



Identifizierung und Charakterisierung von AUM, einer neuen humanen Tyrosin-Phosphatase

Identification and characterization of AUM,
a novel human tyrosine phosphatase

Dissertation zur Erlangung des naturwissenschaftlichen Doktorgrades
der Fakultät für Biologie,
Julius-Maximilians-Universität Würzburg

Vorgelegt von

Prashant S. Duraphe

aus

Pune (Indien)

Würzburg, 2009

Eingereicht am: 13-11-2009

Mitglieder der Promotionskomitees:

Vorsitzender: Prof. Dr. Thomas Dandekar

1. Betreuer: Prof. Dr. Antje Gohla

2. Betreuer: Prof. Dr. Dr. Manfred Scharl

Tag der Promotionskolloquiums : 13-01-2010

Doktorurkunde ausgehändigt am :

Contents

1	<u>INTRODUCTION</u>	1
1.1	PRINCIPLES OF PHOSPHOREGULATION	1
1.1.1	KINOME	3
1.1.2	PHOSPHATOME	3
1.2	THE HAD SUPERFAMILY OF HYDROLASES	5
1.2.1	STRUCTURAL AND FUNCTIONAL ASPECTS OF HAD ENZYMES	7
1.3	IDENTIFICATION OF A NOVEL HAD-TYPE PHOSPHATASE RELATED TO CHRONOPHIN	8
1.3.1	IDENTIFICATION AND BIOINFORMATIC ANALYSIS OF AUM, A NOVEL CHRONOPHIN-RELATED HAD PHOSPHATASE	8
1.3.2	RT-PCR EXPRESSION ANALYSIS OF AUM	12
1.3.3	SUBCLONING OF AUM INTO BACTERIAL AND MAMMALIAN EXPRESSION VECTORS	13
1.3.4	CATALYTIC PROPERTIES OF RECOMBINANT AUM	13
1.3.5	AUM PHOSPHATASE INHIBITOR PROFILE	14
2	<u>AIM OF THE STUDY</u>	17
3	<u>MATERIALS</u>	18
3.1	LIST OF MANUFACTURERS AND DISTRIBUTORS	18
3.2	CHEMICALS	19
3.3	NUCLEOTIDES, NUCLEIC ACIDS AND PRIMERS	21
3.4	PLASMIDS	21
3.5	ANTIBODIES	22
3.6	ANIMALS AND CELL LINES	23
3.7	TISSUE CULTURE REAGENTS AND MATERIALS	23
3.8	OTHER MATERIALS	24
3.9	COMMERCIAL KITS	25
3.10	SOFTWARE AND DATABASES	25
3.11	RNA INTERFERENCE TOOLS	26
3.12	SOLUTIONS & BUFFERS	26
4	<u>METHODS</u>	30

4.1 IDENTIFICATION OF A CHRONOPHIN-RELATED, HYPOTHETICAL PROTEIN BY DATABASE ANALYSIS	30
4.1.1 PHYLOGENETIC ANALYSIS OF HAD PHOSPHATASES	30
4.2 MOLECULAR BIOLOGY METHODS	30
4.2.1 TRANSFORMATION OF COMPETENT <i>E. COLI</i>	30
4.2.2 PLASMID PREPARATION	31
4.2.3 QUANTIFICATION OF NUCLEIC ACIDS BY PHOTOMETRIC MEASUREMENT	32
4.2.4 RESTRICTION DIGESTS OF PLASMID DNA	32
4.2.5 DNA GEL ELECTROPHORESIS	32
4.2.6 ELUTION OF DNA FROM AGAROSE GELS	32
4.2.7 ISOLATION OF RNA FROM MURINE TISSUES	33
4.2.8 POLYMERASE CHAIN REACTION	33
4.2.9 SITE-DIRECTED MUTAGENESIS	35
4.2.10 DNA CONSTRUCTS AND CLONING PROCEDURES	35
4.2.11 COMPUTER-ASSISTED ANALYSIS OF DNA SEQUENCES	36
4.2.12 DIGOXIGENIN-LABELED RIBOPROBE SYNTHESIS	36
4.2.13 NORTHERN BLOT	36
4.3 CELL BIOLOGY METHODS	37
4.3.1 CELL LINES	37
4.3.2 TRANSIENT TRANSFECTION	37
4.3.3 IMMUNOFLUORESCENCE	38
4.3.4 CONFOCAL LASER-SCANNING MICROSCOPY	39
4.3.5 RNA INTERFERENCE	39
4.3.6 LENTIVIRAL TRANSDUCTION OF SHRNA	40
4.3.7 VALIDATION OF THE RNAI TOOLS	41
4.4 PROTEIN BIOCHEMICAL METHODS	43
4.4.1 BACTERIAL EXPRESSION AND PURIFICATION OF RECOMBINANT AUM	43
4.4.2 DESIGN OF AUM PEPTIDE ANTIBODY	44
4.4.3 SAMPLE PREPARATION FOR IMMUNOBLOT ANALYSIS	46
4.4.4 MOUSE SPERM PREPARATION AND ANALYSIS	46
4.4.5 ESTIMATION OF PROTEIN CONCENTRATION	47
4.4.6 SDS-POLYACRYLAMIDE GEL ELECTROPHORESIS	48
4.4.7 DETECTION OF PROTEINS IN SDS-POLYACRYLAMIDE GELS	48
4.4.8 IMMUNOBLOT ANALYSIS	49
4.4.9 IMMUNOPRECIPITATION	50
4.4.10 IMMUNOHISTOCHEMISTRY	50
4.4.11 ENZYMATIC ACTIVITY ASSAYS	51

4.4.12	HIGH THROUGHPUT PHOSPHOPEPTIDE SCREEN	52
4.4.13	<i>IN VITRO</i> PROTEIN PHOSPHATASE ACTIVITY ASSAYS	52
4.4.14	CELL BIOLOGICAL ASSAYS	53
4.4.15	CELL AREA DETERMINATION OF FIXED CELLS	55
5	RESULTS	57
5.1	PHYLOGENETIC ANALYSIS OF AUM ORTHOLOGS AND OF ITS EVOLUTIONARY RELATIONSHIP WITH CIN	57
5.2	AUM IS A MAGNESIUM-DEPENDENT HAD PHOSPHATASE	61
5.2.1	ENZYMATIC ACTIVITY ASSAY	61
5.2.2	AUM IS AN ASPARTATE-DEPENDENT HAD PHOSPHATASE	62
5.3	HIGH THROUGHPUT PEPTIDE SCREEN	64
5.4	AUM IS A PROTEIN TYROSINE PHOSPHATASE	65
5.4.1	PHOSPHATASE OVERLAY ASSAY	65
5.4.2	ROLE OF AUM FOR EPIDERMAL GROWTH FACTOR-INDUCED TYROSINE PHOSPHORYLATION IN CELLS	66
5.5	UBIQUITOUS EXPRESSION OF AUM IN MOUSE TISSUES	68
5.5.1	REAL-TIME PCR	68
5.5.2	NORTHERN BLOT	69
5.5.3	WESTERN BLOT	71
5.6	IMMUNOHISTOCHEMICAL ANALYSIS OF AUM IN MOUSE TESTES	74
5.6.1	EXPRESSION PATTERN OF AUM IN MOUSE SEMINIFEROUS TUBULES	75
5.6.2	EXPRESSION PATTERN OF AUM IN MALE REPRODUCTIVE SYSTEM	75
5.6.3	EXPRESSION OF AUM IN DEVELOPING GERM CELLS	76
5.7	AUM KNOCKDOWN BY RNA INTERFERENCE	78
5.7.1	TRANSIENT AUM DEPLETION	78
5.7.2	STABLE AUM DEPLETION	79
5.8	POTENTIAL ROLE OF AUM IN EPIDERMAL GROWTH FACTOR SIGNALING	81
5.9	EFFECT OF AUM ON ACTIN DYNAMICS	82
5.10	ROLE OF AUM FOR CELL ADHESION	86
5.10.1	EFFECT OF AUM ACTIVITY ON CELL ADHESION TO FIBRONECTIN	86
5.10.2	EFFECT OF AUM DEPLETION ON CELL ADHESION TO FIBRONECTIN	87
5.10.3	EFFECT OF AUM DEPLETION ON CELL AREA DURING SPREADING	88
5.10.4	AUM LOCALIZATION IN SPREADING CELLS	90
5.10.5	EFFECT OF AUM DEPLETION ON PHOSPHOTYROSINE CONTENT OF FOCAL ADHESIONS IN SPREADING CELLS	91

5.10.6	EFFECT OF AUM DEPLETION ON FOCAL ADHESION MATURATION IN SPREADING CELLS	92
5.11	AUM-SRC PHOSPHOCYCLING	94
6	DISCUSSION	98
6.1	AUM IS NOT A CIN ISOFORM	98
6.2	AUM EXPRESSION ANALYSIS	100
6.3	ROLE OF AUM IN ACTIN DYNAMICS	101
6.4	CONSEQUENCES OF AUM DEPLETION	102
6.5	WAYS AND MEANS OF FINDING AUM SUBSTRATES	104
7	SUMMARY	112
8	ZUSAMMENFASSUNG	114
9	REFERENCES	116
10	SUPPLEMENTARY DATA	124
10.1	JPT PHOSPHOPEPTIDE SCREEN ANALYSIS	124
11	CURRICULUM VITAE	128
12	ACKNOWLEDGMENTS	132

Figure Index

Figure 1: Classification of phosphatases.....	4
Figure 2: Characteristics of HAD phosphatases	6
Figure 3: Structure-function aspects of the HAD superfamily	7
Figure 4: Sequence of murine AUM	9
Figure 5: Amino acid sequence alignment of murine AUM and CIN	10
Figure 6: Genomic organization of mouse CIN and AUM genes.	11
Figure 7: Sequence alignment of putative AUM orthologs	11
Figure 8: RT-PCR expression analysis of AUM	13
Figure 9: Concentration dependent AUM activity in <i>p</i> -NPP assay	14
Figure 10: Phosphatase inhibitor analysis of AUM.....	15
Figure 11: A model for gene inactivation <i>via</i> RNA interference.....	40
Figure 12: Localization of the mAUM siRNA/shRNA in open reading frame of mouse AUM .	43
Figure 13: Amino acid sequence alignment of CIN and AUM and sequence used for the generation of an AUM-specific peptide antibody.....	45
Figure 14: Phylogenetic analysis of human HAD phosphatases.....	58
Figure 15: Phylogenetic comparison of primary amino acid sequence of AUM and CIN	59
Figure 16: Phylogenetic analysis of human and yeast HAD phosphatases	60
Figure 17: AUM is an efficient <i>p</i> -NPP phosphatase	62
Figure 18: Generation of a catalytically impaired AUM mutant	63
Figure 19: AUM preferentially dephosphorylates tyrosine phosphorylated peptides	64
Figure 20: AUM dephosphorylates tyrosine phosphorylated proteins in phosphatase overlay assays.	66
Figure 21: Effect of AUM on cellular tyrosine phosphorylation in EGF-stimulated cells.....	67
Figure 22: Relative quantification of AUM transcript by real-time PCR.....	69
Figure 23: AUM expression analysis by Northern blot	70
Figure 24: Characterization of AUM rabbit polyclonal antibody	71
Figure 25: Analysis of AUM expression in mouse tissues.....	72
Figure 26: Schematic representation of male reproductive system of mouse.....	73
Figure 27: AUM protein expression analysis in mouse testis.....	74
Figure 28: Immunohistochemical analysis of AUM in mouse testis	75
Figure 29: Expression pattern of AUM in the male reproductive system	76
Figure 30: Expression pattern of AUM during spermiogenesis	77
Figure 31: Transient AUM depletion by siRNA.....	78
Figure 32: Stable AUM depletion by shRNA	79
Figure 33: Effect of AUM on cellular tyrosine phosphorylation in EGF-stimulated cells.....	80
Figure 34: Effect of AUM on EGFR tyrosine phosphorylation	82

Figure 35: Effect of AUM overexpression on actin cytoskeleton in spreading HeLa cells.....	83
Figure 36: Effect of AUM overexpression on actin dynamics in HeLa cells	84
Figure 37: Effect of stable AUM depletion by shRNA on steady-state actin dynamics	85
Figure 38: Effect of AUM activity on cell adhesion	87
Figure 39: Effect of AUM on area of spreading cells.....	90
Figure 40: AUM localization in spreading cells.....	91
Figure 41: Effect of AUM depletion on phosphotyrosine content of focal adhesion in spreading cells	92
Figure 42: Effect of AUM on focal adhesion maturation in spreading cells	93
Figure 43: Effect of AUM on Src phosphorylation upon fibronectin stimulation	94
Figure 44: Cross talk between Src and AUM	95
Figure 45: Effect of AUM on Src kinase activity	96
Figure 46: Effect of Src on AUM phosphatase activity	97
Figure 47: Approach for the characterization of PTP substrates.....	106
Figure 48: Suggested mechanism for AUM acting as a novel Src kinase activator	110

Abbreviations

Commonly used abbreviations and units of measurements according to the SI system (Cordes, 1972) are not listed.

µg	microgram
µl	microliter
A431	human epidermoid carcinoma cell line
ABC	avidin biotin complex
ADP	adenosine diphosphate
APS	ammonium peroxide sulphate
ATP	adenosine triphosphate
mAUM, hAUM	murine or human actin remodeling, ubiquitously expressed, magnesium-dependent phosphatase hAUM (NM_001042371), mAUM (NM_025954)
BCA	bicinchoninic acid
BLAST	basic local alignment search tool
BPB	bromophenol blue
cDNA	complementary deoxyribonucleic acid
CIN	Chronophin
CIP	calf intestinal phosphatase
CoT	COT fraction of human placental DNA (rapidly annealing, repetitive elements)
<i>C_t</i>	crossing-point threshold cycle
DAB	3,3'-diaminobenzidine tetrahydrochloride
DAPI	4,6-diamidino 2-phenylindole
DEPC	diethylpyrocarbonate
DIG	digoxigenin
DMEM	Dulbecco's modified Eagle's minimal essential medium
DMSO	dimethylsulfoxide
DNA	deoxyribonucleic acid
DTT	dithiothreitol
<i>E. coli</i>	<i>Escherichia coli</i>
EB	elution buffer
EDTA	ethylene diamine-N,N,N',N'-tetraacetic acid
EGF	epidermal growth factor
EK	enterokinase
F-actin	filamentous actin
FAK	focal adhesion kinase
FCS/FBS	fetal calf/bovine serum

FITC	fluorescein-5-isothiocyanate
G-actin	globular actin
GAPDH	glyceraldehyde-3-phosphate dehydrogenase
GC1-spg	mouse spermatogonial cell line
GFP	green fluorescent protein from the jellyfish <i>Aequoria Victoria</i>
HAD	haloacid dehalogenase
HEK 293T	human embryonic kidney cell line
HeLa cell line	human cell line derived from a cervical cancer patient, Henrietta Lacks.
HEPES	N-(2-hydroxyethyl)piperazine-N'-(2-ethanesulfonic acid)
HRP	horseradish peroxidase
Ig	immunoglobulin
IPTG	isopropyl β -D-thiogalactopyranoside
Kbp	kilo basepair
kDa	kilo Dalton
LB medium	Luria-Bertani medium
LIMK	LIM kinase (acronym for Lin-11, Isl-1 and Mec-3)
LSM	laser scanning microscopy
MCS	multiple cloning site
mM	millimolar
MWCO	molecular weight cut-off
NCBI	National Centre for Biotechnology Information
nm	nanometer
ORF	open reading frame
OUT	operational taxonomic unit
PCR	polymerase chain reaction
PFA	<i>para</i> -formaldehyde
pH	negative decadic logarithm of the hydrogen ion concentration
Pi	inorganic phosphate
pI	isoelectric point
PLP	pyridoxal 5'-phosphate
PNA	lectin from <i>Arachis hypogaea</i> (peanut)
<i>p</i> -NPP	<i>para</i> -nitrophenylphosphate
PMSF	phenylmethyl sulfonylfluoride
PP	protein phosphatase
PPM	phosphoprotein phosphatase, magnesium-dependent
PPP	phosphoprotein phosphatase
PuroR	puromycin resistance gene for selection of mammalian cells

RE	restriction enzyme
RIPA	radioimmunoprecipitation assay
RNA	ribonucleic acid
RNAi	RNA interference
RT	room temperature
RT-PCR	reverse transcriptase polymerase chain reaction
RZPD	German resource centre for genome research
SDS-PAGE	sodium dodecylsulphate polyacrylamide gel electrophoresis
shRNA	short hairpin RNA
siRNA	short interfering RNA
SLO	streptolysin O
SOC	super optimal broth with catabolic repression
TBS	Tris-buffered saline
TEMED	N,N,N',N'- tetramethylethylenediamine
Tris	Tris (hydroxymethyl)-aminomethane
Triton X-100	t-octylphenoxypolyethoxyethanol
Tween-20	polyoxyethylen-(20)-monolaurate
UV	ultra violet (light)
v/v	volume per volume
w/v	weight per volume
wt	wild type
x g	acceleration due to gravity (9.81 m/s ²)
YFP	yellow fluorescent protein

1 Introduction

Cells within multicellular organisms communicate *via* diffusible molecules or by direct cell-cell interactions. Hormones, growth factors, neurotransmitters and other external stimuli induce various cellular processes such as gene activation, alterations in metabolism, proliferation, motility or cell death (Bradshaw 2003). The mechanisms by which extracellular agents transmit information *via* specific receptors to evoke intracellular processes are known as 'signal transduction' or 'cell signaling' or 'transmembrane signaling' pathways.

In general, signals are transduced by changes in the activity and/or localization of proteins. Such changes can occur in a rapid and often reversible fashion by posttranslational modifications of the proteins involved in the respective signaling cascade. Protein phosphorylation on serine, threonine and tyrosine residues was the first discovered mechanism of posttranslational protein modification (Krebs and Beavo, 1979). Since then, numerous human diseases have been attributed to dysregulated protein phosphorylation (Hunter 2002). In addition, many other posttranslational modifications that alter protein functions have been found, such as protein acetylation, glycosylation, ubiquitination, SUMOylation, NEDDylation, methylation, biotinylation or ADP-ribosylation (Hunter 2007).

1.1 Principles of phosphoregulation

Protein phosphorylation (that is, the addition of a phosphate $[(\text{PO}_4)^{3-}]$ moiety to certain amino acid residues) is governed by the opposing action of protein kinases and protein phosphatases (Hunter 1995). The enzymatic activity of a protein kinase results in the covalent attachment of a phosphate group [derived from the γ -phosphate of adenosine triphosphate (ATP)], to the side chain of an amino acid that contains free hydroxyl groups (Hunter 1998). The discovery of the cyclic AMP (cAMP)-dependent protein kinase A (PKA) and its pleiotropic substrate specificity was the basis of the establishment of field called signal transduction (Hunter 2000).

Proteins can be phosphorylated on nine different amino acid residues: tyrosine, serine, threonine, cysteine, arginine, lysine, aspartate, glutamate, and histidine (Hunter 2004). Out of these, serine, threonine and tyrosine play key regulatory roles in eukaryotic cells. In humans, the relative phosphorylation on serine, threonine or tyrosine residues is approximately 86.4, 11.8, and 1.8% respectively (Olsen et al., 2006). Several recent phospho-proteomic studies have established that, along with aspartate and histidine residues, bacterial proteins are also phosphorylated on serine, threonine and tyrosine residues (Soufi et al., 2008). Thus, it appears that protein phosphorylation is a universal mechanism of protein regulation. Genome wide analysis has provided a means to compile inventories of protein kinases and phosphatases across a wide selection of organisms.

These efforts have supplied insights into the evolution of this group of enzymes and their roles in various signaling pathways (Moorhead et al., 2009).

The reversible phosphorylation or dephosphorylation of one or more amino acid residues can alter the protein conformation and hence affect its function (Cohen 1992). Posttranslational modifications in general and reversible phosphorylations in particular add another level of protein regulation in addition to post transcriptional modifications, such that the same gene product can have specific functions under different conditions. Until recently, kinases were considered as the active partner of the reversible phosphorylation process and phosphatases as a passive housekeeping counterpart, most of the times acting as a negative regulator in the process of reversible phosphorylation. But now it is amply clear that kinase and phosphatase activities are coordinated in the regulation of signalling processes (Tonks 2006). Also, in contrast to initial views of signaling pathways as simple linear arrangements of phosphorylation cascades that function in isolation to switch protein activities on or off, it is now clear that there are multiple and interacting signaling networks that determine the physiological outcome.

Reversible phosphoregulation can have many additional and subtle effects on the function and fate of a protein, such as the modulation of protein enzymatic activity and its subcellular localization, the generation of binding sites for interacting protein partners or for divalent ions such as calcium, the control of the duration of a given response, or the control of protein degradation, to name a few of them. In particular, by creating binding sites for interacting proteins and by acting as scaffolds in protein-protein complexes, protein (de)phosphorylation can integrate inputs from multiple signaling pathways and regulate synergistic responses to agonists (Cohen 2000).

It is estimated that about thirty percent of all proteins (Hunter 2000), or 2 – 4% of the genes (Manning et al., 2002) are phosphorylated at any given time in most cells. In addition, the potential of protein regulation by phosphorylation is enhanced many fold due to multisite phosphorylation (that is, the phosphorylation of more than one amino acid residue in the same protein). This principle was first shown in the epidermal growth factor (EGF) receptor (Cohen 2000). The existence of phosphorylation and -dephosphorylation events on protein serine/threonine (Ser/Thr)-residues was identified well before the discovery of protein tyrosine (Tyr) phosphorylation in 1979 (Eckhart et al., 1979). It appears that the use of tyrosine phosphorylation as a signaling mechanism evolved along with multicellularity as a signaling mechanism for intercellular communication (Hunter 2002).

The first eukaryotic protein phosphatase was identified a decade later to that of protein kinase (Bradshaw 2003). The initial research on protein phosphorylation was therefore focused on kinases. Even after the discovery of protein phosphatases, these enzymes were considered as passive partners merely responsible for signal termination. As

the field progressed, it became increasingly clear that phosphatases can no longer be viewed as passive partners but can play active and often dominant roles in the process of reversible protein phosphoregulation (Alonso et al., 2004; Hornberg et al., 2005). Whereas kinases appear to control the amplitude of a given signaling response, phosphatases appear to control the rate and duration of the response (Tonks 2006).

1.1.1 Kinome

The molecular analysis of kinases has revealed that all eukaryotic protein kinases (ePKs) contain a conserved, bilobate catalytic domain structure. Eukaryotic protein kinases with no apparent sequence homology to the superfamily of ePKs are grouped as atypical protein kinases (aPKs). Kinases are divided in 120 families of ePKs and 134 families of aPKs (Hanks and Hunter 1995). The human genome has 518 protein kinase genes, of which 478 belong to the ePK and the others to aPK family. That means over 2% of the genes in the human genome belong to protein kinases. This number may vary, *e.g.* due to the expression of splice variants of individual genes. Out of the over 500 kinase genes, 90 are tyrosine kinases and the rest are serine/threonine kinases. Based on functional and phylogenetic analysis (<http://kinase.com/>), this vast numbers of kinases can be grouped into a revised classification scheme of 9 groups (Morrison et al., 2000) as follows: 1) Tyrosine Kinases: All active members phosphorylate tyrosine residues and are related by sequence similarity. 2) Tyrosine Kinase-like: This is the most diverse of all groups. Families in this group are close to tyrosine kinases. 3) AGC: Group named after the family members PKA, PKG, PKC. 4) CAMK: Calcium/Calmodulin regulated kinases and structurally related kinases. 5) CK1: Casein kinase 1 group. 6) Others: Families that do not fit into any of the main groups. 7) STE: MAP kinase cascade kinases. 8) RGC: Catalytically inactive kinase family named after Receptor Guanylate Cyclases. 9) Atypical: Families of eukaryotic kinases whose kinase domains do not have significant sequence similarity to eukaryotic protein kinases.

The protein kinase catalogue has many implications for the understanding of the basis for human diseases and for the development of small molecule drugs that target individual disease-causing protein kinases. Importantly, this kinome analysis has also paved the way for the analysis of the phosphatome.

1.1.2 Phosphatome

Like protein kinases, the study of protein phosphatases initiated in the field of glycogen metabolism and through biochemistry, molecular biology and now with the advent of genomics we are in the position to catalogue the phosphatase complement of various organisms (Moorhead et al., 2009). The evolution of protein kinases and phosphatases has been different. Whereas kinases have similar catalytic pockets and conserved ATP binding sites and can be traced back to a common ancestor, phosphatases are not derived from a

common ancestral molecule and have evolved in structurally and mechanistically distinct families (Alonso et al., 2004). Phosphatases are classified into three major families as schematically represented in figure 1.

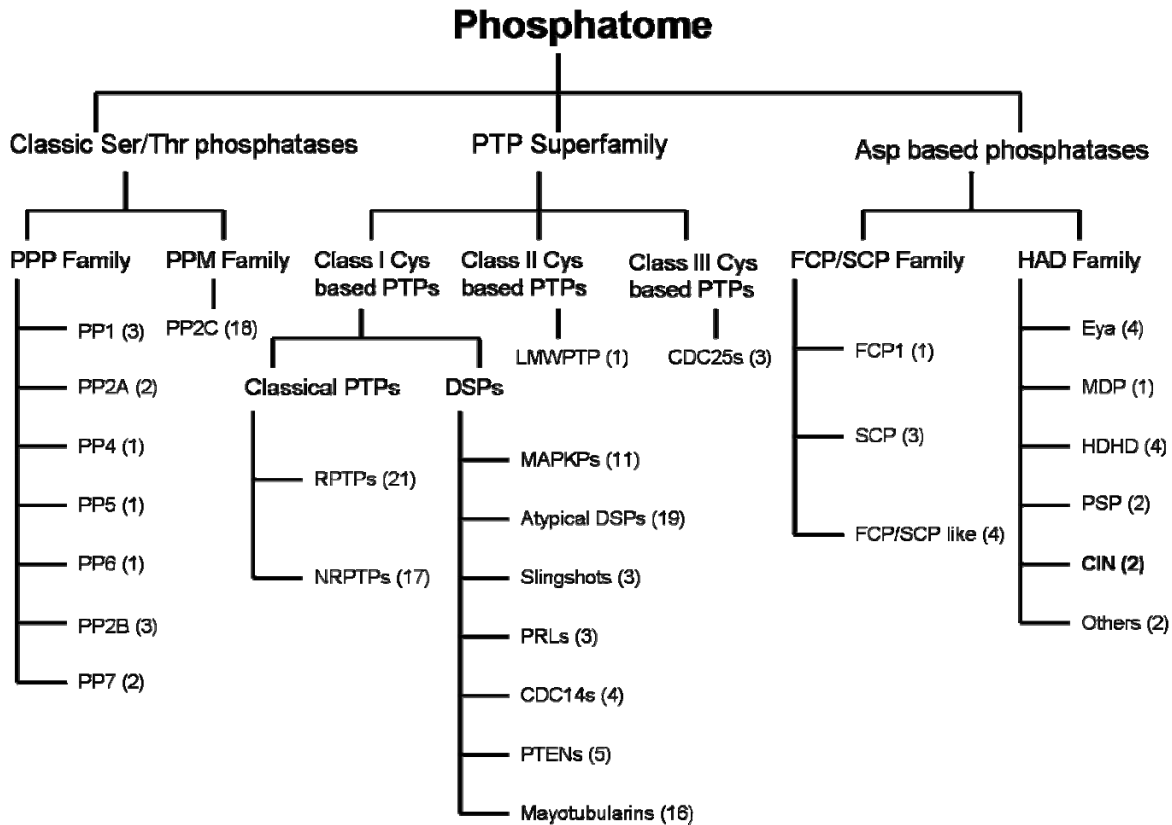


Figure 1: Classification of phosphatases

Based on substrate specificity, phosphatases are classified as either Ser/Thr-phosphatases, cysteine-based Tyr phosphatases or aspartate-based phosphatases. Numbers in the brackets represent gene numbers. For details of each class please refer to the text. Abbreviations used in the figure are as follows: PPP, Phospho Protein Phosphatase; PPM, Metallo dependent Protein Phosphatase; PP, Protein Phosphatase; PTP, Protein Tyrosine Phosphatase; RPTP, Receptor-like PTP; NRPTP, Non Receptor PTP; CDC, Cell Division Control proteins; LMWPTP, Low Molecular Weight PTP; DSP, Dual Specificity Phosphatases; MAKP, Mitogen Activated kinase Phosphatase; PRL, Phosphatase of Regenerating Liver; PTEN, Phosphatase and Tensin homolog; FCP/SCP, transcription initiation factor IIF (TFIIF)- associated component of C-terminal domain (CTD) phosphatase/small CTD phosphatase; HAD, Haloacid Dehalogenase; MDP, Magnesium dependent protein phosphatase; HDHD, Haloacid dehalogenase like Hydrolase Domain containing protein; PSP, Phospho Serine Phosphatase; CIN, Chronophin; Others, proteins that do not belong to major groups of HAD family of phosphatases.

Phosphatases have acquired specificity during the course of evolution through additional modular domains or by the ability to dock to novel regulatory subunits (Moorhead et al., 2009). Most of the PTP family members have evolved through domain fusion on the gene level (Alonso et al., 2004), whereas most of the PPP and PPM family members have evolved *via* complex formation at the protein level. The best understood example of this is the serine/threonine phosphatase 1 (PP1) that can associate with over 100 regulatory subunits (Das et al., 1996; Hendrickx et al., 2009).

The PPP catalytic domain possesses the signature motif –GDxHG-GDx(V/I)DRG– and –GNHE– (spread out over a region of 280 amino acids), which is crucial for binding of divalent metal ions. Otherwise there is no overall sequence homology among the PPP phosphatases. Most members of the PPP family are high molecular weight complexes containing one or more regulatory subunits (Bradshaw 2003). The PPM family phosphatases are Mn^{2+}/Mg^{2+} -dependent serine/threonine-specific enzymes. All eukaryotic PPM enzymes have 11 conserved motifs with nine highly conserved amino acids that coordinate metal ions necessary for catalysis (Zhang and Shi 2004).

The PTP family is defined by the catalytic signature motif –CX₅R– with diverse domain structure and substrate preferences. The three subclasses of cysteine based PTPs have evolved independently during evolution (Moorhead et al., 2009). Class I cysteine based PTP is the largest among three subclasses and the members are strictly tyrosine specific and evolved from common ancestor. Class II cysteine based PTPs is represented by a single member in human genome which codes for low molecular weight (18 kDa) phosphatase. Third subclass is from rhodanese-derived PTPs comprise three cell cycle regulators. The human genome encodes 107 PTP genes. Taking into account inactive PTPs and the ones having non-protein substrate specificities, the number of active protein tyrosine phosphatases and protein tyrosine kinases is very similar and hence one can assume that both tyrosine kinases and tyrosine phosphatases have comparable substrate specificities (Alonso 2004). Similar to the existence of pseudokinases (Kannan and Taylor 2008), the phosphatome also contains phosphatase-inactive, yet conserved members, as exemplified by the STYX-domain proteins (Wishart and Dixon 1998).

The most recently classified group of phosphatases are aspartate-based phosphatases, in which catalysis is driven by an aspartic acid residue in the signature motif –DXDXT/V– (Alonso et al., 2004). While the other families of protein phosphatases have been characterized for over two decades now, those utilizing aspartate-based catalysis have been noted only very recently (Archambault et al., 1998). This is partially due to the fact that aspartate-based phosphatases are insensitive to inhibitors of “classical”, thiol-based phosphatases. Even though aspartate-based catalysis group is divided into FCP/SCP-like and HAD-family phosphatases, both share the same catalytic core motif and also belong to different groups within the HAD superfamily.

1.2 The HAD superfamily of hydrolases

The haloacid dehalogenase (HAD) superfamily of hydrolases, named after the archetypal enzyme haloacid dehalogenase includes enzymes catalyzing carbonyl or phosphoryl group transfer reactions on a diverse range of substrates (Koonin and Tatusov 1994).

The HAD superfamily is represented in the proteomes of organisms from all three superkingdoms of life. The enzymes of this superfamily are involved in numerous disparate biological functions such as metabolism, membrane transport, signal transduction and nucleic-acid transfer, but have so far primarily been characterized in lower organisms (Burroughs et al., 2006). Among the over 2000 different members of this superfamily, ATPases (PO-P cleavage) and phosphatases (CO-P cleavage) are most prevalent, whereas a diversification of catalytic activities toward phosphonate hydrolysis (P-C bond), or dehalogenase hydrolysis (C-Cl bond) occurs less frequently (Allen and Dunaway-Mariano 2004).

Sequence comparisons have shown that there is no overall sequence homology among HAD enzymes but practically all members contain three highly conserved sequence motifs, called HAD domains which correspond to the catalytic pockets and determine the substrate specificities (Ridder and Dijkstra 1999) as shown in figure 2A. N-terminal HAD motif determines the enzymatic characteristics of HAD domains. Haloacid dehalogenase have $-DXYGT-$, p-type ATPases have $-DKTGT-$ whereas HAD phosphatases are characterized by the first N-terminal HAD motif with the signature sequence $-DXDX(V/T)-$. All HAD phosphatases are Mg^{2+} -dependent enzymes that share similar mechanism of substrate dephosphorylation, by forming a phosphoaspartate intermediate where the first aspartate residue in the signature sequence acts as a nucleophile (Allen and Dunaway-Mariano 2004). A schematic representation of the enzymatic mechanism of HAD phosphatases is depicted in figure 1B.

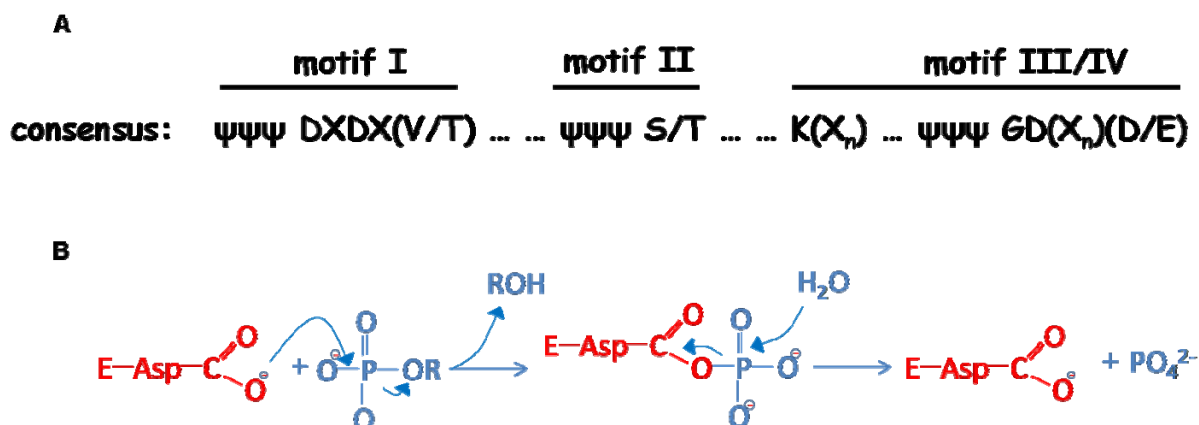


Figure 2: Characteristics of HAD phosphatases

A: Consensus sequence of catalytic motifs. First aspartate residue in motif I act as nucleophile. X represents any amino acid. Ψ : represents any hydrophobic amino acid, D: aspartic acid, V: valine, T: threonine, K: lysine, G: glycine, E: glutamic acid

B: Catalytic mechanism of HAD phosphatases: Moieties originating from the substrate or solvent are colored in blue, and those originating from the enzyme are colored in red. E: Enzyme with aspartate at active site, R: positive charged ion attached to phosphate (modified from Burroughs et al 2006).

1.2.1 Structural and functional aspects of HAD enzymes

Over 40 X-ray crystal structures and an enormous amount of sequence data have made it possible to understand the structure-function relationships of the HAD enzymes (Aravind and Koonin 1998). Aspartate (Asp) nucleophile dependent hydrolysis is the basic theme of HAD enzymes. The carboxylate group of the first Asp and the backbone C=O of the second Asp in motif I coordinate the Mg^{2+} cofactor (Fig. 1B). Second acidic residue acts as a general acid-base which binds and protonates the substrate leaving group in the first step and deprotonates the nucleophile of the second step (Lahiri et al., 2002). The second motif is characterized by a conserved threonine along with hydrophobic amino acids. Motif II along with a lysine in motif III contributes to the stability of the phosphoaspartate intermediate of the hydrolysis reaction. Terminal acidic residues of motif III along with motif I are required for coordinating the Mg^{2+} -ion in the active site (Peisach et al., 2004). Motifs I-III are spatially arranged around a single 'binding cleft' at the C-terminal end that forms the active site of HAD enzymes. Crystal structures of many HAD hydrolases have predicted a variable region around the active site, which is termed "cap domain" (Zhang et al., 2002) as shown in figure 3. Cap domains are thought to provide the necessary 'substrate space' for diversification of the enzymes of this large family of hydrolases.

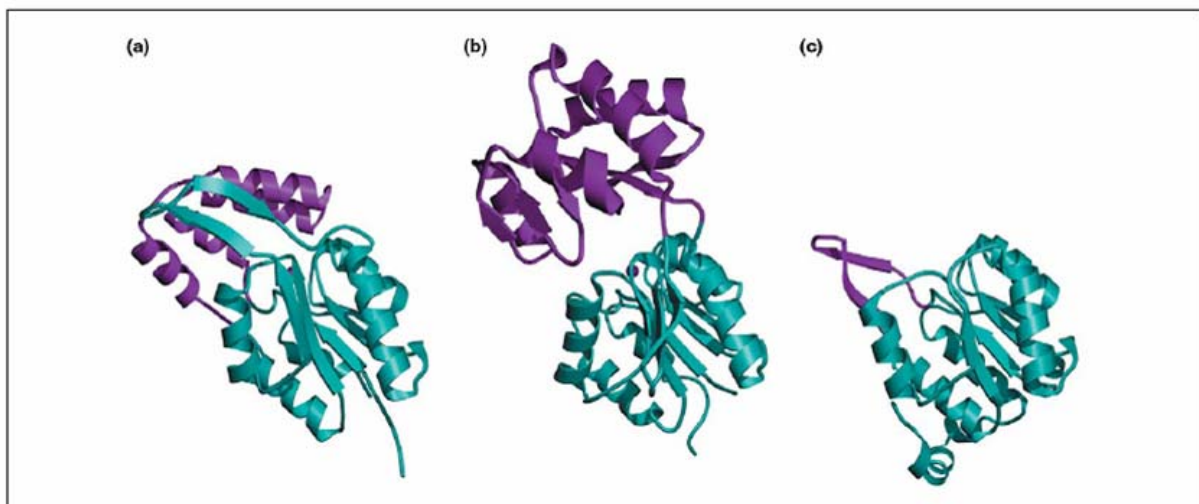


Figure 3: Structure-function aspects of the HAD superfamily

Ribbon diagram highlighting how the common catalytic core domain (cyan) and the divergent cap domain (magenta) contribute to the diverse catalytic mechanisms of HAD hydrolases. Letters a, b, c represents three classes within HAD superfamily. Class a: enzymes with C-Cl, C-P, PO-P cleavage mechanism, class b: enzymes with CO-P cleavage/formation mechanism, class c: CO-P cleavage mechanism (from Allen and Mariano 2004).

Very few HAD phosphatases are so far characterized for their function in higher organisms. Most prominent among them are the human phosphoserine phosphatase (PSP) involved in the L-serine biosynthetic pathway (Collet et al., 1998), the transcription factor Eyes Absent (Eya), which is involved in organogenesis and immunity (Okabe et al., 2009), and the cofilin phosphatase Chronophin (CIN, (Gohla et al., 2005). On the basis of sequence similarity,

UBLCP1 was inferred to have similar functions as EYA proteins (Zheng et al., 2005) and TIMM50 to act as an essential regulator of mitochondrial protein translocation (Guo et al., 2004). These examples emphasize the biological importance of this largely unexplored enzyme family, and support the hypothesis that HAD phosphatases are one of the major players in the diversification of enzymatic potential of organisms by providing the raw evolutionary material for the generation of novel enzymes (Burroughs et al., 2006). Hence it appears to be interesting to characterize the biological roles of HAD phosphatases in higher organisms, which is one of the focus areas in our research group.

1.3 Identification of a novel HAD-type phosphatase related to Chronophin

Our group has identified Chronophin (CIN), an actin cytoskeletal regulatory phosphatase of the HAD-family. CIN was found to dephosphorylate the actin severing protein cofilin on its inhibitory serine residue and thereby activate it (Gohla et al., 2005). Cofilin is a ubiquitously expressed and essential protein that accelerates actin filament turnover (Bamburg and Bloom 2009). The stimulus-dependent cofilin phosphoregulation is one of the key convergence points in cellular signaling networks that regulate actin cytoskeletal dynamics under both physiological and pathophysiological conditions such as tumor initiation, progression and metastasis (Bamburg and Wiggan 2002). It can thus be expected that CIN functions in these processes as well.

1.3.1 Identification and bioinformatic analysis of AUM, a novel Chronophin-related HAD phosphatase

In order to better understand the biological roles of mammalian HAD-type phosphatases, one focus of our group is to characterize CIN-related enzymes. By performing a saturating search of the non-redundant database for human phosphatases that contain HAD domains (using a datamining approach similar to the one described by (Andersen et al., 2005), we were able to identify a previously undescribed, putative CIN homolog (Fig. 4). We initially referred to this novel protein as CIN-2, but later renamed it AUM (acronym for actin remodeling, ubiquitously expressed, magnesium-dependent HAD phosphatase), because it turned out not to be a CIN-isoform, but rather a distinct protein tyrosine phosphatase. The basic characterization of this novel enzyme was conducted during my diploma thesis work. The following sections summarize as yet unpublished information that provided the basis for my present Ph.D. thesis work.

Human AUM is 46% identical and 59% similar in its amino acid sequence to human CIN; mouse AUM and CIN proteins share 45% identity and 61% similarity. A full amino acid sequence alignment of mouse CIN and AUM is shown in figure 5. As highlighted, three HAD domains (HAD I-III) can be found in AUM. Thus, AUM contains all the invariant residues

characteristic of HAD phosphatases, and these residues are almost identical to the respective residues contained in the equivalent positions in CIN.

Mouse AUM has a predicted molecular weight of 34.5 kDa, and its calculated isoelectric point (pI) is 5.35 (as compared to mouse CIN with a molecular weight of 31.5 kDa and a pI of 5.53). Mouse AUM contains seven serine-, as well as three threonine- and three tyrosine residues, which may serve as regulatory phosphorylation sites (Fig. 4). No additional posttranslational modifications were predicted for AUM, using the scansite database (<http://scansite.mit.edu/>).

mAUM	
1	GGCGGGTGGC GCGCGGGGCA GCGGTCAGCG GTCGACCATG GCAGAGGCGG AAGCCGGTGG CGACGAGCC CGCTGCGTGC M A E A E A G G D E A R C V
81	GGCTGAGCGC CGAGCGGGCC AAGTTGCTGC TGGCCGAGGT GGACACGCTG CTGTTGACT GCGATGGCGT GCTGTGGCGC <u>R L S A E R A K L L L A E V D T L L F D C D G V L W R</u>
161	GGCGAGACGG CCGTGCCGGG GCGCGGGAG ACTCTGCGG CTCTGCGGGC CCGCGGCAG CGACTGGGCT TCATCACCA <u>G E T A V P G A P E T L R A L R A R G K R L G F I T H</u>
241	CACACGACG AAGACTCGCA CGGCCTACG GGAGAGCTA AGGCGCTTG GTTTCGGCGG CCGGTGGGG CCCGAGCTG <u>N S S K T R T A Y A E K L R R L G F G G P V G P E A</u>
321	GCCTCGAGGT GTTCGGCAGC GCCTATTGCA GCGCGCTCA TCTGCGCCA CGCCTGGCGG GCGTGCCGA CCCGAGGCC G L E V F G T A Y C S A L Y L R Q R L A G V P D P K A
401	TACGTGCTGG GCAGCCCGG CTTAGCAGCC GAGCTGGAGG CCGTGGGTGT CACTAGCGTG GCGTGGGCC CCGACGTGT <u>Y V L G S P A L A A E L E A V G V T S V G V G P D V L</u>
481	TCACGGGAT GGCCCCAGCG ACTGGCTAGC CGTCCGCTC GACCCGACG TCCGCGCGT AGTGGTGGC TTCGACCCAC H G D G P S D W L A V P L E P D V R A V V V G F D P
561	ACTTCAGCTA CATGAGCTC ACCAAGCCG TCCGTACCT GCAGCAGCC GACTGTCTG TCGTGGCAC CACATGGAC H F S Y M K L T K A V R Y L Q Q P D C L L V G T N M D
641	AACCGCTCC CGTAGAGAA CGGCCGTTT ATTGCGGTA CCGCTGTCT GGTCCGACC GTGAGATGG CCGCCAGCG N R L P L E N G R F I A G T G C L V R A V E M A A Q R
721	CCAGCGGAC ATCATCGGA AGCCTAGCC CTTATCTTC GACTGCGTG CCCAGGATA TGATATCAC CCGAGCCGA <u>Q A D I I G K P S R F I F D C V S Q E Y G I N P E R</u>
801	CCGTCATGGT GGGAGACCG CTGGACACG ACATCTCCT GGGCTCCAC TGTAGCCTGA AGACTATCCT GACCTCACC <u>T V M V G D R L D T D I L L G S T C S L K T I L T L T</u>
881	GGAGTCTCCA GTCTTGAGG TGTGAGAGC ATCAGGAAA GTGACTGCAT GTTCAGAGG AAATGTCC CTGACTTCTA <u>G V S S L E D V K S N Q E S D C M E K K K M V P D F Y</u>
961	TGTTGACAGC ATTGCCGACC TCTGCCTGC CCTTCAGGT TAAAGATCTA GTGCTTTAA TCTCTGCAAT AAAAAAAAAA <u>V D S I A D L L P A L Q G *</u>
1041	AAAAA

Figure 4: Sequence of murine AUM

Nucleotide and deduced amino acid sequence of a full length cDNA encoding for a hypothetical murine CIN homolog, which we refer to as AUM (GenBank accession number NM_025954). Possible phosphorylation motifs are underlined. No other posttranslational modification sites were predicted for this protein. The numbers on the left refer to nucleotide positions.

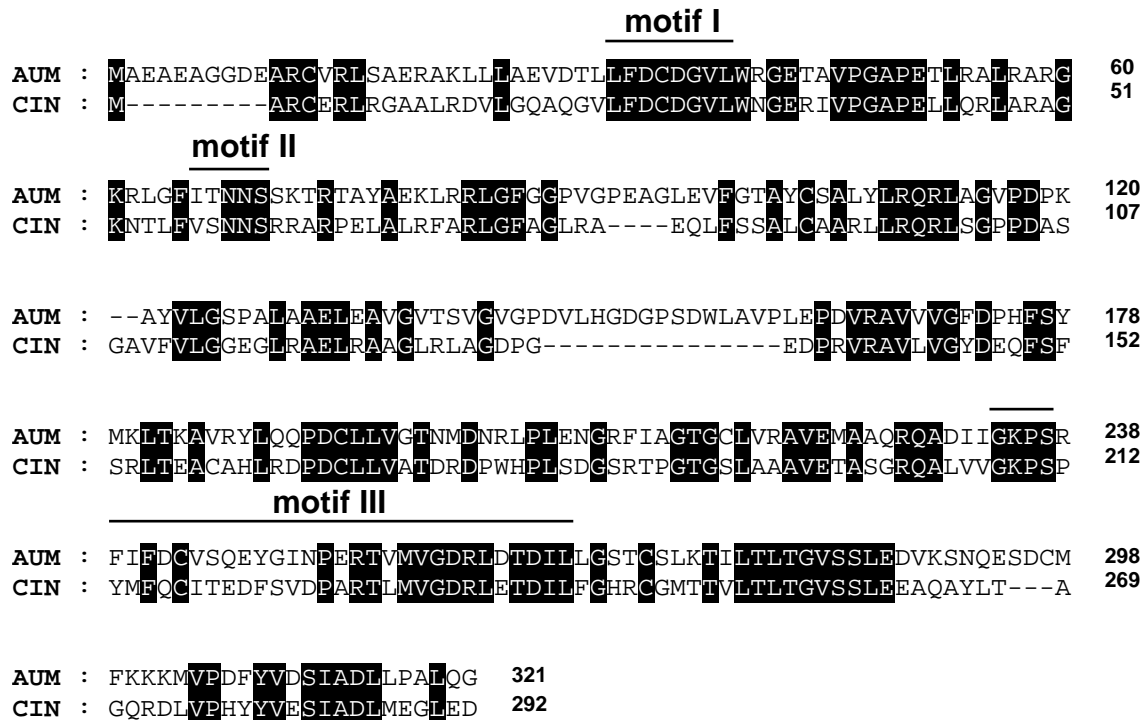


Figure 5: Amino acid sequence alignment of murine AUM and CIN

Both sequences share 45% identity (141/312 residues) and 61% similarity (193/312 residues). This alignment was performed using the 'multiple sequence alignment' tool of the program ClustalW (Version 1.83) program. Identical residues are highlighted in black. Most of the essential amino acid residues in three HAD motifs are conserved. Numbers given on right refer to amino acid positions.

Human and mouse CIN are known to map to chromosome 22q12.3 and 15E1, respectively. Using AUM cDNA as a query sequence, a BLAST analysis of the genomic sequence available through the NCBI Web site mapped the human AUM gene to chromosome 16. The murine AUM gene is located on chromosome 17A3.3. Thus, CIN and AUM are located on different chromosomes in humans and mice. The genomic organization of the human and murine CIN and AUM genes is very similar, with the open reading frames encoded by two exons, as shown in figure 6.

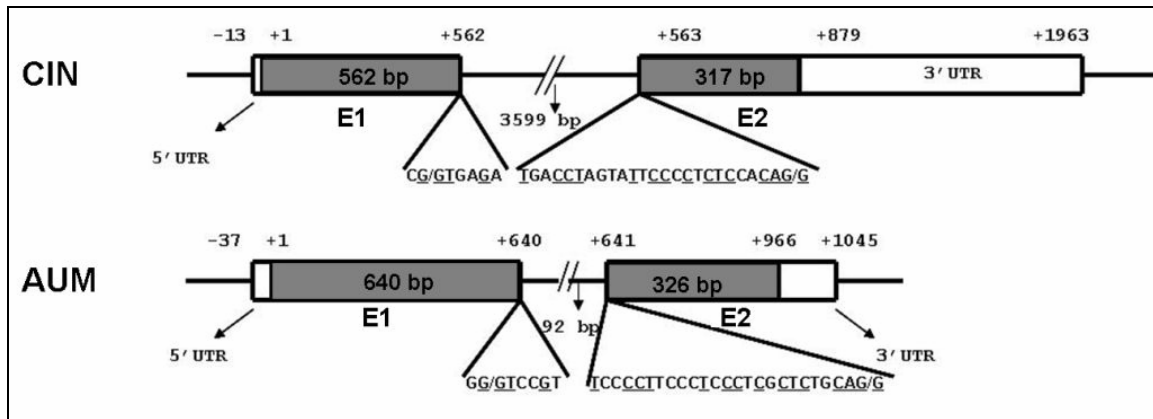


Figure 6: Genomic organization of mouse CIN and AUM genes.

Mouse CIN and AUM are located on chromosomes 15E1 or 17A3.3, respectively. The open reading frames of CIN and AUM are encoded by two exons. AUM has a very small intron as compared to CIN.

The distribution of AUM across species was analyzed in multiple sequence alignments using the program ClustalW. Figure 7 demonstrates that orthologs of AUM are present in species ranging from bacteria to mammals, as shown here by the presence of three HAD phosphatase motifs. In addition, the HAD motifs are similarly distributed in the protein (the adjacent motifs I and II are located at the N-terminus and are separated by a relatively large insert from the bipartite motif III in the C-terminus). The amino acid sequence identities/similarities of mouse AUM to the respective hypothetical proteins from *Rattus norvegicus*, *Homo sapiens*, *Danio rerio*, *Drosophila melanogaster*, *Caenorhabditis elegans*, *Arabidopsis thaliana*, *Saccharomyces cerevisiae*, *Anopheles gambia*, *Dictyostelium discoideum* and *Escherichia coli* are 99/99.6, 90/94, 57/76, 39/60, 33/55, 39/56, 33/51, 40/59, 33/53 and 32/43%, respectively. These results suggest that AUM has been highly conserved throughout evolution.

	Motif I	Motif II	Motif III	
M. musculus	30 TLLFDODGVL	60 GKRLGFITNN	234 DIICKPS.....	259 VMVGDRLDTD BC040100
R. norvegicus	30 TLLFDODGVL	60 GKRLGFITNN	234 DIICKPS.....	259 VMVGDRLDTD XP_213235
H. sapiens	30 TLLFDODGVL	60 GKRLGFITNN	234 DIICKPS.....	259 VMVGDRLDTD XP_208887.1
B. taurus	30 TLLFDODGVL	60 GKRLAFITNN	234 DIICKPS.....	259 VMVGDRLTDD ENSBTAG0000009951
X. tropicalis	24 TVLFDCDGVL	54 NKRVFVLTNN	228 QVIKGPS.....	253 VMVGDRLDTD ENSXETG0000016097
D. rerio	23 CVLFDCDGVV	53 GKQVFFVTNN	227 QVVGKPS.....	252 LMVGDRLDTD AAH45860
S. cerevisiae	26 TFLFDODGVL	56 GKQLIFVTNN	230 SYCGKPN.....	255 CMVGDRLNTD YDL236W
A. gambiae	38 TVLTDODGVI	68 GKKLFFVTNN	242 IVMGKPN.....	257 LMIGDRCNTD XP_309300
D. melanogaster	41 SVITDODGVL	71 GKSIYFCTNN	245 VVIKPN.....	270 LMIGDRANTD CG5567
C. elegans	31 TFI F DADGVL	61 NKQIIVLTNN	235 LTVGKPC.....	260 MMIGDRTNTD NP_504509
D. discoideum	24 TFI F DODGVL	54 GKKILFVTNN	228 ITIGKPE.....	253 LFGDRLDTD DDB0186160
E. coli	05 NVICDHDGVL	35 GLPLVLLTNY	172 FYVGKPS.....	197 VIVGDNLRTD NP_752680
A. thaliana	28 TFI F DODGVI	58 GKRLVFTNN	204 LVVGKPS.....	229 CMVGDRLDTD BAA97552
Consensus	DXDXV	T	K(X _n).....	GD(X _n)D

Figure 7: Sequence alignment of putative AUM orthologs

Sequence alignment of putative AUM orthologs in various species with respect to conserved HAD motifs. The numbers preceding the HAD motifs I-III designate the respective amino acid number. The catalytically essential residues of HAD motifs I-III are identical in the aligned proteins, and are indicated by a black box. GenBank accession numbers are shown on the right.

1.3.2 RT-PCR expression analysis of AUM

A search in the UniGene EST Profile Viewer (<http://www.ncbi.nlm.nih.gov/unigene>) indicated that AUM may be widely expressed in mammals, but with marked tissue-specific differences in transcript abundance. The major AUM expression sites in the mouse were predicted to be male genitals, mammary gland, skeletal muscle and brain stem. Interestingly, the AUM and CIN expression patterns are predicted to be partially non-overlapping (see also Gohla et al. 2005).

In order to examine the expression of AUM experimentally, we first used the cDNA preparations provided in a mouse multiple tissue cDNA panel as a template, and PCR-amplified AUM with gene-specific primers. In this panel, the mRNA expression levels of several housekeeping genes such as α -actin, glyceraldehyde-3-phosphate dehydrogenase (GAPDH), phospholipase A2 and the ribosomal protein S29 are used to standardize the amount of cDNA present in each tissue sample. This normalization procedure accounts for tissue specific differences in the levels of transcription, thus allowing estimating the relative abundance of a gene of interest. GAPDH is known to be expressed at high levels in skeletal muscle and at low levels in testes. As shown in the upper panel of figure 8, the principal expression sites of AUM appear to be testes and skeletal muscle. AUM expression during embryonic development was maximal at E17. Interestingly, testicular development commences at around 18 days post conception (Livera et al., 2006). To investigate AUM expression in more detail, total RNA was isolated from various adult mouse tissues, and subjected to RT-PCR analysis with AUM gene-specific primers. The lower panel in figure 8 shows that relative to the housekeeping gene GAPDH, AUM is differentially expressed in a tissue-specific manner. Highest transcript levels were found in brain stem, cerebellum, brain cortex, and the eye.

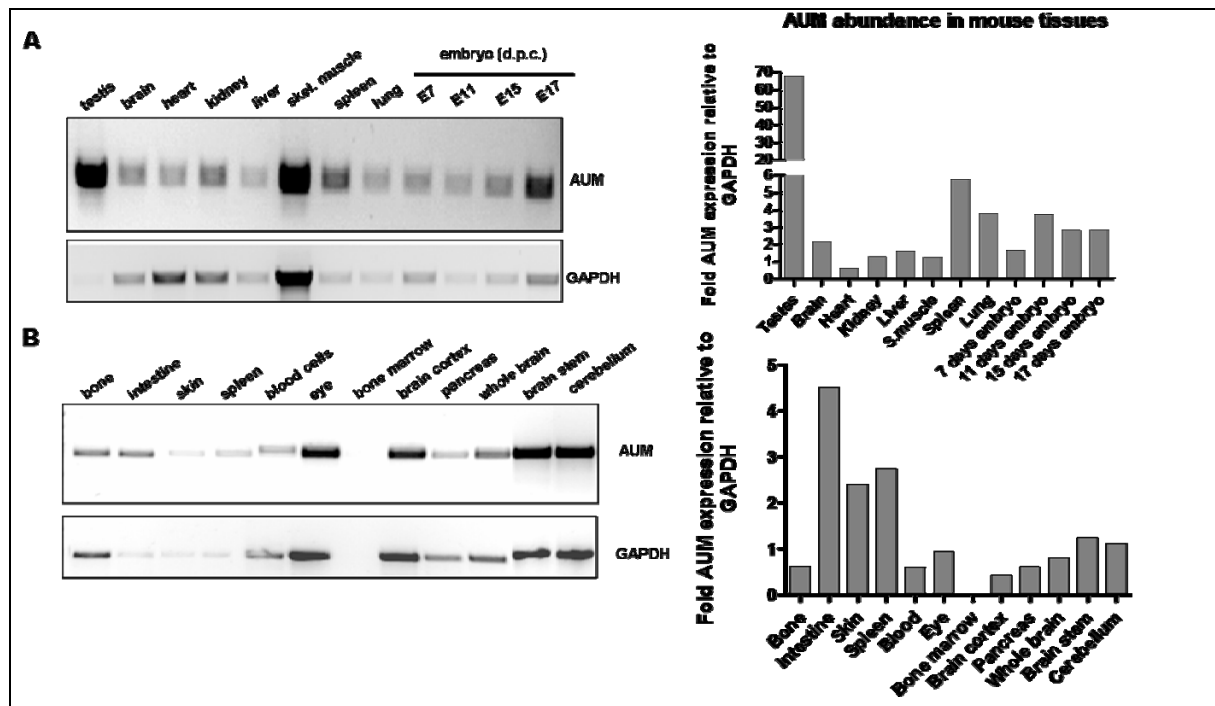


Figure 8: RT-PCR expression analysis of AUM

A: Expression analysis of AUM in cDNA preparations provided in a mouse multiple tissue cDNA panel. AUM is widely expressed, with highest levels found in testes, skeletal muscle, 17 days-old embryo, brain and eye. B: Total RNA was isolated from the indicated mouse tissues and reverse transcribed. AUM message is prominently expressed in the eye and in certain brain regions as well as in pancreas. Comparable amounts of cDNA were loaded in each lane. The amplicon size for AUM is 780 bp. 30 cycles of PCR amplification were used for both panels. The expression of the housekeeping gene GAPDH is shown as an internal control. Densitometric quantitation of the AUM expression plotted as fold expression relative to GAPDH.

1.3.3 Subcloning of AUM into bacterial and mammalian expression vectors

As a basis for the initial characterization of AUM, we generated AUM expression constructs. A full-length mouse AUM cDNA clone (pCMV-SPORT6 IRAVp968H1184D) was obtained from the German Resource Centre for Genome Research (RZPD). AUM was PCR-amplified with gene-specific primers, and subcloned into the bacterial expression vector pTrc-His (containing an N-terminal His₆-tag for the purification of the recombinant enzyme on immobilized metal affinity matrices), as well as into the mammalian expression vector pcDNA4-myc/His (containing a C-terminal myc-tag for subcellular localization analysis, in addition to an adjacent His₆-tag inserted for purification purposes). Positive clones were verified to be full-length and error-free by sequencing.

1.3.4 Catalytic properties of recombinant AUM

Murine AUM was expressed as a His₆-tagged protein in bacteria and subsequently affinity-purified by IMAC. We then tested the enzymatic activity of purified AUM in *in vitro* phosphatase assays. We first employed the broad-spectrum phosphatase substrate *para*-nitrophenylphosphate (*p*-NPP). *p*-NPP is a colorless compound that can be enzymatically

dephosphorylated to the yellow substance *p*-nitrophenol. This conversion can be spectrophotometrically measured over time, and both the kinetics and the endpoint of the reaction can be determined. Figure 9 demonstrates that purified AUM dose-dependently dephosphorylates *p*-NPP.

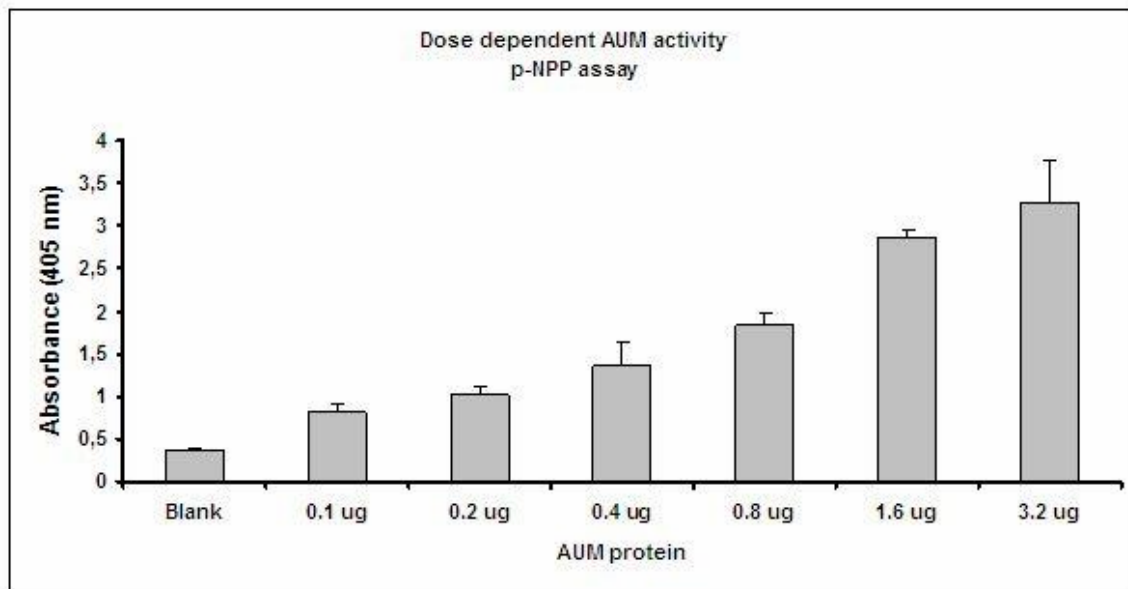


Figure 9: Concentration dependent AUM activity in *p*-NPP assay

Purified AUM concentration-dependently dephosphorylates *p*-NPP (3.5 mM final concentration). The absorbance of the product *p*-nitrophenyl was continuously measured at 405 nm over 30 min at 30°C. Samples were measured in duplicates, and the mean values of the end points are plotted.

1.3.5 AUM phosphatase inhibitor profile

Further evidence for the HAD-phosphatase nature of AUM was obtained by testing its susceptibility profile to various standard phosphatase inhibitors in a *p*-NPP assay. Figure 10, upper panel, shows that AUM was insensitive to inhibitors of classical thiol-based serine/threonine phosphatases, such as the PP2A-inhibitor okadaic acid, the PP1-inhibitor calyculin A, and the PP2B-inhibitor cypermethrin. These results support the idea that AUM utilizes an unconventional catalytic mechanism. In agreement with these findings, AUM was insensitive to the commercial phosphatase inhibitor cocktail I (containing the PP2A/PP1-inhibitor microcystin LR, the PP2A/PP1-inhibitor cantharidin and the alkaline phosphatase inhibitor (-)-*p*-bromotetramisole), but was inhibited by the phosphatase inhibitor cocktail II (containing sodium vanadate, an inhibitor of tyrosine and alkaline phosphatases; sodium molybdate and sodium tartrate, inhibitors of acid phosphatases, and imidazole, an inhibitor of alkaline phosphatases). Figure 10, lower panel, shows that AUM was effectively and concentration-dependently blocked by molybdate and orthovanadate, which act as phosphate analogs. Furthermore, AUM was strongly inhibited by NaF, which inactivates magnesium-dependent phosphatases. In addition, Zn²⁺, Ca²⁺ and Mn²⁺, which may compete

with the catalytically essential Mg^{2+} , inhibited AUM activity. The Mg^{2+} -chelator EDTA completely abolished AUM activity.

The inhibitor profile of AUM thus closely resembles CIN (Gohla et al., 2005). Thus, the homology between the AUM and CIN phosphatase domains, the high extent of conservation of the active-site residues among AUM orthologs across evolution, together with the observed AUM inhibitor profile suggest that AUM is a CIN-related, Mg^{2+} -dependent HAD-type phosphatase.

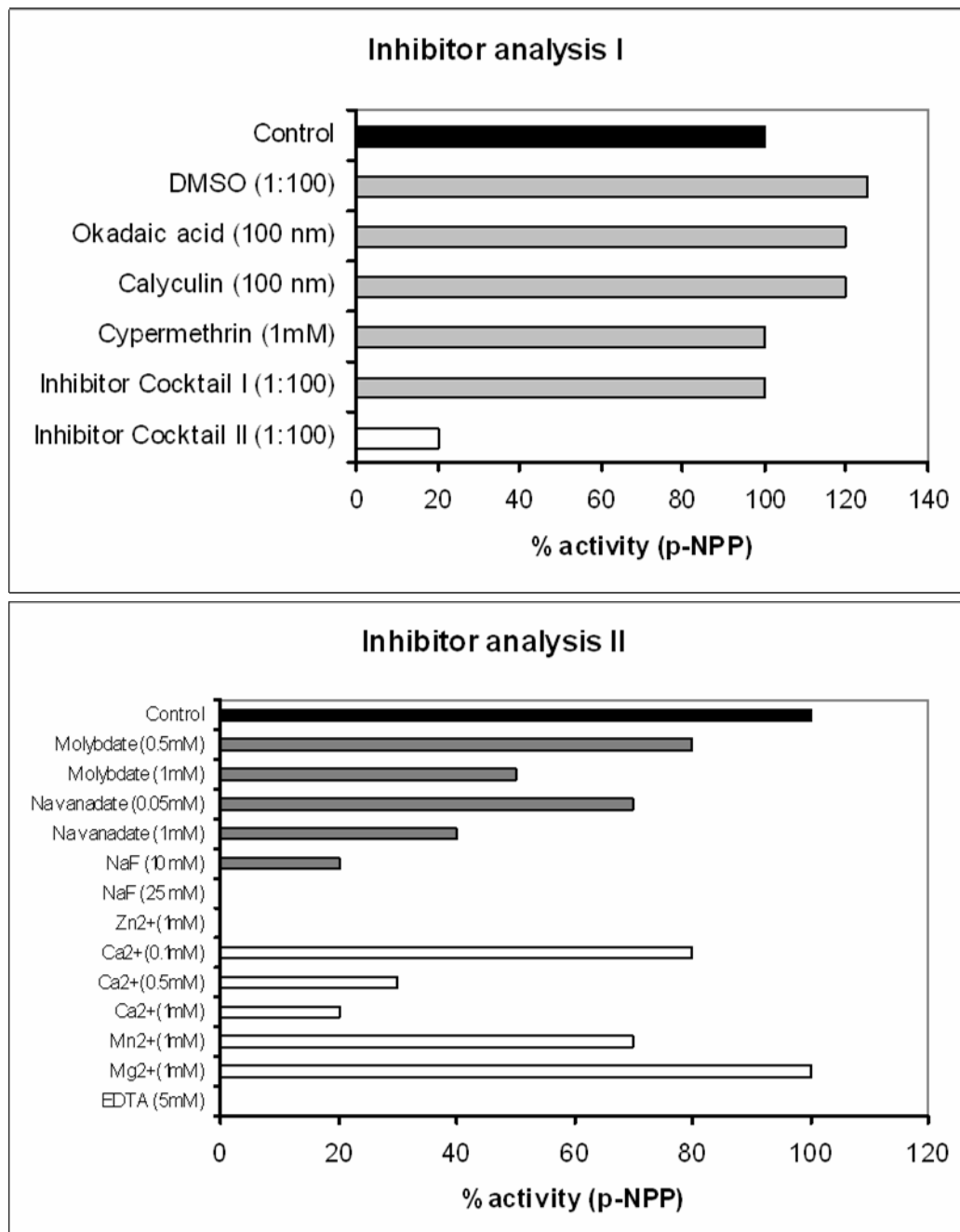


Figure 10: Phosphatase inhibitor analysis of AUM

Eight hundred nanograms of AUM were preincubated with the indicated inhibitors for 30 min at 30°C. Subsequently, the kinetics of *p*-NPP-dephosphorylation was followed at 405 nm for 30 min at 30°C. Two independent experiments were performed in duplicate. In the initial, linear phase of the reaction, the slopes of mean values were calculated and compared to the appropriate controls. The

percentages of the activities as compared to the control are shown. The inhibitor cocktail II (containing vanadate, molybdate, tartrate and imidazole), but none of the tested PP1-, PP2A or PP2B-inhibitors blocks AUM phosphatase activity. DMSO was included as a solvent control for Calyculin A and the inhibitor cocktail I. AUM was inhibited by phosphate analogs like vanadate, molybdate and fluoride. Various cations that may compete with Mg^{2+} during the enzymatic reaction were tested. Calcium dose-dependently inhibits AUM activity with 30% inhibition at 0.5 mM. Mn^{2+} leads to 40% inhibition, whereas AUM activity is completely inhibited in the presence of Zn^{2+} .

Taken together, the basic characterization of AUM identifies an evolutionarily conserved novel phosphatase in higher organisms with yet unknown physiological function. AUM is found to be a novel HAD-type phosphatase with similarities to CIN, but with a distinct, tissue-specific expression pattern.

2 Aim of the study

The haloacid dehalogenase (HAD) superfamily of hydrolases represents a ubiquitous enzyme family with approximately 2000 members, the majority of which are magnesium-dependent phosphatases. Although the existence of 58 human HAD enzymes has been predicted (Allen and Dunaway-Mariano 2004), our understanding of their cellular and physiological functions remains rudimentary.

By database mining of human HAD phosphatases, we have recently discovered a previously undescribed enzyme with homology to Chronophin, a cytoskeletal regulatory HAD phosphatase. The aim of this study was the characterization of this novel enzyme using phylogenetic, biochemical and cell biological approaches.

The following questions were addressed:

- 1) Is AUM an isoform of Chronophin?
- 2) What are the substrate preferences of AUM?
- 3) What are the cellular functions of AUM?

Answering these questions is expected to enhance our understanding of the biological importance of an emerging class of poorly understood human phosphatases.

3 Materials

3.1 List of manufacturers and distributors

- 1) Abgent, San Diego, CA, USA
- 2) Abnova, Taipei, Taiwan
- 3) Addgene Inc. Cambridge, MA, USA
- 4) Amersham Biosciences, Little Chalfont, UK
- 5) AnaSpec Inc. San Jose, CA, USA
- 6) AppliChem, Darmstadt
- 7) Applied Biosystems, Foster city, CA
- 8) ATCC, Manassas, VA, USA
- 9) BD Becton Dickinson GmbH, Heidelberg
- 10) Beckman Coulter, Krefeld
- 11) Biomol Research Lab, Plymouth Meeting, PA, USA
- 12) Bio-Rad, Munich
- 13) BMG Labtech, Offenburg
- 14) Calbiochem, Darmstadt
- 15) Carl Zeiss AG, Jena
- 16) Cell Signaling Technologies, Danvers, CO, USA
- 17) Charles River Laboratories, Kisslegg
- 18) Clontech, Palo Alto, CA, USA
- 19) Cytoskeleton Inc., Denver, CO, USA
- 20) Dako, Glostrup, Denmark
- 21) Dharmacon RNAi Technologies, Schwerte
- 22) Fermentas, St. Leon-Rot
- 23) Fujifilm, Düsseldorf
- 24) GE Healthcare, Munich
- 25) Genaxxon Bioscience, Biberach
- 26) GeneTex, Irvine, CA, USA
- 27) Hartmann Analytic GmbH, Braunschweig
- 28) Invitrogen, Karlsruhe
- 29) JPT Peptide Technologies GmbH, Berlin
- 30) Leica microsystems, Wetzlar
- 31) Mediatech, Jylling, Denmark
- 32) Merck, Darmstadt
- 33) Millipore, Billerica, MA, USA

- 34) MP Biomedicals, Eschwege
- 35) Operon Biotechnologies, Cologne
- 36) PAN Biotech GmbH, Aidenbach
- 37) Pierce, Rockford, USA
- 38) Promega, Heidelberg
- 39) Qiagen, Hilden
- 40) Raytest, Straubenhardt
- 41) Roche Applied Science, Mannheim
- 42) Roth, Karlsruhe
- 43) German Science Center for Genome Research (RZPD), Berlin
- 44) Santa Cruz, Heidelberg
- 45) Serva, Heidelberg
- 46) Sigma Aldrich, Munich
- 47) Stratagene, La Jolla, CA, USA
- 48) Thermo Scientific, Rockford, IL
- 49) TPP, Trasadingen, Switzerland
- 50) Upstate, Lake Placid, NY, USA
- 51) US Biological, Swampscott, MA, USA

3.2 Chemicals

β-Mercaptoethanol	6
2-Propanol	42
Acetic acid	32
Acrylamide/bisacrylamide	42
Ammonium persulfate	46
Aprotinin	46
Bovine serum albumin	45
Bromophenol Blue	46
Calcium chloride (CaCl ₂ · 6 H ₂ O)	32
Calyculin A	15
Crystal Violet	46
Cypermethrin	15
Difco Agar Noble	9
DMSO	6
DNase	46
DTT	46

EDTA	46
EGTA	46
Ethanol	42
Ethidium bromide	46
Gelatin	46
Glycerol	6
Glycine	32
Hepes	46
Hydrochloric acid (HCl)	42
Isopropanol	42
LB agar	6
LB powder	6
Leupeptin	42
Low-melting agarose	46
Magnesium acetate [$\text{Mg}(\text{CH}_3\text{COO})_2 \cdot 4 \text{H}_2\text{O}$]	46
Magnesium chloride (MgCl_2)	46
Methanol	42
Okadaic acid	46
Paraformaldehyde	32
Phosphatase Inhibitor Cocktail I	46
Phosphatase Inhibitor Cocktail II	46
Pepstatin	46
PMSF	46
Polybrene	46
(1,5-dimethyl-1,5-diazaundecamethylene polymethobromide)	
Ponceau S	28
Potassium acetate ($\text{CH}_3\text{COO}^-\text{K}^+$)	42
Protease Inhibitor Cocktail Tablets (complete, EDTA-free)	39
Puromycin	15
RNase A	38
SDS	42
Sodium azide (NaN_3)	46
Sodium chloride (NaCl)	6, 32
Sodium deoxycholate	32
Sodium hydroxide (NaOH)	32
TEMED	42
Tris base / Tris-HCl	42

Triton X-100	46
Tween 20	46
Water (PCR quality)	32

3.3 Nucleotides, nucleic acids and primers

CoT Human DNA	41
Custom primers	35
DIG-labeled dNTP mix	41
DNA ladder	22
dNTPs	47
[γ - ³² P]ATP	27
On-Target Plus, set of individual siRNA oligonucleotides (targeting human or mouse AUM)	21
RNA ladder	22
Salmon testes DNA (sodium salt)	46

3.4 Plasmids

pCMV-SPORT6- IRAVp968H1184D	43
pcDNA4-myc/His ₆	28
pTrcHis-A	28
pECFP-N1	18
pEYFP-C1	18
pGEX-4T-1	24
pGEX-4T1 SHP1 ^{wt}	3
pGEX-4T1 SHP2 ^{wt}	3
pLKO.1-puro	46
psPAX2 (packaging vector)	Trono laboratory http://tronolab.epfl.ch/
pCR-VSV-G (envelop vector)	
pcDNA4-myc/His ₆ -mAUM ^{D34N}	present work
pcDNA4-myc/His ₆ -mAUM ^{wt}	present work
pCR 2.1-TOPO-AUM	present work
pECFP-C1- mAUM ^{wt}	present work
pEYFP-C1- mAUM ^{D34N}	present work

pEYFP-C1- mAUM ^{wt}	present work
pGEX-4T-1-mAUM ^{wt}	present work
pTrcHis A-mAUM ^{D34N}	present work
pTrcHis A-mAUM ^{wt}	present work

3.5 Antibodies

AlexaFlour-488-conjugated goat anti-mouse, highly cross absorbed	28
AlexaFlour-488-conjugated goat anti-rabbit, highly cross absorbed	28
AlexaFlour-546-conjugated goat anti-mouse, highly cross absorbed	28
AlexaFlour-546-conjugated goat anti-rabbit, highly cross absorbed	28
AlexaFlour-633-conjugated goat anti-mouse, highly cross absorbed	28
AlexaFlour-633-conjugated goat anti-rabbit, highly cross absorbed	28
Anti-DIG-AP Fab fragments	41
Anti-phosphotyrosine, clone 4G10, mouse monoclonal	50
Anti-phosphotyrosine, pTyr100, mouse monoclonal	16
AUM, rabbit polyclonal	17
EGF receptor, rabbit polyclonal	16
EGF receptor, rabbit polyclonal	51
EGFR (for immunoprecipitation), mouse monoclonal	16
FAK, rabbit polyclonal	16
FAK (clone 4.47), mouse monoclonal	33
GAPDH, mouse monoclonal	26
Goat anti-mouse IgG (Fc), peroxidase conjugated	48
Goat anti-rabbit IgG (Fc), peroxidase conjugated	48
HER2/ErbB2 (clone 29D8), rabbit monoclonal	16
HER2/ErbB2, rabbit polyclonal	16
Immobilized phosphotyrosine antibody (pTyr -100)	16
Paxillin, mouse monoclonal	9
Paxillin, rabbit polyclonal	16
Phospho-EGFR (clone 1H12), mouse monoclonal (Tyr 1068)	16
Phospho-EGFR (clone 53A5), rabbit monoclonal (Tyr 1173)	16
Phospho-EGFR, rabbit polyclonal (Tyr 1045)	16
Phospho-EGFR, rabbit polyclonal (Tyr 992)	51
Phospho-EGFR, rabbit polyclonal (Tyr 1045)	51
Phospho-EGFR, rabbit polyclonal (Tyr 1068)	51
Phospho-HER2/ErbB2, rabbit polyclonal (Tyr 877)	16

Phospho-HER2/ErbB2, rabbit polyclonal (Tyr 1221/1222)	16
Phospho-FAK, mouse monoclonal (Tyr 397)	9
Phospho-FAK, rabbit polyclonal (Tyr 576/577)	16
Phospho-p130 Cas, rabbit polyclonal (Tyr 165)	16
Phospho-Paxillin, rabbit polyclonal (Tyr 118)	16
Phospho-Src Family, rabbit polyclonal (Tyr 416)	16
Phospho-Src, rabbit polyclonal (Tyr 527)	16
Progesterone receptor, mouse monoclonal	2
Src (clone 36D10), rabbit monoclonal	16
Src (clone 17AT28) mouse monoclonal	1
Tubulin (clone DM1A), mouse monoclonal	46
Vinculin (clone hVIN-1), mouse monoclonal	46
β -Actin (clone C4) mouse monoclonal	33

3.6 Animals and cell lines

C57BL/6 mice	17
<i>E. coli</i> TOP 10	28
<i>E. coli</i> DH5 α	28
<i>E. coli</i> BL21(DE3) pLysS	32
HeLa (CCL-2)	8
HEK 293T/F (CRL-1573)	8
GC1 (CRL-2053)	8
A431 (CRL-2592)	8

3.7 Tissue culture reagents and materials

Culture dishes/flasks	49
DMEM	36
Fetal bovine serum	36
L-Glutamine	36
Lipofectamine 2000	28
Opti-MEM	28
Penicillin G, sodium salt	36
Phosphate buffered saline 10X (with/without MgCl ₂ /CaCl ₂)	36
Streptomycin sulphate	36

Trypsin/EDTA	36
--------------	----

3.8 Other materials

5-Bromo-4-chloro-3-indolyl-phosphate (BCIP)	41
Abl protein tyrosine kinase, bacterial recombinant protein	15
Alexa Fluor -488 phalloidin	28
Alexa Fluor -546 phalloidin	28
Alexa Fluor -633 phalloidin	28
Apyrase	46
BD CELL-TAK	9
Biomol Green reagent	11
Centricons, 10 MWKO	33
c-Kit, His ₆ -tagged, recombinant human protein	16
Consensus phosphopeptide (CAAEQPLY*LNPLDP)	5
Coomassie Brilliant Blue (G250)	48
Csk kinase, recombinant human protein	16
Enterokinase (from calf intestine)	41
Epidermal growth factor, recombinant protein	15
Ethidium bromide	46
FAK, GST-tagged, recombinant human protein	16
Fibronectin from bovine plasma	46
FITC-PNA	46
HER/ErbB2 kinase, recombinant protein	16
Hybond C nitrocellulose membrane	24
IPTG	42
Kanamycin	46
Latrunculin A	28
Lysozyme	42
Nitroblue tetrazolium chloride (NBT)	41
PageRuler prestained protein ladder	22
Phospholipase C γ 1, human recombinant protein	16
Phospholipase C γ 2, human recombinant protein	16
Phospholipase C γ 2, phosphopeptide (CRDINSLY*DVSARMY)	5
Phospholipid scramblase 1, human recombinant protein	1
Phosphopeptide scramblase 4, phosphopeptide (CRYQPGKY*PMPNQS)	5
PP2 (Src kinase inhibitor)	16

Progesterone	46
Prolong gold, antifade medium	28
Puromycin	15
QIAzol	39
Restriction enzymes	22
RNase free DNase I	38
Signal transduction peptide, biotinylated (core sequence EGIY*DVP)	16
Sodium butyrate	46
Sperm preparation medium	31
Src, GST-tagged, recombinant human protein	16
Streptolysin O	46
SYBR Green mix	7

3.9 Commercial kits

DIG Wash & block buffer set	41
JPT phosphopeptide panel	29
Micro BCA kit	38
Mouse epididymis cDNA library	44
Mouse tissue cDNA panel	9
Omniscript RT kit	39
PCR purification kit	39
PIPER phosphate detection kit	28
Plasmid purification kit	39
Gel extraction kit	39
p-NPP assay kit	15
Src Kinase Assay kit	16
TOPO cloning kit	28
Quickchange XL site directed mutagenesis kit	47

3.10 Software and Databases

BLAST	NCBI;NLM, Bethesda, MD
ClustalW	EMBL, Hinxton, Cambridge, UK
ClustalX	EMBL, Heidelberg, Germany
ExpASy Server	Swiss Institute of Bioinformatics

GraphPad Prism version 4.00	GraphPad software, San Diego, CA, USA
Metamorph version 7.1.3.0	MDS Analytical Technologies, Downingtown, PA, USA
Primer express	Applied Biosystems, Foster City, CA, USA
Proweb.org	http://www.proweb.org/
PhyloDraw version 0.8	Graphics Application Lab, Pusan National University, Pusan, South Korea
SDS v1.3	Applied Biosystems, Foster City, CA, USA

3.11 RNA Interference tools

All siRNA oligoribonucleotides were purchased from Dharmacon. Four different synthetic siRNA oligoribonucleotides for mouse and human AUM were ordered as ON-TARGET plus set of four (catalog # LQ-041844-01-0002 or # LQ-022877-00-0002, respectively). ON-TARGET plus siCONTROL non-targeting siRNA (catalog # D-001810-01-05) was used as a control in all siRNA experiments.

Lentiviral vectors used for establishing stable cell lines expressing shRNA for stable AUM depletion were purchased from Sigma-Aldrich as bacterial glycerol stocks from the MISSION shRNA Program (catalog # SHCLND-NM_025954). The corresponding control shRNA plasmid (catalog # SHC002) was obtained as a DNA stock.

3.12 Solutions & Buffers

(in alphabetical order)

ABC mix	5 ml	TBS
	50 μ l	Avidin
	50 μ l	Biotin
Antibody diluent	10 mM	Hepes, pH 7.4
	0.5 M	NaCl
	1%	BSA
	0.2%	Tween-20
	0.2%	NaN ₃
Blocking buffer	50 mM	Tris-HCl, pH 8.0

	2 mM	CaCl ₂
	80 mM	NaCl
	5% (w/v)	nonfat milk powder
	0.2%	NP-40
DAB solution	50 ml	0.05 M Tris-HCl, pH 7.6
	1 tablet	DAB (10 mg)
	50 µl	nickel sulfate (13 mg/ml)
	6.5 µl	30% H ₂ O ₂
dNTP stock solutions (PCR)	25 mM	of dATP, dCTP, dGTP, dTTP (each)
Laemmli buffer (SDS-PAGE sample buffer)	62.5 mM	Tris-HCl, pH 6.8
	10% (v/v)	glycerol
	5% (v/v)	β-mercaptoethanol
	2% (w/v)	SDS
	0.02% (w/v)	Bromophenol Blue
Lysis buffer I (for lysis of mouse tissues)	50 mM	Tris-HCl, pH 7.4
	150 mM	NaCl
	1% (v/v)	Triton X-100
	0.1% (w/v)	SDS
	1% (w/v)	sodium deoxycholate
	1 mM	EDTA
	0.5 mM	sodium orthovanadate
	1 mM	sodium fluoride
	1x	protease inhibitor cocktail
Lysis buffer II (for immunoprecipitation)	20 mM	Tris-HCl, pH 7.5
	150 mM	NaCl
	1% (v/v)	Triton X-100
	1 mM	β-glycerophosphate
	2.5 mM	sodium pyrophosphate
	1 mM	sodium orthovanadate
	1x	phosphatase inhibitor cocktail 1
	1x	phosphatase inhibitor cocktail 2
	1x	protease inhibitor cocktail

RIPA buffer (for cell lysis)	50 mM 150 mM 1 % (v/v) 0.1% (w/v) 0.5% (w/v) 1x	Tris-HCl, pH 8.0 NaCl NP-40 SDS sodium deoxycholate protease inhibitor cocktail
Running buffer (10x), pH 8.7 (SDS-PAGE)	250 mM 2 M 10%	Tris base glycine SDS
Stripping buffer (for immunoblotting)	62.5 mM 2% 100 mM	Tris-HCl, pH 6.7 SDS β -mercaptoethanol, added immediately before use
TAE (50x) (for DNA gels)	2 M 100 mM	Tris-Acetate, pH 8.0 EDTA
TBS (10x)	0.5 M 1.5 M	Tris-HCl, pH 7.5 NaCl
TBS-T	50 mM 150 mM 0.1%	Tris-HCl, pH 7.5 NaCl Tween 20
Transfer buffers (for semi-dry blotting)		
Anode buffer I	0.3 M 40%	Tris base methanol
Anode buffer II	25 mM 40%	Tris base methanol
Cathode buffer	25 mM 40 mM	Tris base glycine

10% methanol
For high molecular weight proteins, 20% methanol was used in Anode buffers I and II. Whereas additional 0.005% SDS was used in cathode buffer

All other compounds used in this work were purchased from Roth or Sigma-Aldrich with “*pro analysi*” (pA) grade.

Confocal images were taken on LSM 510 Meta or Leica TCS SP5 confocal microscopes.

TIRF images were taken on Leica AM TIRF MC microscope.

Epifluorescence images were taken on a Nikon TE 2000 Eclipse.

All oligonucleotides/primers used in this work were synthesized by Operon.

DNA bands in agarose gels were detected with the DIANA III Camera System (Raytest, Straubenhardt). In some cases, protein bands detected by Western blotting were semiquantitatively measured on X-ray films using the DIANA III Camera System and quantitated using ImageJ software. For the quantitative analysis of Western blot signals, membranes were analyzed on Alpha Innotech (San Leandro, CA, USA).

DNA and RNA photometrical analysis was performed on a DU800 spectrophotometer.

Measurement of protein concentration and *in vitro* kinase and phosphatase assays were performed on a FLUOstar OPTIMA microplate reader and on a Perkin Elmer Envision 2104 multilabel reader.

4 Methods

4.1 Identification of a Chronophin-related, hypothetical protein by database analysis

In a search for previously uncharacterized, Chronophin (CIN)-related haloacid dehalogenase (HAD)-type phosphatases, an EST database search was performed according to the method described by Anderson (Andersen et al., 2005). A text search was performed in Entrez and Swiss-Prot using the terms "haloacid dehalogenase AND phosphatase AND human" to retrieve a protein master set. These protein sequences were used to query NCBI's non-redundant database with TBLASTN searches, using a cut-off value of $E < 10^{-4}$ in addition to a manual inspection of the obtained sequences for the presence of HAD motifs. Using the Proweb.org server, the obtained sequences were blasted against each other to sort out overlapping/redundant sequences. The remaining hits were included in PSI-BLAST searches. This approach revealed the presence of a Chronophin (CIN)-related, hypothetical protein that we termed AUM, for actin remodeling, ubiquitously expressed, magnesium-dependent phosphatase.

The basic physical characteristics, genomic organization, primary structural analysis of AUM and its sequence similarities with CIN were determined using the NCBI database and bioinformatic tools available on the ExPASy Server (<http://expasy.org/>).

4.1.1 Phylogenetic analysis of HAD phosphatases

Based on the presence of the characteristic HAD motif I, HAD phosphatases from model organisms across the animal kingdom were retrieved using BLAST searches (Altschul et al., 1990). The phylogenetic analysis of AUM orthologs as well as of HAD phosphatases in species ranging from slime mold to human beings was performed using ClustalX (<ftp.embl-heidelberg.de>) and PhyloDraw, version 0.8).

4.2 Molecular biology methods

4.2.1 Transformation of competent *E. coli*

For the transformation of chemically competent *E. coli* TOP10, DH5 α , or BL21(DE3)pLysS cells, 50 μ l of thawed competent cells were mixed with either 50 ng of plasmid DNA or 5 μ l of ligation reaction and incubated on ice for 30 min. After a heat shock (2 min, 42°C in waterbath) and successive incubation on ice (2 min), 250 μ l of preheated SOC-medium (2% tryptone, 0.5% yeast extract, 10 mM NaCl, 10 mM MgCl₂, 10 mM MgSO₄ and 20 mM glucose, pH 7) was added to the bacteria, and the cells were incubated at 37°C for 30 – 60

min. Use of SOC-medium in the final step of *E. coli* cell transformation was shown to yield maximal transformation efficiency (Hanahan 1983). This was followed by incubation for one hour at 37°C in a shaker (120 rpm). Cells were then centrifuged (10,000 x *g*, 1 min, RT) and the supernatant was removed. Cells were resuspended in 100 µl of LB medium and plated on LB agar plates containing the appropriate antibiotics. Plates were incubated at 37°C overnight. Antibiotic resistant colonies were screened for the expression of the respective plasmid and positive strains were stored as glycerol stocks (LB medium supplemented with 25 % (v/v) glycerol) at -70°C or as DNA stock at -20°C. The verification of positive clones was carried out by plasmid isolation (see 4.2.2), restriction digestion (see 4.2.4), and, when appropriate, by sequencing (GATC, Konstanz).

4.2.2 Plasmid preparation

Small scale plasmid isolation

For the screening of positive colonies and preparation of small amounts of DNA, the Mini-prep DNA extraction kit (Qiagen) was used. Plasmids were isolated according to the manufacturer's instructions. Briefly, 3 ml LB medium containing the appropriate antibiotic was inoculated with a single bacterial colony and was incubated overnight at 37°C with constant agitation. Cultures were transferred into 2 ml Eppendorf tubes and cells were pelleted by centrifugation (Centrifuge 5415 D, Eppendorf, Hamburg; 12,000 rpm, 1 min, RT). The DNA was eluted from the columns by the addition of 50 µl of elution buffer (10 mM Tris-HCl, pH 8.0) and subsequent centrifugation (12,000 rpm, 2 min, RT). Following the 1:100 dilution of DNA in elution buffer, the DNA concentration was determined photometrically (see 4.2.3). DNA was stored at -20°C.

Large scale plasmid isolation

For preparation of large quantities of DNA, the Maxi-prep DNA extraction kit (Qiagen) was used according to the instructions of the manufacturer. A single bacterial colony was inoculated in 2 ml LB medium containing appropriate antibiotics, and cells were grown at 37°C for 6-8 h with constant agitation. Afterwards, this culture was added to 100 ml of LB medium with appropriate antibiotics and the culture was incubated at 37°C with constant agitation overnight. Cells were pelleted by centrifugation (Avanti J-20 XP Centrifuge, Beckman Coulter, Krefeld; 6,000 x *g*, 15 min, 4°C), and DNA was isolated as described in the manufacturer's protocol. Finally, the DNA pellet was resuspended in 500 µl of Tris-HCl (10 mM Tris-HCl, pH 8.0), and the DNA concentration was determined. After that, the DNA was diluted 1:100, and the concentration was determined photometrically (see 4.2.3). DNA samples were adjusted to a concentration of 0.5 – 1 µg/µl, aliquoted and stored at -20°C.

4.2.3 Quantification of nucleic acids by photometric measurement

The photometric determination of nucleic acid concentrations was carried out using a DU 800 spectrophotometer (Beckman Coulter). The absorbance A was measured in quartz cuvettes ($d = 1$ cm) at 260 and 280 nm (A_{260} and A_{280}) against H_2O . The nucleic acid concentration was calculated based on the fact that an absorbance of 1 at 260 nm corresponds to an average DNA concentration of 50 $\mu\text{g/ml}$, and that an absorbance of 1 at 280 nm corresponds to an average RNA concentration of 40 $\mu\text{g/ml}$. The purity of isolated DNA was determined using the ratio A_{260}/A_{280} . Ratio of 1.8 to 1.9 is considered to be of optimum purity for most of the downstream applications.

4.2.4 Restriction digests of plasmid DNA

The enzymatic digestion of DNA with restriction endonucleases was carried out using the manufacturer's recommended buffers for single and double digestions (Fermentas, St. Leon-Rot). 10 U of enzyme was used to digest 1 μg of DNA at 37°C in a ThermoMixer (ThermoMixer compact, Eppendorf) for one hour. The efficiency of digestion was checked by agarose gel electrophoresis (see 4.2.5).

4.2.5 DNA gel electrophoresis

Agarose gels were prepared by heating 1% (w/v) agarose (Sigma or Genaxxon) in 1xTAE buffer in a microwave oven, followed by the addition of ethidium bromide (0.5 $\mu\text{g/ml}$). DNA sample buffer (orange DNA loading dye or bromophenol blue) was added to the DNA samples, and the gel was run at constant voltage. The separation was evaluated on a UV table and documented using the DIANA III Camera System (Raytest, Straubenhardt).

4.2.6 Elution of DNA from agarose gels

The extraction of DNA from the agarose gel was carried out with the QIAquick Gel Extraction Kit (Qiagen) according to manufacturer's instructions. Briefly, the agarose gels were illuminated with UV light and the appropriate DNA bands were excised from the gel with a scalpel and transferred into Eppendorf tubes. The gel slices were weighted and three volumes of the supplied buffer were added to each gel slice, followed by incubation at 50°C for 10 min to solubilize the agarose. Afterwards, one volume of isopropanol was added to the samples, and the DNA was separated from the obtained mixture by binding it to the supplied columns and subsequently washing it one time with washing buffer. Afterwards, the DNA was eluted from the columns by the addition of 20 – 30 μl of elution buffer (10 mM Tris-HCl, pH 8.0) and subsequent centrifugation (12,000 rpm, 1 min, RT). DNA was stored until use at -20°C.

4.2.7 Isolation of RNA from murine tissues

Total RNA from HeLa cells or mouse tissues was isolated with the QIAzol reagent according to the manufacturer's protocol. This method is a single-step RNA isolation with slight modifications from the original method, described by Chomczynski and Sacchi (Chomczynski and Sacchi 1987). Basically, an appropriate amount of QIAzol reagent (one ml of QIAzol per 50 to 100 mg tissue or per one 3.5 cm dish with adherent cells) was added to samples. Tissue samples were uniformly homogenized before proceeding further. After sample dissociation, an appropriate amount of chloroform (0.2 ml per 1 ml of QIAzol) was added, and samples were centrifuged to separate the organic and the RNA-containing aqueous phases. RNA was precipitated from the aqueous phase by mixing it with isopropanol (0.5 ml of isopropanol per 1 ml of QIAzol reagent that was used for the initial homogenization). The resulting RNA pellet was washed once with 1 ml of 75% ethanol, was briefly air-dried, and was then redissolved in 20 μ l of DEPC-treated water. To reduce the contamination of the RNA with genomic DNA, the dissolved RNA was subjected to a digestion with RNase-free DNase. The reaction was set as follows: 20 μ l RNA, 2.5 μ l 10 x DNase buffer and 2.5 μ l DNase. The reaction was carried out for 30 min at 37°C. After that, the enzyme was heat inactivated at 65°C for 15 min. The extracted RNA was subjected to a photometric concentration determination (see 4.2.3). The ratio of A_{260}/A_{280} was used to determine the purity of the RNA sample. Ideally, a value of 1.8 to 2 indicates sufficiently pure samples for downstream applications. The RNA was stored at -80°C.

4.2.8 Polymerase Chain Reaction

The polymerase chain reaction (PCR) was used for the amplification of DNA regions, which were defined by specific oligonucleotides (primers). As part of this work, different thermostable polymerases were used for PCR. For the reverse transcriptase-PCR (see below) the reverse transcriptase of the high fidelity RNA PCR kit (Takara Bio Inc.) was used. For synthesizing DNA fragments, where the accuracy of the sequence is of particular importance, a proof-reading DNA polymerase from *Thermococcus sp.* (Platinum Pfx DNA polymerase, Invitrogen) was used, which has a 5'→3' exonuclease activity. For real-time PCR, a commercially available SYBR Green PCR Master Mix was purchased from Applied Biosystems. All PCR reactions were performed in the PCR cycler (Eppendorf or Applied Biosystems) in a single tube or in a 96-well plate. The analysis of the PCR results was carried out on agarose gels (see 4.2.5).

Standard PCR

The standard PCR reaction was set in 25 μ l of reaction volume by a 5 min initial denaturation of DNA at 95°C, and followed by 25 reaction cycles of denaturation, annealing of primers and elongation. The elongation of the primers for 1 min was carried out at a temperature which is

usually calculated 3°C below that of the melting temperature of both oligonucleotides. The elongation was carried out for 1 min at a temperature of 68°C. After a terminal elongation of 1 min the PCR products were analyzed by agarose gel electrophoresis (see 4.2.5).

Reverse transcriptase-PCR (RT-PCR)

PCR can be used for the production of cDNA from tissue or cell lysates. For this purpose, the RNA is reverse transcribed (RT) using reverse transcriptase and specific primers. In this study, RT-PCR was performed for the generation of AUM cDNA from murine tissues. Total RNA was isolated as described in Section 4.2.7, and the reaction was set as follows: 1 µg of RNA, 0.25 µl RNase inhibitor (40 U/µl), 1.25µl dNTPs (10mM), 1µl random hexamer concentration (Roche, Mannheim) 2 µl 10x RT buffer. The total reaction volume was adjusted to 20 µl with DEPC-treated water. RNA was reverse transcribed at 37°C for 1 hr followed by 95°C for 5 min.

One microlitre of cDNA generated in the RT reaction was used as a template in the subsequent PCR reaction using Platinum Pfx DNA polymerase with the forward primer 5'-CTGCTGTTCTGACTGCGATGG-3' and the reverse primer 5'-CTCTTCACATCCTCAAGA CTG-3'. The mixture was initially denatured for 5 min at 95°C, followed by 30 amplification cycles (95°C for 1 min, 58°C for 1 min, 72°C for 1 min). After the terminal elongation step (72°C for 2 min), the PCR product was analyzed by agarose gel electrophoresis.

Real-time PCR

Real time PCR allows quantification and analysis of amplified product in real time. In this study we quantified the AUM signal in various mouse tissues using SYBR Green chemistry (Applied Biosystems). SYBR green dye present in master mix binds to each newly synthesized double stranded DNA in the minor groove and the fluorescence can be measured in real time during the exponential phase of the amplification. Real Time PCR primers for AUM and GAPDH were designed with Primer express software (Applied Biosystems). For AUM, forward primer sequence is

5'-ACCGCCTGGACACAGACATC-3' and the reverse primer sequence is

5'-CCGGTGAGGGTCAGGATAGTC-3', whereas for GAPDH, forward primer sequence is

5'-CGAGAATGGGAAGCTTGTCATC-3' and the reverse primer sequence is

5'-CGGCCTCACCCATTTG-3'. The PCR cycling conditions were 95°C for 15 s, 62°C for 1 min. The reaction was set as follows: 12.5 µl of 2x SYBR mix, 1 µl of 10 µM primer mix, template 2 µl (100 ng of RNA equivalent cDNA). The reaction volume was adjusted to 25 µl with DEPC-treated water. Real-time fluorescence data were captured during the elongation (62°C) step of the cycle on 7500 Real Time PCR system (Applied Biosystems). A crossing-point threshold cycle (C_T) value was obtained for each well as the fractional cycle number at which the measured fluorescence crossed the threshold, a value chosen by the software such that all reactions in all plates were in log phase. The signal was quantified using System

Detection Software (SDS v1.3) relative to GAPDH and calibrated against signal in testis. Software allows us to calibrate the signal with respect to any sample in the given dataset and also to integrate different experiments together.

4.2.9 Site-directed mutagenesis

The catalytic aspartate in AUM was point mutated to asparagine (AUM^{D34N}) using site-directed mutagenesis according to the Quickchange XL site directed mutagenesis kit purchased from Stratagene (La Jolla, USA). Briefly, 100 ng of pTrcHis-mAUM plasmid was employed as a template in the mutagenesis reaction with the primer 5'-GTGGACACGCTGCTGTTCAACTGCGATGGCGTGCTGTGG-3' and its reverse complement. The PCR reaction was performed with Platinum Pfx Polymerase (5 min at 94°C, 12 cycles at 94°C for 30 sec, 58°C for 1 min, and at 68°C for 5 min, followed by 1 min at 68°C). One µl of DpnI enzyme was added to the PCR mix for digestion of the methylated template. The PCR product was transformed into competent DH5α cells (see 4.2.1), and the obtained colonies were screened for the desired mutation by sequencing (see 4.2.11).

4.2.10 DNA constructs and cloning procedures

The full length clone (pCMV-SPORT6- IRAPv968H1184D) encoding for mouse AUM (1700012G19Rik) was obtained from the German Resource Centre for Genome Research (RZPD, Berlin). The full length AUM cDNA was amplified using Platinum Pfx Polymerase (PCR conditions 5 min at 95°C, 25 cycles at 95°C for 1 min, 60°C for 1 min, and 68°C for 1 min followed by 30 sec at 68°C) and the forward primer 5'-CTTCCGGATCCATGGCAGAGGCGGAAGCC-3' and the reverse primer 5'-CTTCCGAATTCTTATCTAGAACCTTGAAGGGCAGGCAAG-3'. The PCR product was cloned into pCRII-TOPO vector and sequenced. As a part of my diploma work, AUM was subcloned into the bacterial expression vector pTrcHis A (Invitrogen) *via* the BamH1-EcoRI sites to allow the expression of N-terminally His₆-tagged AUM, and into the eukaryotic expression vector pcDNA4-myc/His₆ (Invitrogen) *via* the BamH1-XbaI sites to generate C-terminally myc/His₆-tagged AUM.

As part of this thesis work, AUM^{wt} and AUM^{D34N} were subcloned into pECFP-N1 to generate AUM-CFP, into pEYFP-C1 to generate YFP-AUM (both vectors from Clontech, Palo Alto, CA, USA) and into pGEX-4T-1 (GE Healthcare, Munich) to generate GST-AUM for bacterial expression. YFP and CFP-AUM were cloned *via* BamH1-XbaI sites whereas GST-AUM was cloned *via* BamH1-NotI restriction sites. All generated plasmids were verified by sequencing (GATC Biotech) and stored as glycerol stocks at -80°C and as plasmid DNA at -20°C.

4.2.11 Computer-assisted analysis of DNA sequences

The analysis of sequences and their graphic representation was carried out with the programs ContigExpress and AlignX from the program package VectorNTI Suite 10 (Invitrogen) as well as with the Chromas program, version 1.43 (C. McCarthy, Brisbane, Australia).

4.2.12 Digoxigenin-labeled riboprobe synthesis

An AUM RNA probe (riboprobe) was generated for the detection of AUM expression at the RNA level in Northern blots. To that end, 300ng of the pCMV-Sport6-AUM plasmid were amplified using the forward primer 5'-CTTCCGGATCCATGGCAGAGGGCGGAAGCC-3' and the reverse primer with the T7 polymerase promoter sequence 5'-CTAATACGACTCACTATAGGGAGAGAATTCTTATCTAGAACCTTGAAGGGCAGGCAAG-3' with platinum Pfx polymerase (5 min at 94°C, 25 cycles of 94°C for 1 min, 60°C for 1 min, and at 68°C for 1 min followed by final extension for 1 min at 68°C). After a terminal elongation of 1 min, the PCR products were analyzed by agarose gel electrophoresis (see 4.2.5).

Amplified DNA was purified from the gel as detailed in section 4.2.6. Gel-extracted DNA was precipitated in 3 M ammonium acetate, vacuum-dried and resuspended in 5 µl of DEPC-treated water. The purified plasmid DNA was used as a template for the synthesis of the digoxigenin-labeled riboprobe. The *in vitro* transcription was carried out with T7 RNA polymerase at 37°C for 2 hrs (2 µl of 5x transcription buffer, 2 µl of digoxigenin-labeled dNTP mix containing 10 mM of each nucleotide, 2 µl of 0.1 M DTT, 1 µl (40 U/µl) of RNasin). Transcription buffer was provided along with polymerase. DIG labeled dNTP mix was purchased from Roche. To remove plasmid DNA, the reaction mix was treated with 2 µl of RNase-free Dnase RQ1 (Promega, Madison, WI, USA) at 37°C for 15 min. Unincorporated dNTPs were removed by LiCl (4M) purification. The pellet was washed in 70% ethanol, dried under vacuum and resuspended in 50 µl of 10mM TE (10 mM Tris-HCl, pH 7.5, 1 mM EDTA).

The purified AUM riboprobe was analyzed in a 1% denaturing agarose gel. The sample was prepared in 2x orange DNA loading dye, heated at 70°C for 10 min, chilled on ice and loaded on the gel along with an appropriate RNA ladder. The riboprobe was visualized under an UV illuminator and documented.

4.2.13 Northern blot

A commercial dot blot containing membrane-bound total RNA from various mouse tissues (BD Biosciences, San Jose, CA, USA) was used to analyze the AUM tissue expression pattern. The array was incubated in 10 ml of prehybridization solution containing 1.5 mg of salmon testes DNA at 65°C for 1 hr. The hybridization solution contained the denatured AUM riboprobe (10 ng/ml), 30 µg of COT DNA and 150 µg of salmon testes DNA and was

prepared in 20x SSC. The array was transferred into the hybridization solution and was incubated at 65°C overnight with gentle shaking. Afterwards, the array was washed twice in low stringency buffer (1x SSC, 0.5% SDS) and 2x each in low and high stringency buffer (0.1 x SSC, 0.5% SDS). After washing, the array was blocked in blocking buffer at RT for 1 hr. Ready to use blocking, washing and detection buffers were purchased from Roche (Cat. No. 11585762001).

Alkaline phosphatase (AP)-labeled anti-digoxigenin antibody (150 U/200µl, Roche) was prepared at a dilution of 1:10,000 in blocking buffer, and the array was incubated for 30 min at RT in the antibody solution. After washing twice in 1x washing buffer for 15 min at RT, the array was equilibrated in 1x detection buffer for 10 min at RT. Bound antibodies were detected in a chemiluminescent reaction using the CDP-star solution (Roche) for 5 min at RT. The array was then exposed to X-ray film for 20 min at RT and developed. For future use, the array was stored in 2x SSC at -20°C after stripping in 0.5% SDS for 10 min.

4.3 Cell biology methods

4.3.1 Cell lines

All cell lines used in this work (HeLa, GC1-sp, A431, and HEK293T) were purchased from ATCC (Manassas, VA, USA), cultured in Dulbecco's modified Eagle's medium (DMEM) containing 4.5 g/l glucose, supplemented with 10% FCS (PAN Biotech GmbH, Aidenbach), 2 mM L-glutamine, 100 U/ml penicillin and 100 µg/ml streptomycin at 7% CO₂ and 37°C in a standard cell culture incubator. All cell lines were grown on standard cell culture dishes (TPP, Trasadingen, Switzerland and Nunc, Roskilde, Denmark) and passaged for further cultivation every 3-4 days at a ratio of 1:5 to 1:10. To passage cells, the culture medium was removed, cells were briefly washed with calcium- and magnesium-free D-PBS (Dulbecco's phosphate buffered saline; PAN Biotech) and incubated with trypsin-EDTA (0.05% trypsin/EDTA) for 5 min at 37°C. Trypsin was neutralized by the addition of FCS-containing culture medium and detached cells were then brought into a single cell suspension by repeated pipetting. Cells were counted under the microscope Axiovert 25 (Carl Zeiss, Jena) using a Neubauer chamber. The average cell numbers per square were multiplied with 10⁴ in order to determine the number of cells per millilitre of cell suspension.

4.3.2 Transient transfection

The day preceding the transfection, cells were seeded at the appropriate density in 6-well plates or 6 cm dishes. For immunofluorescence experiments, cells were seeded at a density of 1 – 1.5 x 10⁵ cells on a round 22 mm glass coverslip. For immunoblotting assays in overexpression experiments, cells were seeded at a density of 4 – 4.5 x 10⁵ cells per well of

a 6-well plate; for RNAi experiments, $2 - 2.5 \times 10^5$ cells were seeded per well of a 6-well plate.

Next day, plasmids or siRNA oligoribonucleotides and the Lipofectamine™ 2000 reagent were mixed separately with OptiMEM in polystyrene tubes. In case of 6-well plates, 3 μ l of Lipofectamine™ 2000 reagent and 0.1 – 0.5 μ g of the respective plasmids or 12.5 to 50 nM of siRNA oligoribonucleotides were each mixed with 250 μ l of OptiMEM medium and were incubated for 5 min at room temperature. Afterwards, DNA (or siRNA) and Lipofectamine™ 2000 solutions were combined and incubated for another 20 min at room temperature to form transfection complexes. In the meanwhile, cells were washed 3 times with DMEM without any additives and the medium was then replaced with 1 ml of OptiMEM. The transfection mix (500 μ l in case of 6-well plates) was added, and the cells were incubated in a cell culture incubator for 4 hours. After that, the transfection medium was replaced with 2 ml of standard growth medium. Eighteen hours (for overexpression experiments) or 48 – 72 h (for RNAi experiments) after transfection, cells were either used for further experiments, fixed for immunofluorescence or lysed with RIPA buffer for immunoblotting (see 4.4.6).

When plates other than 6-well plates were used, the number of cells was adjusted proportionally to the effective growth area of the employed plates. The volume of transfected solutions was increased (e.g., to 1 ml for a 6 cm plate, to 2 ml for a 10 cm plate), along with proportional increase of the transfection mix.

4.3.3 Immunofluorescence

To determine the subcellular localization of endogenous or transiently (over)expressed proteins, cells were fixed for 20 min at RT in 4% paraformaldehyde, followed by permeabilization with 0.5% Triton X-100 for 10 min. The permeabilized cells were blocked for one hour in 3% BSA prepared in $\text{Ca}^{2+}/\text{Mg}^{2+}$ -free D-PBS, and were subsequently incubated for 2 h with appropriate primary antibodies (diluted 1:100-1:400 in 1% BSA prepared in $\text{Ca}^{2+}/\text{Mg}^{2+}$ -free D-PBS). The cells were washed twice in 1% BSA, and were incubated for 1 h at RT with appropriate secondary, Alexa Fluor-labeled anti-rabbit or anti-mouse IgG (1:400, prepared in 1% BSA). To stain filamentous actin, samples were incubated in Alexa Fluor-labeled phalloidin (1:400) along with the secondary antibodies. Phalloidin is a bicyclic heptapeptide isolated from the death cap (*Amanita phalloides*) that specifically binds to actin filaments. After washing the samples three times with $\text{Ca}^{2+}/\text{Mg}^{2+}$ -free D-PBS, cell nuclei were counterstained with DAPI (1 μ g/ml in D-PBS) for 5 min and the specimen were embedded in ProLong Gold Antifade reagent. When fluorescent proteins were overexpressed (e.g., AUM-YFP), the cells fixed and were embedded directly in ProLong Gold Antifade reagent. Cells were analyzed using confocal microscopy (see 4.3.4).

4.3.4 Confocal Laser-Scanning Microscopy

The subcellular localization of endogenous or exogenous proteins was examined with a confocal laser scanning microscope. Confocal microscopy allows the analysis of defined optical slices by minimizing scattered fluorescence from out-of-focus cell areas. A laser beam passes through a light source aperture which is then focused by an objective lens into a small focal volume at optimum depth of the specimen. A beam splitter which divides light into two portions separates off fluorescent wavelengths from original excitation wavelength. After passing a pinhole, the light intensity is detected by a photodetection device which converts the light signal into an electrical signal that is then recorded by a computer. The out of focus light is suppressed by a pinhole, which results in sharper images than those of conventional epifluorescence microscope. The detector aperture obstructs the light that is not coming from the focal point permits one to obtain images of planes at various depths within the sample (Taylor and Wang 1980). The live or fixed and antibody-labeled cells were analyzed under the confocal laser scanning microscope LSM 510 Meta (Carl Zeiss, Jena) or TCS SP5 (Leica, Wetzlar) with a Plan-Apochromat 40x/NA1.3 or 63x/NA1.4 objectives. The confocal aperture was set so that the optical film thickness was in between 0.5 – 1.0 μm . Focal adhesion structures in fixed cells were imaged under TIRF microscope with 100x objectives.

4.3.5 RNA interference

Gene knockdown through RNA interference (RNAi) has developed into a widely used method for gene silencing (Elbashir et al., 2001). Two types of small RNA molecules – microRNA (miRNA) and small interfering RNA (siRNA) are central to RNA interference. These small RNA molecules bind to RNA and regulate its stability. Among various post transcriptional modifications of RNA, molecules involved in RNAi shows great potential as drug targets in future medicine.

Double stranded RNA (dsRNA) is RNA with two complementary strands which form the genetic material of some viruses. DsRNA can trigger RNA interference in eukaryotes (Blevins et al., 2006). When dsRNA whose antisense strand is complementary to the transcript of a targeted gene is introduced into cells, it results in the degradation of the targeted mRNA and the consequential silencing of the target gene. Two distinct steps are involved in this process. In the first step, the enzyme Dicer recognizes and cleaves long dsRNA into siRNA molecules, which are between 21 and 23 nucleotides in length. In the second step, these oligoribonucleotides become incorporated in a multicomponent RNA-induced silencing complex (RISC), which uses these siRNAs to guide the sequence-specific cleavage of the RNA transcripts of the target gene at sites homologous to siRNA sequences (Stewart et al., 2003). As a result, the synthesis of the encoded protein is largely suppressed, without its gene being affected (Tuschl and Borkhardt 2002).

Synthetic small interfering RNA (siRNA) and retroviral short hairpin RNA (shRNA) libraries covering most of the known and predicted human and mouse genes are commercially available. To trigger RNA interference-mediated gene silencing, synthetic siRNA oligoribonucleotides can be directly introduced into cells, e.g., by transfection. Alternatively, siRNA oligoribonucleotides can be generated in cells from short hairpin RNA (shRNA). DsRNA molecules consist of a sense and an anti-sense sequence, connected by a short loop of several nucleotides. That allows complementary base-pairing and the production of a hairpin structure. ShRNA oligoribonucleotides can be introduced into cells through transfection or *via* expression vectors and are processed by cellular enzymes into active siRNA oligoribonucleotides through removal of the loop sequence (Fig. 11).

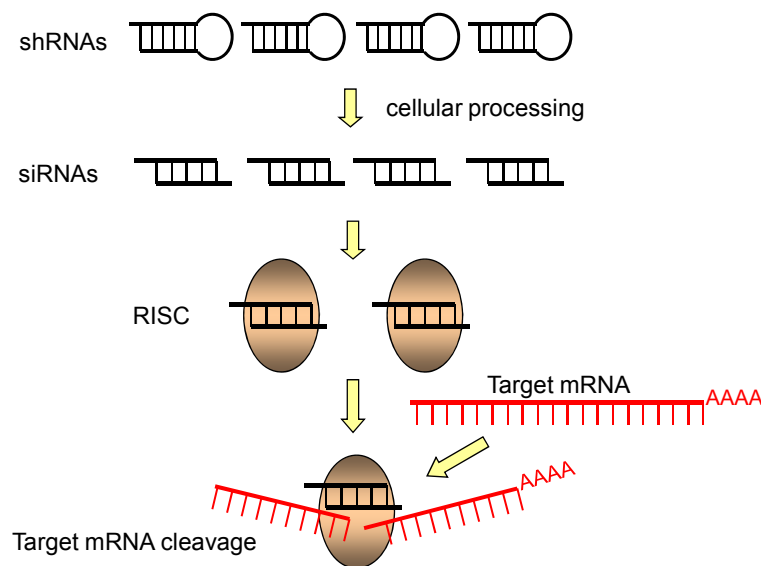


Figure 11: A model for gene inactivation *via* RNA interference.

Short hairpin (sh)RNA oligoribonucleotides are processed to 21-23-nt long short interfering (si)RNA duplexes by intracellular enzymes. The siRNA duplexes are incorporated into an siRNA containing ribonucleoprotein complex, forming the RNA-induced silencing complex (RISC). The RISC mediates sequence-specific target RNA degradation by targeting homologous mRNAs for degradation due to its endonuclease activity (modified from Tuschl and Borkhardt, 2002).

4.3.6 Lentiviral transduction of shRNA

Lentiviruses were generated by transient transfection of human embryonic kidney 293F cells (HEK293 cells constitutively expressing the simian virus 40 (SV-40) F antigen). The cells were seeded the day prior to the transfection at a density of 4.5×10^6 cells per 10 cm dish. A lentiviral shRNA expression vector containing the respective shRNAs of interest (pLKO.1-puro), a packaging vector (psPAX2) and an envelope vector (pCR-VSV-G) were simultaneously transfected (10 μ g of each plasmid). For that, DNA at a concentration of 1 μ g/ μ l was dissolved in 533 μ l ddH₂O, and 62.5 μ l of a 2.5 M calcium chloride solution was added. Building of precipitate complexes of calcium and DNA phosphate residues was induced by the addition of 625 μ l of 2x BES-buffered saline solution (50 mM BES, 280 mM

NaCl, 1.5 mM Na₂HPO₄, pH 7.02). Transfection mixtures were incubated at room temperature for 5 min and pipetted into the culture medium of 293F cells. Cells were then incubated for approximately 16 hours. Afterwards, the medium was replaced by fresh medium supplemented with 10 mM sodium butyrate for 6 hours in order to enhance lentivirus production. Sodium butyrate is known to increase protein expression from CMV promoter-driven vectors by stimulating the enhancer element of the promoter. Furthermore, sodium butyrate was shown to increase lentivirus titer even when the transfection conditions were not optimal (Kolokoltsov et al., 2005). The medium with sodium butyrate was then replaced with fresh growth medium and recombinant lentiviral particles were allowed to form during a 24 h incubation period in a cell culture incubator. Afterwards, the medium was collected with a 20 ml syringe and cellular debris was removed by filtration through sterile 0.45 µm filters. Virus-containing supernatants were directly used to transduce target cells, which had been seeded the day before transduction. The growth medium of the target cells was changed to virus-containing medium and cells were incubated in a cell culture incubator for 24 h. (pLKO.1-puro lentiviral plasmids containing AUM shRNA contain the ampicillin and puromycin antibiotic resistance genes for selection of inserts in bacterial or mammalian cells, respectively.) Afterwards, transduced cells were incubated in selection medium containing 1 µg/ml puromycin for 2 – 3 days.

Cryostocks were made from the obtained puromycin-resistant cells by trypsinizing the cells and by supplementing the cell suspensions with 10% (v/v) DMSO, followed by a slow freeze down to –80°C and subsequent storage in liquid nitrogen. To bring cells back in culture, cryostocks were rapidly thawed in a 37°C waterbath, diluted 1:10 with 37°C prewarmed medium and centrifuged for 5 min at 1000 x g. Cell pellets were then resuspended and seeded in the appropriate medium onto culture dishes.

4.3.7 Validation of the RNAi tools

Cellular AUM expression was downregulated using two different methods. First, a transient transfection of synthetic siRNA oligoribonucleotides into the host cells was used. The corresponding sequences of the employed oligoribonucleotides are presented in Table 1. Host cells were seeded at low density on the day before transfection. Next day, the cells were transfected (see 4.3.2) with four different individual siRNA oligoribonucleotides or a combination of two of them. Forty-eight – 72 h after transfection, cells were lysed in RIPA buffer and lysates were tested for AUM downregulation by immunoblotting with AUM-specific antibodies (see 3.5).

Table 1: siRNA sequences used to downregulate mAUM expression

Construct	Sense Sequence (5'- 3')	Antisense Sequence (5'- 3')
J-041844-09	UCACCAAGGCCGUGCGGUAAU	PUACCGCACGGCCUUGGUGAUU
J-041844-10	CCAAGUUGCUGCUGGCCGAUU	PUCGGCCAGCAGCAACUUGGUU
J-041844-11	AGGCGGACAUCAUCGGGAAUU	PUUCCCGAUGAUGUCCGCCUUU
J-041844-12	GCGGAGAAGCUAAGGCGCUUU	PAGCGCCUUAGCUUCUCCGCUU

The second way of AUM knock-down used in this work is the MISSION lentiviral shRNA expression system developed by the RNAi consortium (TRC). The lentiviral plasmid pLKO.1-Puro (Moffat et al., 2006) carries the puromycin-resistance gene and drives shRNA expression from a human U6 promoter. This system allows the production of lentiviral particles and the delivery of shRNA expression cassettes into the target cells by lentiviral transduction. The lentivirus used here is derived from human immunodeficiency virus (HIV). The unique infectious capacity of this retrovirus is due to the fact that it can permeate the nucleus of the target cell, and is therefore capable of delivering its genetic information even to non-dividing or primary cells. Several shRNA sequences of 21 nucleotides in length targeting mouse AUM were tested for their ability to downregulate AUM protein expression levels in GC1-spg cells, after lentiviral transduction (see 4.3.6). The shRNA sequences employed are presented in Table 2.

Table 2: Sequences of shRNA used to specifically down-regulate mAUM expression

Construct	Insert sequence (5'- 3')
TRCN0000081473	CCGGCGTGGGCACCAACATGGACAACCTCGAGTTGTCCATGTTGGTGCCACGTTTTTG
TRCN0000081474	CCGGCGGACATCATCGGGAAGCCTACTCGAGTAGGCTTCCCGATGATGTCCGTTTTTG
TRCN0000081475	CCGGCCACACTTCAGCTACATGAACTCGAGTTCATGTAGCTGAAGTGTGGGTTTTTG
TRCN0000081476	CCGGACGCTGCTGTTCCGACTGCGATCTCGAGATCGCAGTCGAACAGCAGCGTTTTTG
TRCN0000081477	CCGGCTGTAGCCTGAAGACTATCCTCTCGAGAGGATAGTCTTCAGGCTACAGTTTTTG

As a control, the MISSION non-targeting shRNA control SHC002 was used, which contains a shRNA insert that does not target any known human or mouse genes, due to a minimum of four base pair mismatches to any known human or mouse gene. Following diagram gives an overview of the si/shRNA sequences enlisted above in ORF of mAUM.

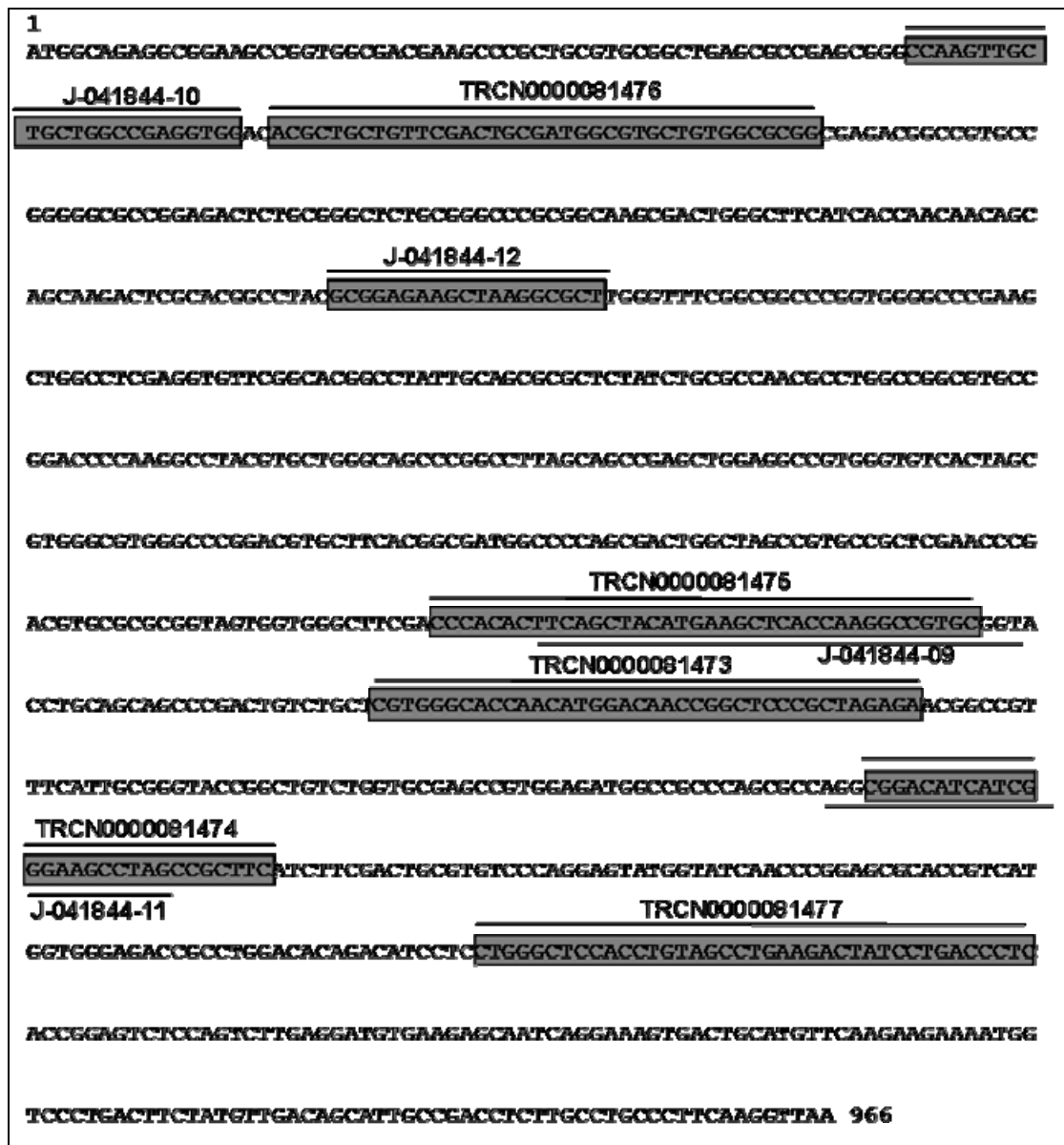


Figure 12: Localization of the mAUM siRNA/shRNA in open reading frame of mouse AUM. Refer to tables 1 and 2 for the designations used in the figure

4.4 Protein biochemical methods

4.4.1 Bacterial expression and purification of recombinant AUM

Recombinant AUM was expressed in competent bacterial system BL21 (DE3) pLysS from Invitrogen (Carlsbad, CA, USA) as described. Proteins were expressed for 4 hrs at 37°C upon induction with 1 mM isopropyl β-D-thiogalactopyranoside (IPTG), and purified under native conditions by standard affinity chromatography on a Talon matrix (Clontech). Purified AUM was stored at 4°C in 40 mM triethanolamine, 5 mM MgCl₂, 150 mM NaCl, 0.002% Triton X-100, 50% glycerol; pH 7.4.

The purity of the eluted protein was evaluated by 12% SDS-PAGE using Coomassie blue staining. Calf intestine Enterokinase (EK) from Roche (Nutley, NJ, USA) was used to

cleave fusion protein. EK was dissolved in millipore water to a final concentration of 1 µg/µl. His₆-tagged protein was digested for 48 hrs at room temperature on a shaker. 30 µg of EK was used to digest 200 µg of purified protein as recommended by the manufacturer. Extent of cleavage was checked on 12% SDS-PAGE and protein was stored at 4°C.

Further purification was facilitated by the anion exchanger column (Resource Q) on an Äkta purifier (Amersham Pharmacia Biotech AB, Uppsala, Sweden). A gradient of 0-500 mM NaCl was used for elution of proteins in fractions of 300 µl. Appropriate fractions were pooled and checked for the extent of purification on 12% SDS-PAGE.

4.4.2 Design of AUM peptide antibody

An AUM-specific peptide antibody was designed by comparing the amino acid sequences of human and mouse CIN and AUM (see Fig. 13). The highlighted amino acid sequence in AUM was selected for peptide generation, because a corresponding region in CIN (boxed region in Fig. 13) was already known to yield a CIN-specific antibody that does not crossreact with AUM. The AUM peptide was synthesized by Squarix biotechnology (Marl, Germany) and two female New Zealand White (NZW) rabbits were immunized with this peptide by Charles River Laboratories (Kisslegg, Germany). Crude sera were purified by Squarix biotechnology using (NH₄)₂SO₄-precipitation and affinity chromatography on immobilized AUM peptide, followed by gelfiltration on a Superdex 200, HR 10/30 column. The specificity and sensitivity of the antibody was analyzed using Western blotting of purified, recombinant as well as of endogenously expressed CIN and AUM (see Figs. 24, 25, 31, 32).

```

CLUSTAL W (1.83) multiple sequence alignment

mCIN      -----MARCERLRGAALRDVLGQAQGVLFDCDGVWNGERIVPGAP 41
hCIN      -----MARCERLRGAALRDVLGRAQGVLFDCDGVWNGERAVPGAP 41
mAUM      MAEAEAGGDEARCVRLSAERAKLLLAEVDTLLFDCDGVWLRGETAVPGAP 50
hAUM      MAAAEAGGDDARCVRLSAERAQALLADVDTLLFDCDGVWLRGETAVPGAP 50
              *** ** . : :* . .: :*****.* ** *****

mCIN      ELLQLRARAGKNTL FVSNNSRRARPELALRFARLGFAGLR----AEQLFS 87
hCIN      ELLERLARAGKAAL FVSNNSRRARPELALRFARLGFAGLR----AEQLFS 87
mAUM      ETLRALRARGKRLGFITNNSKTRTAYAEKLRRLGFGGPGVPEAGLEVF 100
hAUM      EALRALRARGKRLGFITNNSKTRAAAYAEKLRRLGFGGPAGPGASLEVF 100
              * * . * ** *::*** :*: * :: *****.* . :*:

mCIN      SALCAARLLRQRLSGPPDASGAVFVLGGEGLR AELRAAGLR-LAGDP--- 133
hCIN      SALCAARLLRQRLPGPPDAPGAVFVLGGEGLR AELRAAGLR-LAGDPSAG 136
mAUM      TAYCSALYLRQRLAGVPDPK--AYVLGSPALAAELEAVGVTSVGVGPDVL 148
hAUM      TAYCTALYLRQRLAGAPAPK--AYVLGSPALAAELEAVGVASVGVGPEPL 148
              :* *:* *****.* * . :****. .* ****.**: :. .*

mCIN      -GEDPR-----VRAVLVGYDEQFSFSRLTEACAHLRDPD CLLVAT 172
hCIN      DGAAPR-----VRAVLVGYDEHFSFAKLREACAHLRDPD CLLVAT 176
mAUM      HGDGSPDWLAVPLEPDVRAVVVGFDPHFSYMKLTKAVRYLQQPD CLLVGT 198
hAUM      QGEGPGDWLHAPLEPDVRAVVVGFDPHFSYMKLTKALRYLQQPG CLLVGT 198
              * * *****:*:* :* :* :*: * **.*

mCIN      DRDPWHPLSDGSRTPGTGSSLAAAVETASGRQALVVGKPSPYMFQCITEDF 222
hCIN      DRDPWHPLSDGSRTPGTGSSLAAAVETASGRQALVVGKPSPYMFECITENF 226
mAUM      NMDNRLPLENRFIAGTGC LVRVEMAAQRQADIIGKPSRFIFDCVSQEY 248
hAUM      NMDNRLPLENRFIAGTGC LVRVEMAAQRQADIIGKPSRFIFDCVSQEY 248
              : * **.*: * .***.* ** * : * * :***** :*:*:*:

mCIN      SVDPARTLMVGDRLDITDILFGHRCGMTTVLTLTGVS SLEEAQAYLTAG-- 270
hCIN      SIDPARTLMVGDRLDITDILFGHRCGMTTVLTLTGVS RLEEAQAYLAAG-- 274
mAUM      GINPERTVMVGDRLDITDILLGSTCSLKTILTLTGVS SLEDVKSNQESDCM 298
hAUM      GINPERTVMVGDRLDITDILLGATCGLKTILTLTGVS TLGDVKNNQESDCV 298
              .:* *::*****:*****.* *.:*:***** * :.: .

mCIN      -QRDLVPHYYVESIADLMEGLE 292
hCIN      -QHDLVPHYYVESIADLTEGLE 296
mAUM      FKKKMVPDFYVDSIADLLPALQG 321
hAUM      SKKKMVPDFYVDSIADLLPALQG 321
              :.:*:*:*****.*:*.

```

Figure 13: Amino acid sequence alignment of CIN and AUM and sequence used for the generation of an AUM-specific peptide antibody.

This alignment was performed using the 'multiple sequence alignment' tool of the program ClustalW (Version 1.83) program. The highlighted amino acid sequence was selected for antibody generation. Numbers given on the right refer to amino acid positions. (*) means that the residues or nucleotides in that column are identical in all sequences in the alignment, (:) indicates conserved substitutions, (.) indicates semi-conserved substitutions.

4.4.3 Sample preparation for immunoblot analysis

Preparation of cell lysates

GC-1 spg cells or HeLa cells were washed with $\text{Ca}^{2+}/\text{Mg}^{2+}$ -free D-PBS, and then lysed in ice-cold lysis buffer (50 mM Tris-HCl, pH 7.2; 150 mM NaCl; 0.1% SDS; 1% NP -40; 1% sodium deoxycholate; 1 $\mu\text{g}/\text{ml}$ pepstatin; 1 $\mu\text{g}/\text{ml}$ leupeptin; 10 $\mu\text{g}/\text{ml}$ aprotinin; 1 mM PMSF and 1x phosphatase inhibitor cocktails I and II). The cells were scraped from the plate on ice and were homogenized by repeatedly drawing into a syringe with a 20 gauge needle. Insoluble cell components were removed by centrifugation at 15,000 rpm for 10 min at 4°C and the lysate was stored in aliquots at -20°C .

Preparation of mouse tissue lysates

An adult wild type male mouse (C57BL/6) was sacrificed by cervical dislocation and then dissected to obtain various tissues. The tissues were immediately snap-frozen in liquid nitrogen and stored at -80°C until use. Tissue samples were pulverized in liquid nitrogen by grinding with a pestle in a mortar, and were then transferred to pre-cooled Eppendorf tubes on ice. Tissue lysates were prepared by homogenizing 100 mg of tissue in 1ml of lysis buffer [50 mM Tris-HCl, pH 7.2; 150 mM NaCl; 0.1% SDS; 1% Triton X-100; 1 mM EDTA; 0.5 mM sodium orthovanadate; 1 mM sodium fluoride; 1% sodium deoxycholate with freshly added protease inhibitors: 10 $\mu\text{g}/\text{ml}$ aprotinin; 10 $\mu\text{g}/\text{ml}$ leupeptin; 1mM pepstatin; 1 mM PMSF and phosphatase inhibitor cocktail I (1:1000) and II (1:1000)]. The samples were further homogenized by repeatedly drawing them into a syringe through a 20 gauge needle. Subsequently, particulate matter was removed by centrifugation at 15,000 rpm for 10 min at 4°C, and the lysates were stored in aliquots at -20°C .

4.4.4 Mouse sperm preparation and analysis

Preparation of sperm suspension

An adult wild type male mouse (C57BL/6) was sacrificed by cervical dislocation and then dissected to obtain mature spermatozoa from different parts of the sperm carrying duct, the epididymis. Caput and cauda epididymis were cut by clearing adjoining fatty tissue and were immediately put in to a drop of sperm preparation medium (Medicult, Jylling, Denmark) and were incubated at 37°C for 15 min. Motile spermatozoa from caput and cauda epididymis were collected by the swim-up method (Yamashita et al., 2007) and subsequent centrifugation at 1000 rpm for 10 min. Live sperms were counted under the microscope and were adjusted to $1 \times 10^6/\text{ml}$ in sperm preparation medium.

Sperm capacitation and permeabilization

Mature cauda sperms were capacitated in 2x TYH medium (119 mM NaCl, 4.8 mM KCl, 1.7 mM CaCl₂, 1.2 mM KH₂PO₄, 1 mM MgSO₄, 25 mM NaHCO₃, 5.6 mM glucose, 0.5 mM sodium pyruvate, 4 mg/ml BSA) by incubating at 37°C for 30 min. Capacitated sperms were washed in 1X PBS and treated with 10 U of streptolysin O (SLO) prepared in TYH at 37°C for 30 min for permeabilization (Yamashita et al., 2007).

Sperm fixation

Sterile coverslips were coated with BD cell Tak (BD biosciences) as per the manufacturer's instructions. Briefly, a drop of cell Tak was put on sterile coverslip and spread evenly by putting another coverslip on it at RT. After 20 min, the coverslip was washed with distilled water and allowed to air dry. The sperm suspension was spread evenly on the coated coverslip and was allowed to air dry for 1 hr at RT. Coverslip was washed with 1x PBS and sperms were fixed in 70% methanol at -20°C for 5 min. After blocking in 10% BSA, sperms were stained for microscopic analysis (see 4.3.3).

Sperm lysis

Sperm suspensions were prepared in sperm preparation medium that was treated either with pervanadate (for overlay assay), SLO (for permeabilization) or progesterone (for acrosome reaction) before lysing in 2x lysis buffer containing 20 mM Tris-HCl, pH 7.4; 150 mM NaCl; 1% NP40; 1 mM sodium orthovanadate; 10 µg/ml aprotinin; 10 µg/ml leupeptin; 1 mM pepstatin; 1 mM PMSF) and phosphatase inhibitor cocktails I & II (1:1000 dilutions, Sigma-Aldrich). Subsequently, the particulate matter was removed by centrifugation at 15,000 rpm for 10 min at 4°C and the lysates were stored in aliquots at -20°C.

4.4.5 Estimation of protein concentration

The protein concentration of cell or tissue lysates was determined using the Micro BCA Protein Assay Kit. This assay allows the colorimetric detection and quantification of the total protein content. The assay is based on the reduction of Cu²⁺ to Cu¹⁺ by the proteins contained in the reaction under alkaline conditions (the Biuret reaction) and the colorimetric detection of the generated Cu¹⁺ by a reagent containing bicinchoninic acid, BCA (Smith et al., 1985). Chelation of two molecules of BCA with one cuprous cation (Cu¹⁺) leads to the formation of a water-soluble, purple-colored product with maximal absorbance at 562 nm.

To measure the protein concentration, the BCA solution was prepared by mixing together components of the Micro BCA Protein Assay Kit according to manufacturer's instructions. Cell or tissue lysate (5 µl) was diluted in a microtitre plate with water to make a volume of 150 µl of protein solution. Then, 150 µl of BCA solution was added to each probe, and samples were incubated for 2 hours at 37°C. A BSA standard curve ranging from 2 to 10

μg of BSA per well was supplemented with 5 μl of lysis buffer to take into account the absorbance of compounds of the lysis buffer. The extinction of the samples was determined at 560 nm in a FLUOstar OPTIMA microplate reader.

4.4.6 SDS-Polyacrylamide Gel Electrophoresis

SDS-PAGE is a commonly used method for separating proteins according to their molecular masses using polyacrylamide gels as a support medium (see Table 3) and sodium dodecyl sulfate (SDS) for protein denaturation and charge (Laemmli 1970). The technique of SDS-PAGE followed by immunoblotting (see 4.4.5) is a commonly used method for protein expression and phosphorylation analysis.

Protein samples were adjusted to equal protein concentrations, mixed with Laemmli buffer, denatured at 95°C for 5 min and loaded onto SDS-PAGE gels. The electrophoresis was carried out in running buffer at a constant current (25 – 30 mA). Proteins were first run in the stacking gel [4.5 % (v/v) acrylamide solution] to concentrate them, and then they were separated in the running gel [12% (v/v) acrylamide solution]. To separate low molecular weight proteins, running gels with 8% (v/v) acrylamide solution were used. SDS-PAGE was performed on the Bio-Rad mini gel apparatus (Bio-Rad, Munich).

Table 3: Polyacrylamide gel recipe

	Stacking gel	Running gel
30% Acrylamid/Bisacrylamid (37,5:1)	4,5%	8 or 12%
SDS	0,1%	0,1%
APS	0,1%	0,1%
TEMED	0,1%	0,1%
Tris-HCl	125 mM, pH 6.8	375 mM, pH 8.8

4.4.7 Detection of proteins in SDS-polyacrylamide gels

The proteins in SDS-polyacrylamide gels were stained with Coomassie dye (2.5 g/l Coomassie Serva Blue R in 10% acetic acid and 45% methanol) at room temperature directly after electrophoresis for a minimum of one hour or overnight. For destaining, the gels were incubated in the destainer (10% acetic acid and 20% methanol in H₂O) with gentle shaking until the background was clear. The gel was stored in 0.1% sodium azide or was vacuum-dried. The stained gels were scanned (HP Scanjet 8300, Hewlett-Packard, CA, USA) for documentation or further analysis.

4.4.8 Immunoblot analysis

Immunoblotting is an analytical technique commonly used for semiquantitative detection of specific proteins in a given sample of cell or tissue homogenates or lysates. A standard method for the quantitative transfer of proteins from polyacrylamide gels to nitrocellulose membranes, first described in 1979 (Towbin et al., 1979), was used. Briefly, proteins are electrophoretically transferred on membranes, and target proteins are specifically detected using primary antibodies. Bound primary antibodies can then be detected by using secondary antibodies coupled with horseradish peroxidase (HRP).

Proteins were transferred from the SDS-PAGE gels onto nitrocellulose membranes using a TRANSBLOT semidry blotting apparatus (Bio-Rad, Munich). After equilibration of the SDS-PAGE gel in cathode buffer for 5 min, the blotting sandwich was assembled. For that, two lower sheets of Whatman paper were equilibrated in anode buffer I, one sheet of Whatman paper together with the nitrocellulose membrane in anode buffer II and three other sheets of Whatman paper in cathode buffer. Proteins were transferred electrophoretically at constant current (70 mA for 1 mini-gel) for variable times depending on the molecular mass of the proteins of interest. A prestained protein marker was used as a molecular weight marker and to monitor electrophoretic transfer. Western blot membranes were stained for equal protein loading with Ponceau S (0.2% in 5% acetic acid) and were copied for documentation. Afterwards, membranes were blocked in blocking buffer for 30 min at room temperature under constant agitation. Primary antibodies (see 3.5) were applied at dilutions of 1:500-1:1,000 (or 1:10,000 for α -tubulin and β -actin) in antibody diluent, and membranes were incubated overnight at 4°C under constant agitation in primary antibody solution. Afterwards, membranes were washed (3 x 5 min) with TBS-T or rinsing in water and probed for 1 – 2 h with horseradish peroxidase (HRP)-labeled secondary antibodies, diluted 1:10,000 in blocking buffer. After washing (3 x 5 min) with TBS-T or rinsing in water, Western blot membranes were treated with the enhanced chemiluminescent (ECL) Western Blotting Detection System and exposed to X-ray films.

Reprobing of nitrocellulose membranes

In some cases, the same membranes were probed for several different antigens. For this purpose, nitrocellulose membranes were placed in stripping buffer and incubated at 55°C for 30 min under constant agitation to remove primary and secondary antibodies. After that, membranes were washed three times in a large excess of TBS-T, blocked again with blocking buffer for 30 min at room temperature under constant agitation and then reprobed with other primary antibodies to detect the other antigen.

Densitometric analysis of immunoblot bands

For semiquantitative Western blot analysis, Western blot signals from the membranes were directly detected on the DIANA III Camera System, or exposed films were scanned and obtained images were densitometrically evaluated using the ImageJ software (version 1.41, National Institutes of Health, MD, USA. <http://rsbweb.nih.gov/ij/>). Alternatively, digital images of membranes were taken on Alpha Innotech (San Leandro, CA, USA) for quantification of the signal.

4.4.9 Immunoprecipitation

Immunoprecipitation is the antibody-mediated isolation of overexpressed or endogenously expressed proteins from cell or tissue lysates for downstream applications.

AUM overexpressing or stably AUM depleted GC1 cells were washed with $\text{Ca}^{2+}/\text{Mg}^{2+}$ -free D-PBS, and then lysed in ice-cold lysis buffer (see 3.12) supplemented with freshly added protease inhibitors [10 $\mu\text{g}/\text{ml}$ aprotinin; 10 $\mu\text{g}/\text{ml}$ leupeptin; 1 mM pepstatin; 1 mM PMSF) and a 1:1,000 dilution of the phosphatase inhibitor cocktails I & II (Sigma)]. The cells were scraped from the plate on ice and homogenized by repeatedly drawing into a syringe through a 20 gauge needle. Insoluble cell components were removed by centrifugation at 15,000 rpm for 10 min at 4°C and the lysate was stored in aliquots at -20°C. Total protein content of the cell lysate was estimated (see 4.4.3) and lysate containing 250 μg –1 mg of protein was incubated with 2-4 μg (or as recommended by manufacturer) of the immunoprecipitating antibody for 2 hrs at 4°C.

Protein A/G sepharose beads (GE Healthcare, Munich) were equilibrated in lysis buffer and blocked in 5% BSA prepared in lysis buffer for 2 hrs at 4°C. After 2 hrs of incubation with antibody, the complex was incubated in the presence of beads (30 μl of beads for 1 mg of total protein) for another 2 hrs at 4°C with rotation. After washing beads thrice in lysis buffer at 4°C, protein complexes were either released by 5 min of boiling in SDS-PAGE sample buffer or the immunoprecipitates were used in *in vitro* activity assays. The efficiency of immunoprecipitation was assessed by immunoblotting (see 4.4.6) with appropriate controls. It is necessary to examine the nonspecific binding of protein of interest to beads instead of immunoprecipitate complex in an individual experiment. Also, the efficiency of immunoprecipitation was assessed by running an aliquot of the total lysate along with the beads on SDS-PAGE gels followed by immunoblotting.

4.4.10 Immunohistochemistry

Immunohistochemistry refers to the process of localizing proteins in tissue sections exploiting the principle of antibody specificity in biological samples. The principle is that a specific primary antibody is employed to detect an antigen. A biotinylated secondary antibody is then used to detect the bound primary antibody. A horseradish peroxidase (HRP)-coupled

avidin/biotin-complex (ABC) is formed upon addition of HRP-labeled avidin, which can be detected with a HRP substrate, for example 3, 3'-diaminobenzidine tetrahydrochloride (DAB). To perform immunohistochemical analysis, 14 μm sections were cut from paraffin-embedded mouse testis tissue or embryos on a cryostat and mounted on poly-L-lysine coated glass slides. To block the effect of endogenous peroxidase, sections were incubated for 20 min at RT with H_2O_2 (0.3% in TBS). To prevent unspecific binding of the primary antibodies, sections were incubated in the blocking buffer for 30 min at RT. Sections were incubated with the primary antibodies in a humidified chamber at 4°C for 48 hrs. All further steps were done at RT. Sections were washed 3 x 5 min with TBS to remove unbound primary antibodies and then, sections were incubated for 1 h with secondary biotinylated antibodies. Sections were washed 3 x 5 min with TBS to remove unbound secondary antibodies and incubated for 1 h with freshly prepared ABC mix. After 3 x 5 min washing with TBS, sections were placed for 3 – 15 min in DAB-solution and the reaction was stopped in water. After that, sections were washed again in TBS and dehydrated (2 x 70% EtOH for 2 min, 80% EtOH – 2 min, 90% EtOH – 2 min, 100% EtOH – 2 min, Xylene – 2 min, Xylene – 15 min). Dehydrated sections were mounted with Entellan and stored at RT.

4.4.11 Enzymatic activity assays

The phosphatase activity of CIN and AUM towards the broad-spectrum substrate, *para*-nitro phenylphosphate (*p*-NPP, Calbiochem) was measured spectrophotometrically in a 96-well microtitre plate according to the manufacturer's instructions. Briefly, 1 μg of AUM and 2 μl of substrate (final concentration, 3.5 mM) were incubated in a total reaction volume of 100 μl prepared in assay buffer (40 mM TEA, 30 mM NaCl, 0.1% Triton X-100). The release of inorganic phosphate converts the colorless *p*-NPP into the yellow colored *para*-nitrophenyl, which can be measured spectrophotometrically at 405 nm. Thus, the absorbance at 405 nm is proportional to the phosphate release due to phosphatase activity in the reaction. The kinetics of the reaction were followed for 30 min at 405 nm.

Pyridoxal 5'-phosphate (PLP) was used as a CIN substrate (Gao and Fonda 1994; Jang et al., 2003). To detect free inorganic phosphate (P_i) generated in the reaction of PLP dephosphorylation driven by CIN, we employed the PiPer Phosphatase Assay Kit (Invitrogen) according to the manufacturer's instructions. Briefly, the detection of P_i in this assay is based on a cascade of coupled enzymatic reactions. In the presence of P_i , maltose phosphorylase converts maltose to glucose 1-phosphate and glucose. Afterwards, glucose oxidase converts the glucose to gluconolactone and hydrogen peroxide. Finally, received H_2O_2 reacts with the Amplex Red reagent to generate the highly fluorescent product, resorufin. Horseradish peroxidase catalyzes the last reaction. Thus, the resulting increase in fluorescence is proportional to the amount of P_i in the reaction mix.

Michaelis–Menten–Henri kinetics

Enzymatic parameters (K_m & V_{max}) of AUM were calculated by fitting data obtained with various *p*-NPP concentrations into the Michaelis-Menten equation where the rate is plotted as a function of the concentration of substrate:

$$v = \frac{V_{max} \cdot [S]}{K_m + [S]}$$

(*v* is reaction rate, *S* is substrate concentration, *K_m* is Michaelis constant and *V_{max}* is maximum reaction rate).

4.4.12 High throughput phosphopeptide screen

To investigate the peptide substrate preferences of AUM, we performed a high throughput peptide screen at the Max Planck Institute for Physiological Chemistry in Dortmund in the group of Prof. Herbert Waldmann. Phosphatase substrate sets encompassing peptides from 720 human proteins phosphorylated on serine (174), threonine (58) or tyrosine (488) were purchased from JPT Peptide Technologies, Berlin. These peptides were supplied lyophilized in 384-well microtitre plates, each containing 360 phosphopeptides (250 pmol/well) together with 10 calibration standards. To determine the appropriate concentration of recombinant AUM protein under the conditions of this screen, AUM activity was first assayed against *p*-NPP (10 nM): 0.2 mg/ml (5.8 μM) of AUM was diluted 1:60 in assay buffer (40 mM TEA, 30 mM NaCl, 0.1% Triton X-100), and 25 μl of the diluted protein were pipetted in each well of a 384-well microtitre plate with the help of a robotic system. The plate was incubated for 45 min at 37°C with shaking and the reaction was stopped by adding 25 μl malachite green solution. Free phosphate released in solution was detected by malachite green. After allowing color development for 10 min at RT, absorbance was measured at 620 nm and raw data was analyzed. Hits up to 66% of highest optical density (OD) were considered specific.

4.4.13 *In vitro* protein phosphatase activity assays

In vitro phosphatase assay

Immunoprecipitated or recombinant proteins were phosphorylated *in vitro* with either [γ -³²P] ATP (1000 Ci/mmol; for autoradiography) or with unlabeled ATP (for immunoblotting with phosphospecific antibodies) in kinase assay buffer (50 mM HEPES, pH 7.6; 10 mM MgCl₂; 2 mM MnCl₂; 2 mM DTT) at 30°C for 30 min. To remove the unincorporated ATP, the phosphorylated proteins were afterwards either dialyzed against phosphatase assay buffer (50 mM HEPES, pH 7.6; 5 mM MgCl₂; 1 mM DTT) or they were centrifuged in 10 kDa MWCO Centricon tubes (Millipore). For this, the protein was washed 3x in 500 μl of phosphatase assay buffer and finally collected in a volume of 50 μl in the Centricon tubes.

For *in vitro* phosphatase assays, the phosphorylated protein was then incubated with 1 µg of recombinant AUM (active or catalytically dead) at 30°C for 30 min in phosphatase assay buffer (50 mM HEPES, pH 7.6; 5 mM MgCl₂; 1 mM DTT). The phosphatase reaction was stopped by adding sample buffer; samples were boiled for 5 min at 95°C and loaded onto SDS-PAGE gels. Proteins were either stained with Coomassie and the dried gel was exposed to X-ray films, or the proteins were blotted onto nitrocellulose membrane and the dephosphorylation pattern was analyzed by phosphospecific antibodies.

In vitro kinase activity assay

Src kinase activity towards commercial biotinylated peptide (cell signaling Technologies, Danvor) was measured according to manufacturer's instructions. Briefly, 50 ng of recombinant GST-Src was incubated with 1.5 µM substrate peptide in kinase buffer (60 mM HEPES pH 7.5, 5 mM MgCl₂, 5 mM MnCl₂, 3 µM Na₃VO₄, 1.25 mM DTT, 20 µM ATP) for 40 min at RT. After terminating reaction by adding 50 mM EDTA, pH 8.0, reaction mix was transferred to streptavidin coated plate and binding of biotinylated peptide to streptavidin was continued for 60 min at RT. Streptavidin plate was washed extensively with PBS/T (1x PBS, 0.05% Tween-20) and then incubated with primary antibody (1:1000, pTyr-100 prepared in PBS/T with 1% BSA) for 60 min at RT. After incubation with appropriate HRP-linked secondary antibody for 30 min, phosphorylation of biotinylated peptide was measured by colorimetric determination as readout of kinase activity.

4.4.14 Cell biological assays

Phosphatase overlay assays

To determine the effect of the purified AUM phosphatase on the pool of denatured cellular tyrosine phosphorylated proteins, cells were treated with pervanadate. Pervanadate is plasma membrane permeable, and nonspecifically blocks cellular phosphatases due to its structural similarity with phosphate (Gordon 1991). This treatment serves to increase the pool of tyrosine phosphorylated proteins in cells, which is typically very small as compared to serine or threonine phosphorylated proteins (Alonso et al., 2004).

Pervanadate was prepared by mixing equal volumes of 100 mM hydrogen peroxide and 100 mM sodium orthovanadate (pH 10). Cells were treated with 100 µM freshly prepared pervanadate solution for 15 min at 37°C (Selengut 2001). After pervanadate treatment, cells were washed with Ca²⁺/Mg²⁺-free D-PBS, and then lysed in ice-cold lysis buffer (see 3.12) containing freshly added protease inhibitors (10 µg/ml aprotinin, 10 µg/ml leupeptin, 1 mM pepstatin, 1 mM PMSF) and phosphatase inhibitor cocktails I & II (1:1000; Sigma). The cells were scraped from the plate on ice and homogenized by repeatedly drawing into a syringe with a 20 gauge needle. Insoluble cell components were removed by centrifugation at 15,000 rpm for 10 min at 4°C and the lysate was stored in aliquots at -20°C. The total protein content of the cell lysate was estimated using the BCA assay (4.4.5).

The pervanadate-treated cell lysates were separated by SDS-PAGE and transferred onto nitrocellulose membranes by electroblotting. Sample was loaded in one coherent well produced by taping the comb. This procedure ensures a homogenous protein distribution on the gel. Different concentrations of recombinant, purified AUM^{wt} or AUM^{D34N} protein were prepared in phosphatase assay buffer (40 mM TEA, 30 mM NaCl, 0.1% Triton X-100) supplemented with 0.5% non-fat milk powder and 2 mM MgCl₂. The nitrocellulose membrane was cut into vertical strips, the strips were placed in sterile polystyrene tubes, containing either buffer alone as a control, or the respective concentrations of AUM^{wt} or AUM^{D34N} protein. For the phosphatase overlay reaction, the tubes were incubated for 1 hr at 37°C with gentle rotation in incubator. The tyrosine phosphorylation pattern was then analyzed by using the phosphotyrosine-specific antibodies 4G10 or pTyr100 (see 4.4.8).

Analysis of actin cytoskeletal dynamics

Cellular actin exists in a tightly regulated equilibrium between monomeric, globular (G)-actin and polymeric, filamentous (F)-actin pools. This tight regulation poses an experimental hurdle when the effect of a protein on the actin cytoskeleton needs to be visualized. Latrunculin A is a toxin produced by various species of sponge (*e.g.*, *Negombata magnifica*) that binds to and sequesters G-actin. Therefore, *de novo* actin polymerization is inhibited by blocking the incorporation of free actin monomers in actin filaments (Pardo and Nurse 2005). As a result, the use of latrunculin A can uncover direct or indirect effects of a protein on actin dynamics.

Cell overexpressing AUM^{wt} or AUM^{D34N} (see section 4.3.2 or cells stably depleted of endogenous AUM (see section 4.3.6) were treated with 20 nM – 2 μM latrunculin A (Hotulainen et al., 2005) prepared in dilution buffer (5 mM Tris, pH 7.8; 2 mM MgCl₂; 0.1 mM CaCl₂; 0.2 mM ATP; 0.2 mM DTT; 0.05% sodium azide) for different time points. The treatment was terminated by fixing the cells in 4% PFA (see 4.3.3). As the latrunculin A stock solution was prepared in DMSO, control cells were treated with the corresponding concentrations of DMSO as a vehicle control. F-actin was stained as described under section 4.3.3, and the cytoskeleton was analyzed by confocal microscopy (section 4.3.4).

Fibronectin stimulation of cells

Cell adhesion to extracellular matrix (ECM) proteins such as fibronectin, collagen, or laminin triggers signaling cascades involving rapid tyrosine phosphorylation and dephosphorylation events (Sieg et al., 1998). To initiate fibronectin mediated signaling cascades, cells were starved overnight in DMEM containing 0.5% FBS. Serum starved cells were harvested by limited trypsinization (0.05% trypsin/EDTA) for 5 min at 37°C. Trypsin was inactivated by soybean trypsin inhibitor (0.5 mg/ml in DMEM containing 0.25% BSA). The cell suspension was centrifuged at 1,000 rpm for 5 min, and the pellet was resuspended in DMEM containing

0.1% BSA. To avoid sedimentation of cells in tube and to keep them in suspension until spreading on fibronectin coated surface, cell suspension was incubated on rotor at 37°C for 1 hr with gentle rotation.

In parallel, cell culture dishes or 22 mm coverslips were coated with 10 µg/ml of fibronectin (diluted freshly in Ca²⁺/Mg²⁺-free D-PBS) for 1 hr at RT. Excess fibronectin solution was aspirated, and fibronectin-coated dishes/coverslips were dried at 37°C for 1 hr before use. Equal numbers of cells (see 4.3.1) were spread on fibronectin-coated surfaces for different time points. Cells were then either lysed in lysis buffer (see 3.12) containing freshly added protease inhibitors (10 µg/ml aprotinin, 10 µg/ml leupeptin, 1 mM pepstatin, 1 mM PMSF) and phosphatase inhibitor cocktails I & II (1:1000 dilution) for immunoblotting (4.4.8), or fixed and processed for microscopic analysis (see 4.3.3).

EGF stimulation of cells

Epidermal growth factor receptor (EGFR) is a receptor tyrosine kinase which upon stimulation with epidermal growth factor (EGF) initiates signaling cascades and thereby modulates the response of a cell towards its environment (Biscardi et al., 2000). EGFR itself and many of its downstream effector proteins are tyrosine phosphorylated and hence after pervanadate stimulation (see previous paragraph) we used EGF to understand effect of AUM on cells in culture.

To initiate the EGFR signaling cascade, cells were starved in DMEM containing 0.5% FBS either overnight or for a minimum of 6 hrs at 37°C. Upon overnight starvation in DMEM, cells were stimulated with 100 ng/ml (85 nM) EGF for various time points ranging from 1 min to 20 min at 37°C and then washed with ice cold D-PBS containing Ca²⁺/Mg²⁺ on ice. Cells were then lysed in ice cold RIPA buffer (see 3.12) containing freshly added protease inhibitors (10 µg/ml aprotinin, 10 µg/ml leupeptin, 1 mM pepstatin, 1 mM PMSF) and phosphatase inhibitor cocktails I & II (1:1000 dilution). Cells were lysed for 20 min on a rotor at 4°C, and were then centrifuged at maximum speed in a table top centrifuge at 4°C. The supernatants were collected in fresh precooled tubes, and were stored at -20°C.

4.4.15 Cell area determination of fixed cells

For an unbiased and quantitative determination of the cell area of cultured cells, we employed software called Metamorph (version 7.1.3.0) from MDS analytical technologies, Downingtown, PA, USA. To start with, 20,000 cells with stable knock down of AUM were seeded on fibronectin-coated (see 4.4.11) 96-well microtitre plate (15 µ-plate, ibidi, Martinsried) for 10, 20 or 40 min at 37°C and then stain for F-actin with phalloidin (1:400) and nuclei with DAPI (1 µg/ml in D-PBS) after PFA fixation (see 4.3.3). Cells were scored under an epifluorescence microscope with a 10x objective and analyzed with Metamorph. Briefly, the software takes four random pictures per well for nuclei and F-actin. By overlaying

the nuclei and the cell area (stained for F-actin), a single image was created which was then used for segmentation. During segmentation, software recognizes individual cells by nuclei as the center and F-actin as the periphery, and calculates the cell area in arbitrary units from measuring the circumference of all cells in the image. The final value that can be obtained is the average cell area of all cells in a given image.

For validation, the overlay and segmentation files were correlated to ensure correct software operations, especially the correct segmentation of two adjacent cells. The average area of a high number of measured cells gives an unbiased quantitation of a heterogeneous population of cells with different knock down levels of AUM. The cell area of at least 1000 cells per condition was measured in two independent experiments, and the effect of AUM knock down on cell area was plotted as fold increase with respect to control shRNA transduced cells.

5 Results

5.1 Phylogenetic analysis of AUM orthologs and of its evolutionary relationship with CIN

Database searches have predicted the existence of 58 human HAD enzymes (including phosphatases, ATPases, phosphonates, dehalogenases, sugar phosphomutases) with largely unknown functions (Allen and Dunaway-Mariano 2004).

In order to identify the complement of human HAD phosphatases and to understand the evolutionary relationships among them, we performed extensive database searches (see 4.1.1 section in methods) and constructed phylogenetic trees based on the multiple alignment of the identified phosphatases using the program ClustalX 2.0 (Larkin et al., 2007). A phylogenetic tree is a way of describing evolutionary relationships between proteins that are assumed to have a common ancestor. Thus, the basic assumption behind the tree construction is that the respective proteins are evolved over time from a common ancestor.

There are three basic steps in the phylogenetic analysis of proteins. 1) Multiple alignment of amino acid sequences 2) distance calculations depending upon data set and 3) construction of a tree. In the present study we have used the most common program Clustal W to generate multiple alignments of CIN and AUM orthologs. The letter 'W' in Clustal W stands for 'weighted', meaning that different weights are given to sequences and parameters in different parts of the alignment e.g., by inserting gaps to produce biologically significant alignments. The second step towards the tree construction is the calculation of distances between the species on the basis of multiple alignments. There are various methods for distance calculations, depending upon the overall similarity among the sequences. As a first approach we used 'neighbour joining method' for calculations using Clustal X 2.0. The final step of analysis is the tree construction and the data display in various formats.

We used PhyloDraw (version 0.82) for the construction of a tree. Each node of the tree is called a taxonomic unit. Dendrogram is the broad term used for diagrammatic representation of phylogenetic tree. Phylogram is a tree where the branch length is proportional to the character change or to evolutionary distance. In contrast, a cladogram does not represent the evolutionary distance and all branches are of equal length. Trees can be displayed as either rooted or unrooted. Rooted tree shows root as a common ancestor of the given dataset. Root is generally defined as the least related sequence of the given data set which is also called an operational taxonomic unit (OUT). Unrooted tree can be displayed as either radial or slated or rectangular. We choose to display the data as radial, unrooted trees.

We employed phylogenetic analysis for two distinct reasons. One, to understand evolutionary relationship among known human HAD phosphatases and second, to analyze CIN related proteins and their relationship in higher organisms. Figure 14 shows that we could identify a total of 23 human phosphatases (including isoforms) containing HAD motifs. The radial tree of human HAD phosphatases represents the relative sequence similarity among the members at the amino acid level and grouped them in three hypothetical branches. These branches may suggest probable functional similarity between closely related members as it is evident from having all isoforms in single branch. CIN and AUM are close homologs and are grouped with PSP, the only functionally characterized protein in higher organisms (Collet et al., 1998). The green dot represents the root of the tree. As discussed above, the branch distance of radial tree does not correspond to evolutionary distance but merely represents the branching pattern of the members.

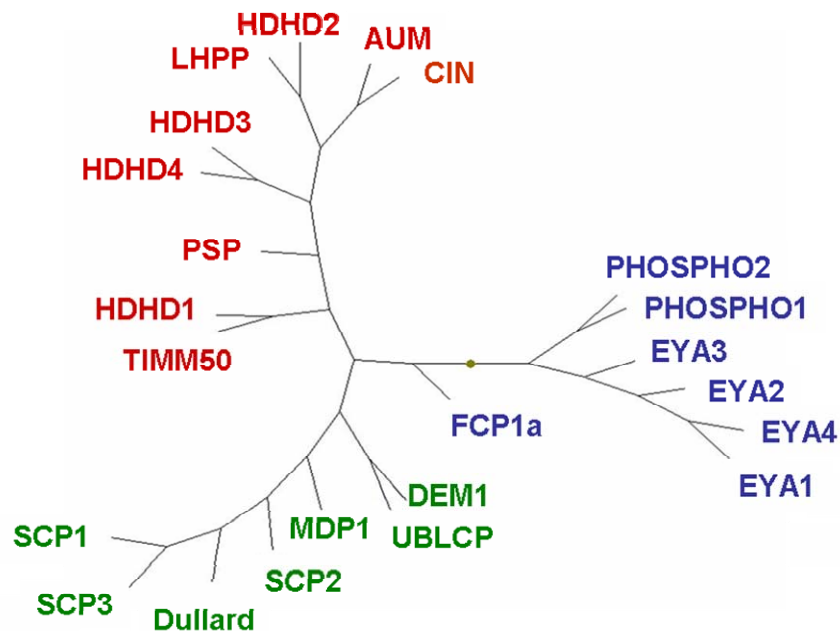


Figure 14: Phylogenetic analysis of human HAD phosphatases.

This radial phylogenetic tree comprises the identified human HAD phosphatases and predicts the probable path of divergence from common ancestors. The tree was constructed by multiple alignment of entire protein sequence and the distance was calculated by neighbour joining (NJ) algorithm. Human HAD phosphatases are grouped in evolutionarily three distinct branches probably with similar function. AUM is the closest CIN relative when compared to all other human HAD members. The following proteins are included (Swiss-Prot identifiers are given in brackets):

AUM, actin-remodeling, ubiquitously expressed, magnesium-dependent HAD phosphatase (A6NDG6) also designated as PGP, phosphoglycolate phosphatase;

CIN, Chronophin (Q96GD0), also known Pdxp, Pyridoxyl phosphate phosphatase (pdxp);

PHOSPHO1, phosphatase, orphan 1 (Q8TCD6);

EYA1, eyes absent 1 (Q99502);

FCP1a, CTD (carboxy-terminal domain, RNA polymerase II, polypeptide A) phosphatase subunit 1 (Q9Y5B0);

DEM1, differentially expressed in malignancies protein (no Swiss-Prot Id, AF120499_1);

UBLCP, ubiquitin-like domain containing CTD phosphatase 1 (Q8WVY7);

MDP1, magnesium-dependent phosphatase 1 (Q86V88);

SCP, small C-terminal domain (carboxy-terminal domain, RNA polymerase II, polypeptide A) phosphatase 1 (Q9GZU7);

Dullard, (O95476);

TIMM50, translocase of inner mitochondrial membrane 50 homolog (Q3ZCQ8);

HDHD1A, haloacid dehalogenase-like hydrolase domain containing 1A (Q08623);

PSP, phosphoserine phosphatase (P78330);

LHPP, phospholysine phosphohistidine inorganic pyrophosphate phosphatase (Q9H008).

AUM was discovered bioinformatically as the closest relative of the cofilin phosphatase Chronophin (CIN; Gohla et al., 2005). Murine AUM shares 45% sequence identity and 61% sequence similarity on the amino acid level with murine CIN when aligned using PSI BLAST (see also Fig. 5). To understand the evolutionary relationship between AUM and CIN, a combined phylogenetic tree of AUM and CIN orthologs was constructed (Fig. 15). We used the entire protein sequence as input for alignment of CIN and AUM orthologs. These data show that both proteins co-evolved closely in lower organisms. Interestingly, the evolution of AUM and CIN diverged in vertebrates and was found to be localized in separate chromosomes in mice and humans (see section 1.3.1).

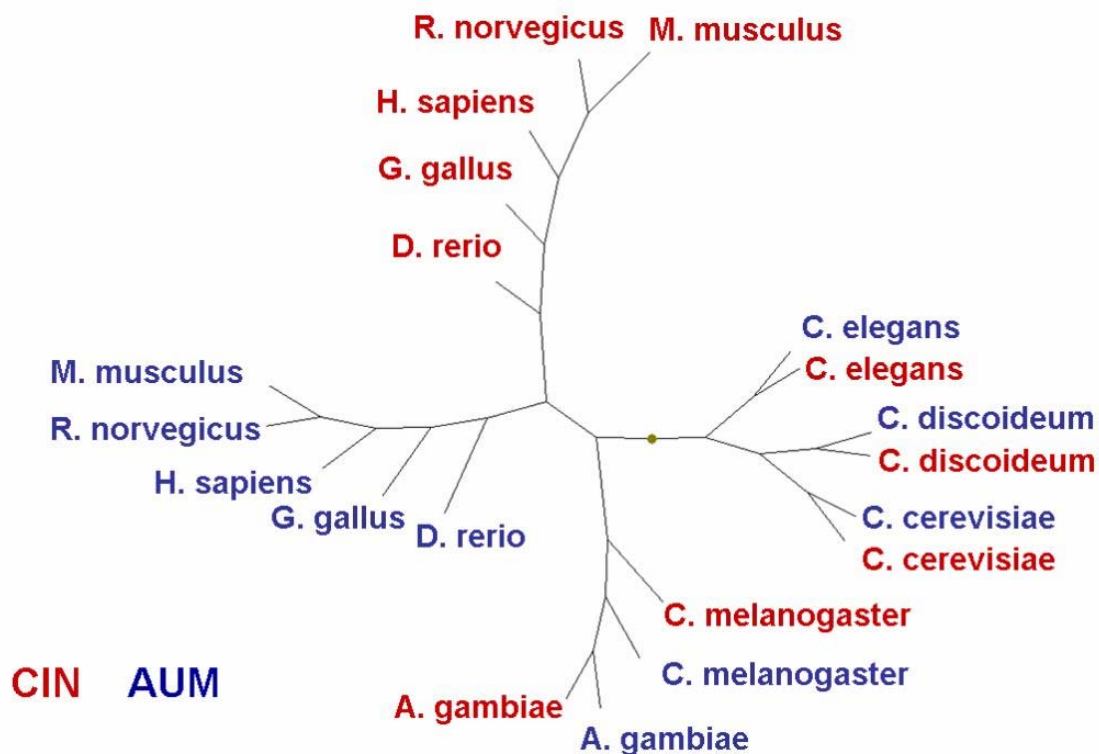


Figure 15: Phylogenetic comparison of primary amino acid sequence of AUM and CIN

This radial phylogenetic tree comprises the identified AUM and CIN orthologs and predicts the probable path of divergence from common ancestors. The tree was constructed by multiple alignment of entire protein sequence and the distance was calculated by the neighbour joining (NJ) algorithm. AUM and CIN orthologs (shown in blue and red, respectively) are closely related in lower organisms, but have evolved independently in vertebrates. The green dot represents the root of the tree. As the tree representation is in radial form, root was not considered while drawing the tree.

The following CIN and AUM orthologs are included (Name of species and accession numbers are given in brackets for CIN and AUM): Human (NP_064711, NM_001042371); Mouse (NM_064667, NM_025954); Rat (AAL37168, XP_213235); Gallus (XP_001234473, NM_001030638); Danio rerio

(NP_848524, AAH45860); Anopheles mosquito (XP_309300; XP_309300.4); Fruitfly (NP_611656, CG5567); Yeast (NP_010045, NP_596255.1); Slime mould (XP_638376.1, XP_638376); Worm (NP_504511; NP_504509.1).

Next we investigated phylogenetic relationship of HAD phosphatases in model organisms. We constructed phylogenetic trees for individual organisms and analyzed how individual isoforms of single protein or two closely related proteins were evolved from prokaryotes to humans. Here we only show trees of yeast and human HAD phosphatases (Fig. 16). Such phylogenetic studies may be helpful to predict probable functions of novel proteins. This analysis can be extended for individual human HAD phosphatases with respect to other family members. We have restricted ourselves only to understand evolution of CIN and AUM. So far, the initial characterization of AUM shows striking differences with CIN (see section 1.3). This may be attributed to differences in primary amino acid sequences in higher organisms as shown in figure 16. Yeast was chosen for comparison with human HAD phosphatases because there no tyrosine kinases were predicted until premetazoans (Pincus et al., 2008).

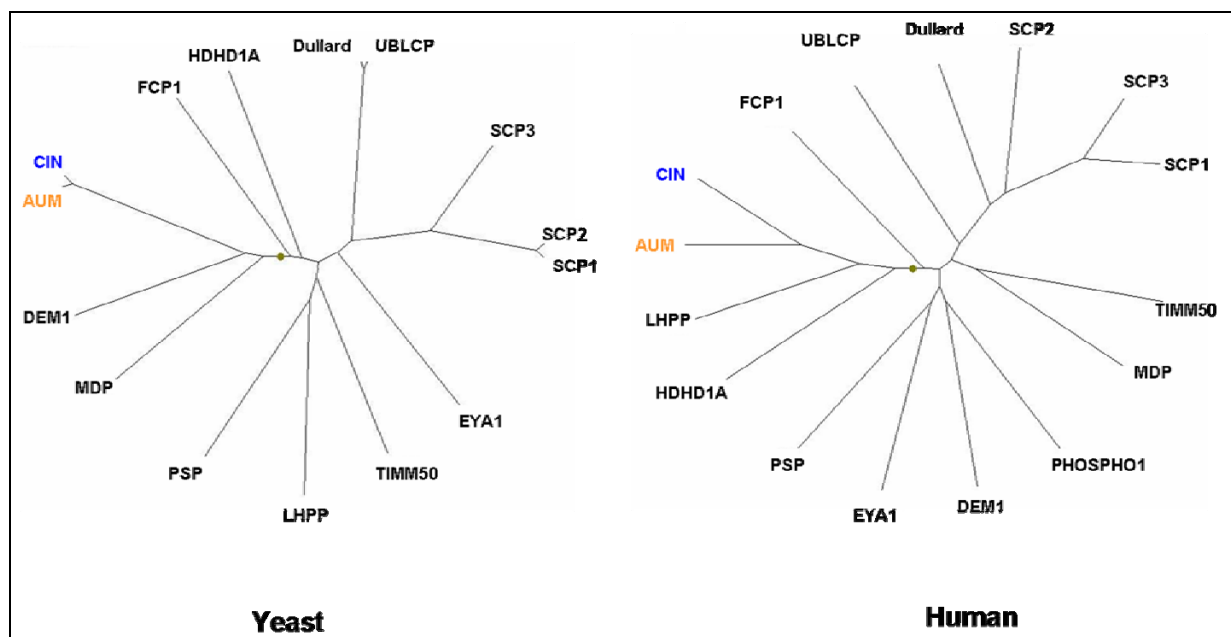


Figure 16: Phylogenetic analysis of human and yeast HAD phosphatases

This radial phylogenetic tree comprises the identified human and yeast HAD phosphatases and predicts the probable path of divergence from common ancestors in this two model organisms. The tree was constructed by multiple alignment of the entire protein sequences and the distance was calculated by neighbour joining (NJ) algorithm. AUM evolved independently of CIN in multicellular organisms. For abbreviations used in this figure, please refer (Fig. 14).

5.2 AUM is a magnesium-dependent HAD phosphatase

Phosphatases of the ancient and evolutionarily conserved HAD superfamily constitute an emerging, yet poorly understood class of enzymes. As of now, very few HAD phosphatases in higher organisms are characterized in terms of their physiological roles (Kim et al., 2007) and even their cognate substrates frequently remain unknown.

Given the sequence similarity between AUM and CIN, we first analyzed the AUM phosphatase activity towards a low molecular weight CIN substrate, pyridoxal phosphate (PLP; (Gao and Fonda 1994; Jang et al., 2003) in comparison to *para*-nitrophenylphosphate (*p*-NPP), a non-specific, broad range phosphatase substrate.

5.2.1 Enzymatic activity assay

To examine the catalytic properties of AUM, murine AUM was recombinantly expressed in bacteria as a His₆-tagged protein (see section 4.4.1), and was subsequently purified by affinity chromatography.

We first tested the activity of AUM against the broad-spectrum phosphatase substrate *p*-NPP. *p*-NPP is a colorless compound that can be enzymatically dephosphorylated to generate inorganic phosphate (P_i) and the yellow-colored *p*-nitrophenol. This conversion can be spectrophotometrically measured over time, and both the kinetics and the endpoint of the reaction can be determined. Figure 17A shows that AUM dephosphorylates *p*-NPP much more efficiently than CIN. A likely explanation for this result is that the phosphorylated phenyl residue of *p*-NPP is structurally similar to a phosphorylated tyrosine residue. This relatively bulky residue may not be easily accommodated in the narrow catalytic pocket of the serine phosphatase CIN (Almo et al., 2007).

As PLP is a known substrate for CIN, we next compared the CIN and AUM activities toward PLP. Free inorganic phosphate (P_i) generated in the reaction of PLP dephosphorylation was detected fluorimetrically as described in section 4.4.11. As this assay is based on coupled enzymatic reactions, picomolar concentrations of released inorganic phosphate can be amplified and detected. But due to its high sensitivity the assay is prone to amplification of experimental errors as well. Figure 17A suggests that AUM can dephosphorylate PLP, but that it is a relatively weak PLP phosphatase as compared to CIN.

The enzymatic characteristics of AUM were determined for *p*-NPP as a substrate as shown in figure 17B. Various substrate concentrations were used to calculate the reaction rate. The data was fitted into a Lineweaver-Burk plot and found to follow Michaelis-Menten kinetics. The K_m and V_{max} values for *p*-NPP were calculated with GraphPad Prism software, version 4.00. K_m is the Michaelis-Menten constant. It is defined as the substrate concentration that is required to achieve a half-maximal enzyme velocity. V_{max} is the maximum velocity of the enzyme extrapolated to very high concentrations of substrate.

Usually, either V_{\max} or K_{cat} is calculated along with K_m to describe enzyme efficiency. Enzyme kinetics of AUM as shown in figure 17B indicates that AUM efficiently dephosphorylate *p*-NPP, as half of the maximal velocity is attained with 370 μM of *p*-NPP.

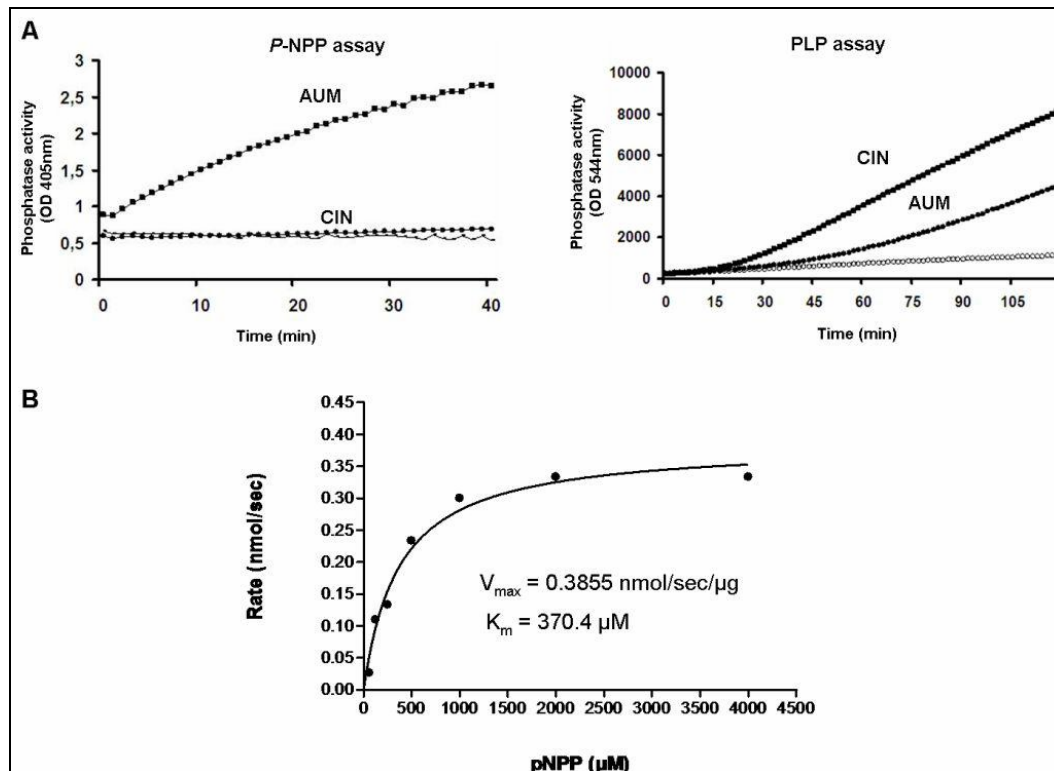


Figure 17: AUM is an efficient *p*-NPP phosphatase

A: Comparison of AUM and CIN enzymatic activities.

Left panel: One microgram of purified, untagged CIN or AUM was incubated with *p*-NPP (3.5 mM) at 30°C, and the dephosphorylation of *p*-NPP was continuously measured for 40 min at 405 nm. Samples were in duplicates. AUM shows a higher activity against *p*-NPP than CIN.

Right panel: One microgram of purified, untagged CIN or AUM was incubated with PLP (50 μM) at 37°C, and the production of inorganic phosphate was continuously measured for 120 min at 544 nm, using the formation of the fluorescent product resorufin as a readout. Samples were in duplicates. PLP is a better substrate for CIN than for AUM. In both the panels, open circles indicate blank reading without protein.

B: Characterization of the AUM enzyme kinetics towards *p*-NPP.

One microgram of AUM was incubated with the indicated concentrations of *p*-NPP for 30 min at 30°C and the kinetics of *p*-NPP-dephosphorylation was followed at 405 nm. Data obtained for the individual substrate concentrations were fitted into the Michaelis-Menten equation to calculate K_m and V_{\max} of AUM for *p*-NPP.

5.2.2 AUM is an aspartate-dependent HAD phosphatase

In contrast to conventional cysteine-based phosphatases, HAD phosphatases employ an unusual catalytic mechanism whereby an aspartate in the catalytic pocket acts as a nucleophile in a phosphoaspartate transferase reaction (Burroughs et al., 2006). After having confirmed that recombinant, purified AUM functions as an active phosphatase *in vitro* (Fig. 17), our next step was to examine whether it was an aspartate-based phosphatase, as suggested by the primary structure and the presence of three HAD-type phosphatase motifs.

To address this question, we generated a point mutant by site-directed mutagenesis as detailed in section (4.2.9). The aspartate at position 34 in the HAD motif I of murine AUM, which is predicted to act as a nucleophile, was mutated to asparagine (AUM^{D34N}). The mutant and the wildtype AUM were then expressed in bacteria and purified by affinity chromatography.

Figure 18A shows a Coomassie Blue-stained SDS-PAGE gel of the purified His₆-tagged AUM^{D34N} and AUM^{wt} proteins. Subsequently, the *in vitro* phosphatase activities of AUM^{D34N} and AUM^{wt} were analyzed against *p*-NPP. In contrast to AUM^{wt}, which efficiently dephosphorylated *p*-NPP in a concentration-dependent manner, even the highest employed AUM^{D34N} concentration of 2 μg only demonstrated only 1-2% of residual activity against *p*-NPP as compared to the same concentration of AUM^{wt} (Fig. 18B).

These data clearly show that AUM is an aspartate-dependent phosphatase. Since aspartate is also known to be needed for Mg²⁺-coordination, AUM is a Mg²⁺-dependent phosphatase. AUM^{D34N} is catalytically massively impaired, indicating that the contribution of other residues to catalysis is secondary to the contribution of aspartate at position 34 in motif I of AUM.

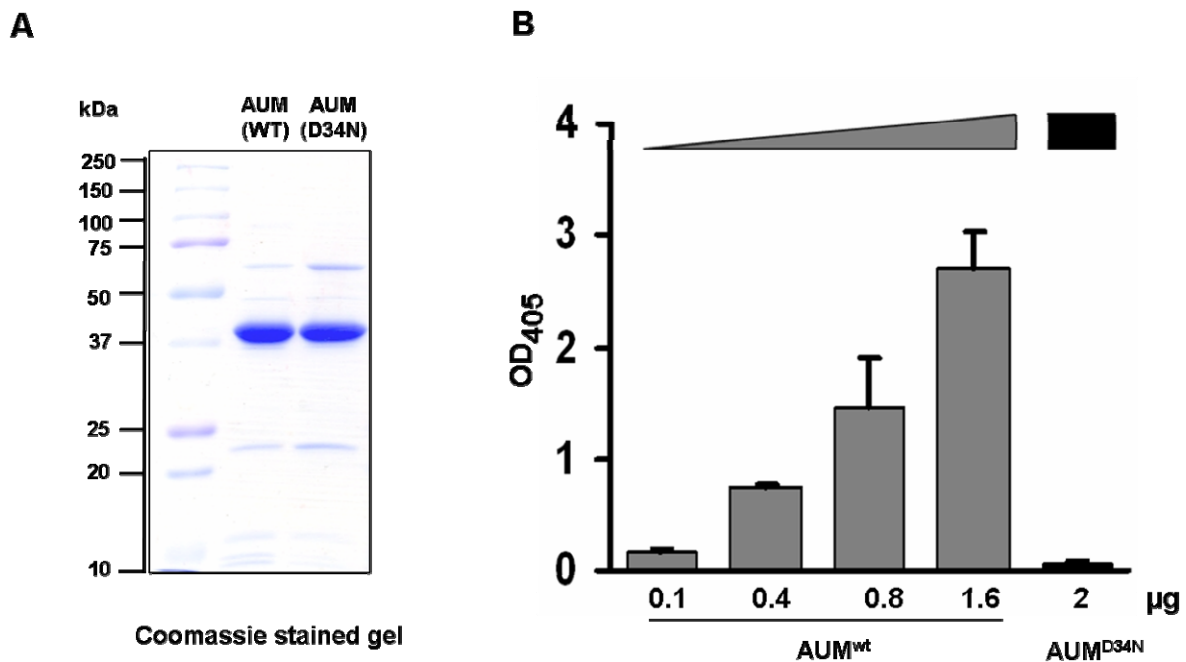


Figure 18: Generation of a catalytically impaired AUM mutant

A: Bacterially expressed and affinity-purified His₆-tagged AUM^{wt} and AUM^{D34N} proteins were run on a 12% SDS-PAGE gel and were stained with Coomassie Brilliant Blue.

B: *In vitro* phosphatase assay using the artificial phosphatase substrate *p*-nitrophenyl phosphate (*p*-NPP). The indicated concentration of the recombinant proteins were incubated with 3.5 mM *p*-NPP for 30 min at 30°C, and the kinetics of the dephosphorylation were followed at 405 nm for 30 min. AUM^{wt} dose-dependently dephosphorylates *p*-NPP, whereas AUM^{D34N} has only residual phosphatase activity towards this substrate.

5.3 High throughput peptide screen

As a first step towards understanding the substrate preference of AUM, we decided to analyze its phosphatase activity against a panel of peptides derived from human proteins experimentally found to be phosphorylated on serine, threonine or tyrosine residues. To that end, we screened a total of 720 commercially available serine-, threonine- or tyrosine-phosphorylated peptides (JPT peptide technologies, Berlin; see section 4.4.12).

Figure 19 shows that AUM was found to be a specific phosphotyrosine (pTyr) peptide phosphatase in this screen, as it dephosphorylated only 17 out of the 488 phosphotyrosine-containing peptides present in the assay (when applying a cutoff at 66% of the maximal reading. The full list of peptides that were dephosphorylated by AUM is given in the Appendix, see 10.1). Interestingly, there was not a single hit for the 232 serine (pSer) - and threonine (pThr)-phosphorylated peptides present in the assay. Although this peptide-based information may not be translated directly to AUM substrate preferences at the protein level, the data clearly indicated that AUM prefers tyrosine-phosphorylated residues. Furthermore, these results are in accordance with the efficient dephosphorylation of p-NPP (see Fig. 17).

Figure 19 shows a graphical representation of the AUM peptide substrates identified in this peptide screen, together with a list of the putative substrates.

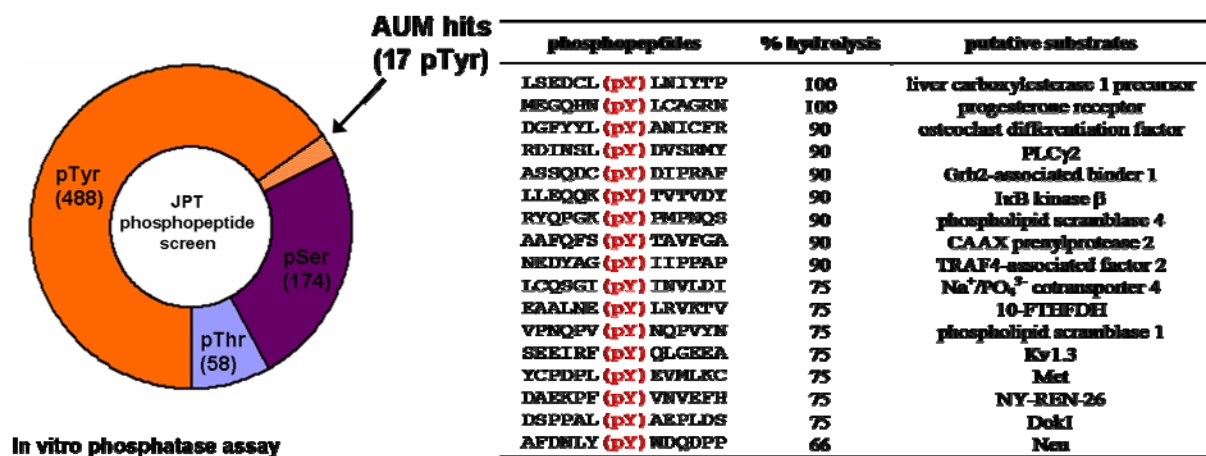


Figure 19: AUM preferentially dephosphorylates tyrosine phosphorylated peptides

720 phosphopeptides derived from human phosphorylation sites were screened for putative AUM substrates using a malachite green assay. 17 pTyr but no pSer or pThr peptides were dephosphorylated by AUM. Putative AUM substrates belong to following signalling pathways: Receptor tyrosine kinase signalling, Metabolism, Cell adhesion, Cytoskeleton, Nuclear signalling, Vesicular traffic, Second messenger, Differentiation, Apoptosis, Voltage gated channels, Growth factors.

Abbreviations used in the figure: PLC γ 2 (Phospholipase gamma 2); Grb2 (Growth factor receptor binding 2); I κ B kinase (Inhibitor of nuclear factor kappa B kinase); CAAX (motif of one 'cysteine, two 'aliphatic amino acids' and one any amino acid at the end); TRAF4 (tumor necrosis factor (TNF) receptor associated factor 4); 10FTHFDH (10-formyltetrahydrofolate dehydrogenase); Kv 1.3 (Potassium voltage-gated channel subfamily A member 3); Met (Hepatocyte growth factor receptor precursor); NY-REN-26 (Breakpoint cluster region protein); Dok1 (Docking protein 1); Neu (C-erbB-2 (epidermal growth factor receptor) precursor)

5.4 AUM is a protein tyrosine phosphatase

So far, we have proved at peptide level that AUM prefers phosphotyrosine residues over phosphoserine or phosphothreonine residues. Next step was to show it on protein level and in also under physiological settings. We decided to employ phosphatase overlay assay and *in vitro* phosphatase assays to address these questions as described in subsequent sections.

5.4.1 Phosphatase overlay assay

In order to investigate whether AUM also acts as a protein tyrosine phosphatase, we performed phosphatase overlay assays. In cells, only a very small fraction of proteins is tyrosine phosphorylated at any given time as compared to the relative abundance of serine- or threonine-phosphorylated proteins (Alonso et al., 2004). Secondly, the dynamic balance between kinase and phosphatase activities generally makes it difficult to assess cellular tyrosine dephosphorylation. To circumvent these difficulties, HeLa cells were stimulated with freshly prepared pervanadate, a nonspecific phosphatase inhibitor that induces an increase in the levels of cellular tyrosine phosphorylation (Gordon 1991). To avoid the effects of kinases that may obscure phosphatase activities, cells were lysed, and cell lysates were separated by gel electrophoresis and were transferred onto nitrocellulose membranes. Finally, the denatured proteins were overlaid with recombinant AUM^{wt} or AUM^{D34N} as detailed in Methods (see 4.4.14). As shown in figure 20, catalytically active AUM was able to dephosphorylate phosphotyrosine-containing proteins in a concentration-dependent manner, whereas the catalytically impaired AUM^{D34N} point mutant did not show detectable phosphatase activity even when 100 µg of recombinant protein were used. Even though the employed amounts of enzyme appear very high, these concentrations are typically required for phosphatase overlay assays, and represent the standard practice in the field (Rayapureddi et al., 2003). Taken together, these results indicate that that AUM acts as protein tyrosine phosphatase in cells

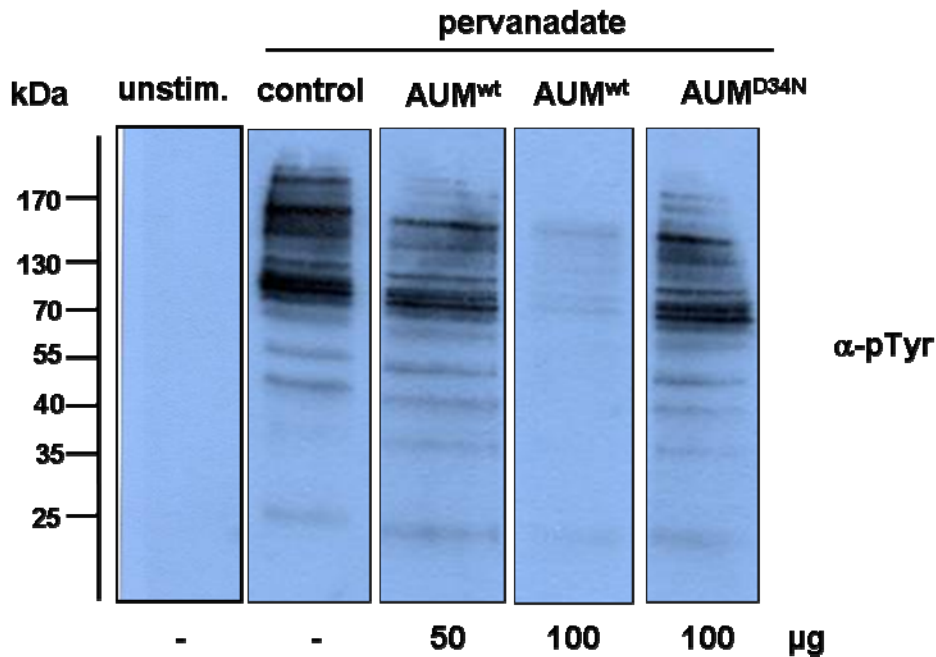


Figure 20: AUM dephosphorylates tyrosine phosphorylated proteins in phosphatase overlay assays.

HeLa cells were stimulated with 100 μ M pervanadate to increase the levels of cellular tyrosine phosphorylation (see 4.4.14). Unstimulated HeLa cells were used as a control for the efficiency of the pervanadate treatment. 20 μ g of the cell lysates were subjected to SDS-PAGE with taped comb to ensure equal loading across the gel and blotted onto a nitrocellulose membrane. The membrane was then cut into vertical strips, and the strips were incubated with the indicated amounts of purified AUM^{wt} or AUM^{D34N} or with assay buffer as a control. Protein tyrosine phosphorylation was analyzed by Western blotting with the phosphotyrosine specific antibody (4G10 clone). AUM^{wt} concentration-dependently dephosphorylated tyrosine-phosphorylated proteins. In contrast, even the highest employed concentration of the catalytically impaired AUM^{D34N} mutant did not induce a detectable protein tyrosine dephosphorylation.

5.4.2 Role of AUM for epidermal growth factor-induced tyrosine phosphorylation in cells

In order to test whether AUM can act as a cellular tyrosine phosphatase, we stimulated cells with epidermal growth factor (EGF) as detailed under Methods (see 4.4.14). EGF was used as a typical growth factor that is well-known to trigger cellular tyrosine phosphorylation cascades (Schlessinger 2002). In addition, the EGF receptor itself and proteins involved in EGF-induced signaling were detected as putative AUM phosphatase substrates in the peptide substrate screen (see 4.4.12).

GC1 or HeLa cells transiently overexpressing AUM^{wt} and AUM^{D34N} were stimulated with 85 nM of EGF for various time points and were probed for global changes in tyrosine-phosphorylated proteins as shown in figure 20. These data suggest that AUM seems to transiently act on tyrosine-phosphorylated proteins, in particular during the initial phase after EGF stimulation. The effect is most prominent around one min of EGF stimulation in GC1 cells and five min of EGF stimulation in HeLa cells. AUM^{D34N} overexpressing cells did not show reversal of the effect, which might be due to the presence of endogenous AUM. In

contrast, the depletion of AUM by shRNA clearly showed that AUM affects tyrosyl phosphorylation upon EGF induction (see section 5.7). Upon reprobing the blot for total EGFR as shown in figure 21B, we observed changes in the total amount of EGFR, suggesting a potential role of AUM in EGFR degradation pathways.

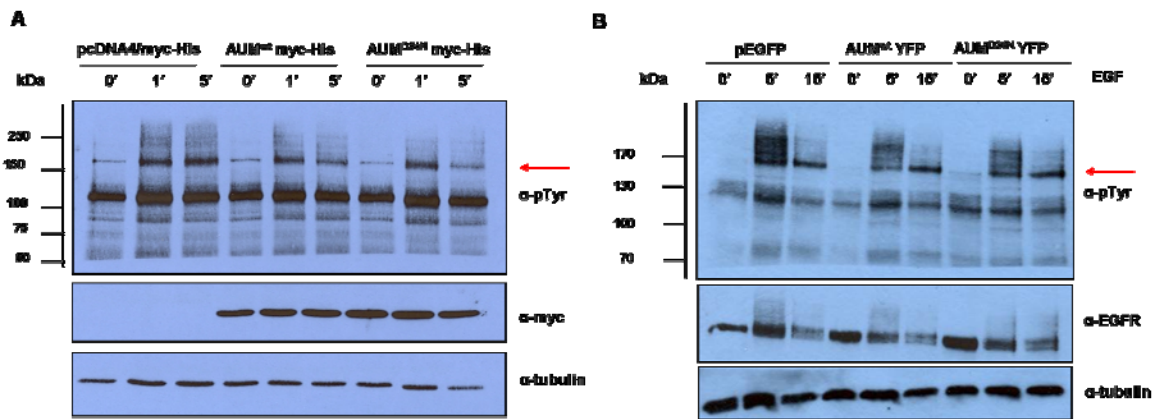


Figure 21: Effect of AUM on cellular tyrosine phosphorylation in EGF-stimulated cells

A: GC1 cells transiently transfected with the indicated plasmids were starved overnight in serum-free culture medium. Cells were stimulated with 85 nM of EGF for the indicated time points, and were subsequently lysed in lysis buffer. Equal protein amounts (20 μ g) of the lysates were separated by SDS-PAGE, transferred onto nitrocellulose membranes and tyrosine-phosphorylated levels were analyzed by immunoblotting with the phosphotyrosine-specific antibody 4G10.

B: HeLa cells transiently transfected with the indicated plasmids were starved overnight in serum-free culture medium. Total phosphotyrosine content was analyzed as above. Total EGFR levels upon AUM overexpression were analyzed by stripping and reprobing the blot. AUM overexpression modulates EGFR levels in cells.

Western blots shown here are representative of 3 independent experiments. The results show that AUM can act as a cellular protein tyrosine phosphatase. Arrow indicates modulation of phosphotyrosine content upon AUM overexpression.

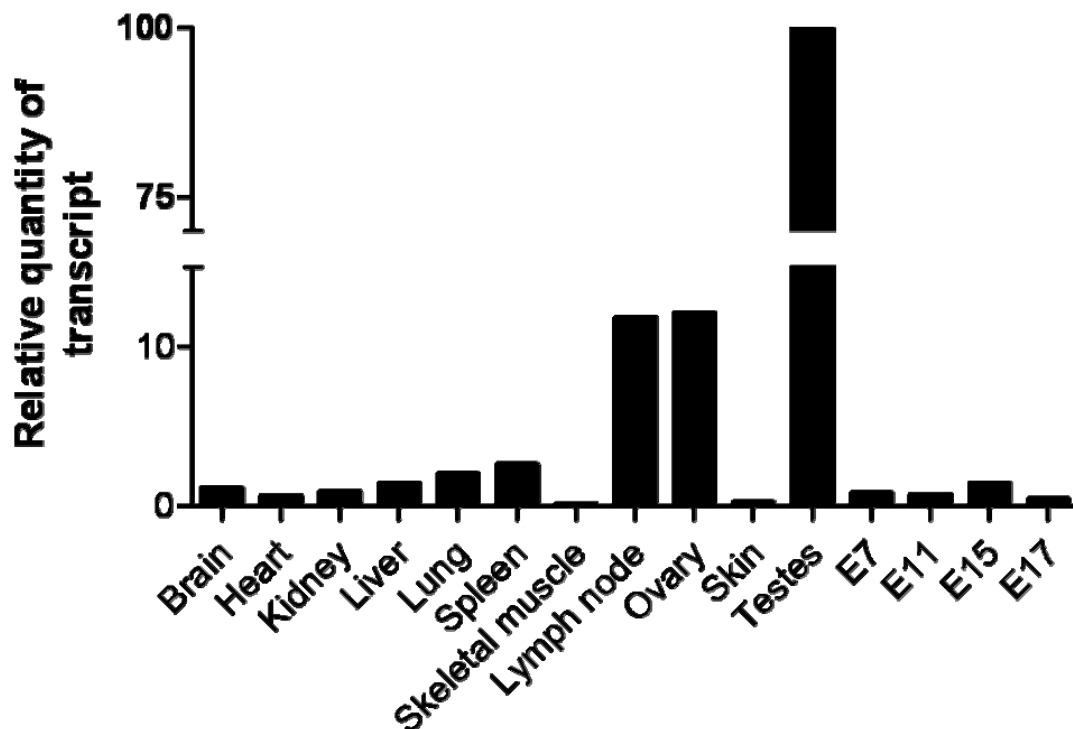
Taken together, these data with pervanadate and EGF stimulations show that AUM can act as a protein tyrosine phosphatase in cells.

5.5 Ubiquitous expression of AUM in mouse tissues

We next investigated the expression pattern of AUM at the RNA and protein level by multiple approaches. Searches in expressed sequence tag (EST) databases (Unigene) predicted a partially non-overlapping AUM and CIN expression pattern. During my diploma work, we compared AUM and CIN expression profiles by reverse transcriptase (RT)-PCR (see section 1.3.2). CIN was found to be broadly expressed with highest levels in brain, whereas AUM was broadly expressed with highest levels found in testis. As a continuation of this preliminary analysis, we now employed quantitative real-time PCR, Northern blot, immunoblot and immunohistochemical analysis with AUM-specific antibodies in the present study.

5.5.1 Real-time PCR

In order to quantify the AUM expression in various tissues and to re-evaluate the expression pattern obtained in the initial RT-PCR experiments, we performed real-time PCR. We analyzed the AUM expression pattern in different mouse tissues and in mouse embryos. The relative abundance of the AUM transcript was quantified with GAPDH as an internal control and testis as a calibrator. Figure 22 shows a ubiquitous expression pattern of AUM in all major mouse tissues. AUM was found to be highly expressed in testis. The crossing point threshold cycle (C_t) value is the measure of transcript abundance (see section 4.2.8 in Methods). Testis has the lowest C_t value among all investigated tissues, implying an early attainment of the threshold cycle due to high transcript abundance. AUM expression can be detected as early as in seven days old mouse embryos. Together, these real-time data are in accordance with the RT-PCR analysis of AUM expression during preliminary characterization (see section 1.3.2 of introduction)



Mouse tissue	C _t value	Mouse tissue	C _t value
Brain	20.48	Ovary	23.47
Heart	23.12	Skin	23.21
Kidney	22.04	Testes	17.70
Liver	23.95	Mouse embryonal stage	C_t value
Lung	23.35	E7	22.37
Spleen	22.39	E11	22.99
Skeletal muscle	20.10	E15	23.26
Lymph node	25.21	E17	22.19

Figure 22: Relative quantification of AUM transcript by real-time PCR

cDNA from the indicated tissues were subjected to real-time PCR with AUM and GAPDH primers. The data were normalized against GAPDH and calibrated against the AUM expression in testis. The crossing point threshold (C_t) value is an indicator of the relative abundance of the transcript in a given tissue. AUM is ubiquitously expressed with highest expression in testis. Values represents results from two independent experiments with each sample run in triplicates.

5.5.2 Northern blot

Along with semi quantitative real-time PCR analysis of AUM transcript, we also designed a digoxigenin (DIG)-labeled AUM riboprobe to analyze the expression pattern of AUM at the RNA level by Northern blot. We used a commercially available dot blot panel of mouse tissues containing total RNA crosslinked on a membrane. Figure 23A shows the validation of the AUM riboprobe using total RNA from mouse testis. The AUM riboprobe was found to detect a single major band at the expected size of AUM (0.96 Kbp). Thus, the AUM RNA probe specifically recognizes AUM. In addition to Northern blot analysis; this probe may also

be a useful tool to analyze the AUM expression pattern at the RNA level by methods such as *in situ* hybridization.

The dot blot was probed with the AUM-specific riboprobe as shown in figure 23B. These results clearly confirm the ubiquitous AUM expression pattern as measured by real-time PCR experiments (Fig. 22). Interestingly, AUM is not only highly expressed in testis, but it also shows high expression in other male and female reproductive organs, such as epididymis, prostate, uterus and ovary.

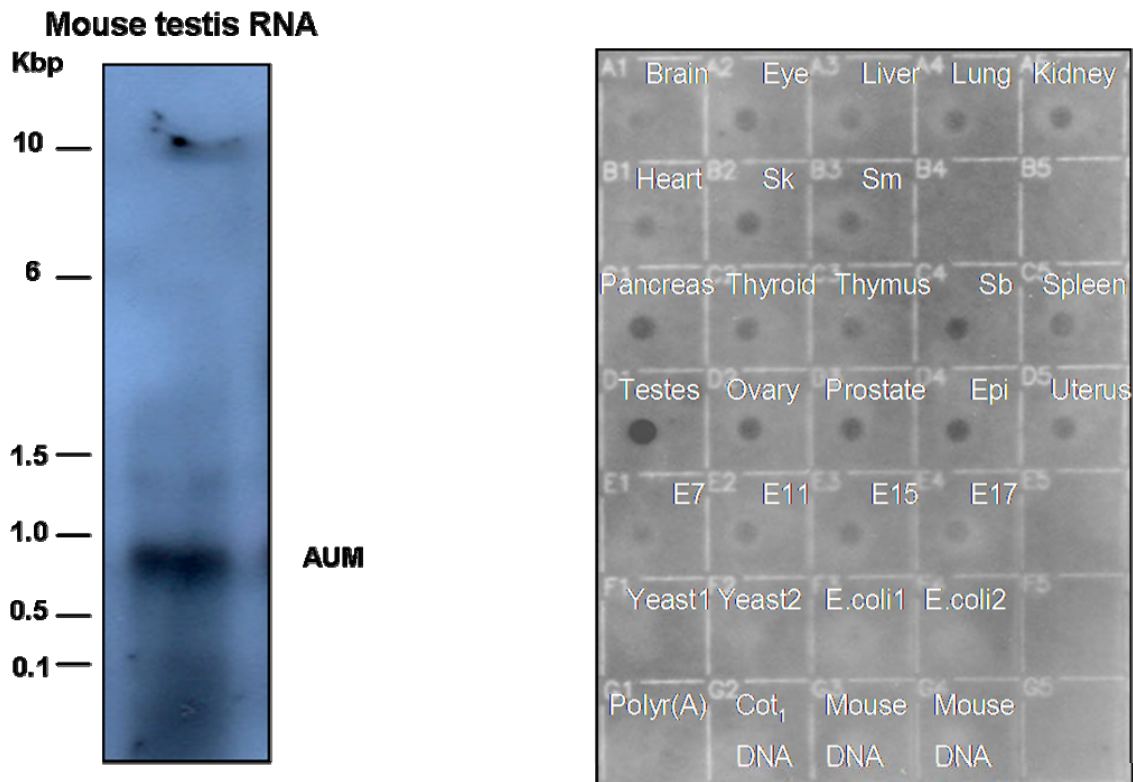


Figure 23: AUM expression analysis by Northern blot

A: AUM RNA probe validation.

Purified AUM RNA probe was analyzed on an RNA agarose gel to check integrity and extent of purity. Total mouse testis RNA cross linked on membrane was probed with DIG labeled AUM riboprobe and the signal corresponding to size of AUM cDNA (966 bp) was obtained after exposing to X-ray film.

B: AUM Northern blot

DIG-labeled AUM riboprobe was probed against total RNA in various mouse tissues. AUM transcript was found to be ubiquitously expressed with highest expression in testis. Controls used were F1: Yeast total RNA; F2: Yeast tRNA; F3: E.coli rRNA; F4: E.coli DNA; G1: Poly r (A); G2: C_ot DNA; G3: Mouse DNA; G4: Mouse DNA. Wells B4, B5 E5, F5, G5 are empty. Abbreviations used in the figure: Sk (Skeletal muscle); Sm (Smooth muscle); Sb (Submaxillary gland); Epi (Epididymis); E7-E17 (mouse embryonal stages)

5.5.3 Western blot

In order to investigate the expression and cellular distribution of AUM at the protein level, we next aimed to generate a sensitive and AUM-specific rabbit polyclonal antibody. For this purpose, we designed an AUM-specific peptide as outlined in Methods (see section 4.4.2).

Figure 24 demonstrates that the affinity-purified AUM-antibody was able to reliably detect as little as 10 ng of recombinant, purified AUM protein. Furthermore, the AUM-directed antibody did not cross-react with CIN, its closest known homolog. The affinity-purified AUM antibody has been successfully used for immunoblotting (1:1000), immunohistochemistry (1:250 – 1:400) and for immunostaining (1:100), as will be shown in the following sections.

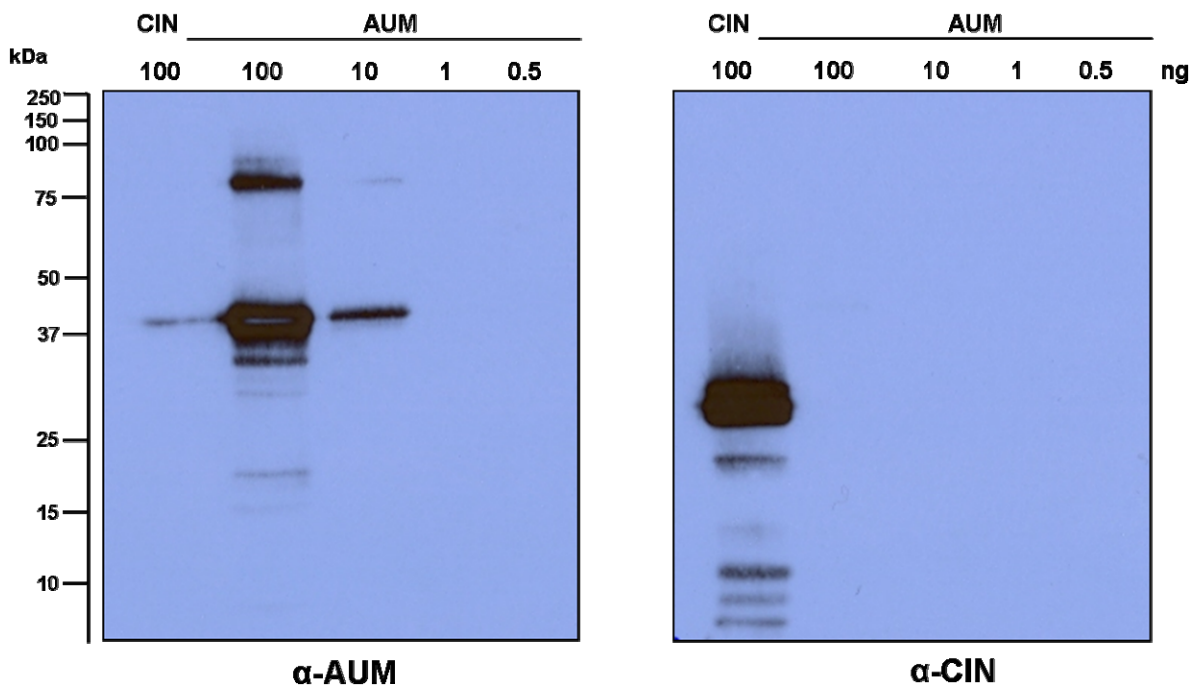


Figure 24: Characterization of AUM rabbit polyclonal antibody

Indicated amounts of recombinant AUM and CIN proteins were loaded on 12% SDS-PAGE and transferred to nitrocellulose membrane.

Left panel: Nitrocellulose membrane probed with AUM specific antibody recognizes 10 ng of recombinant protein but does not cross react with CIN. Faint band in the first lane (with CIN protein) is due to spill over from the adjacent well.

Right panel: Nitrocellulose membrane probed with CIN specific antibody does not cross react with 100 ng of AUM. The AUM antibody can be reliably used for biochemical and cellular assays as there is no cross reactivity with CIN.

In order to analyze the AUM expression pattern at the protein level, we generated lysates of various mouse tissues as detailed in Methods (see 4.4.3). The lysates were then analyzed by immunoblotting using the AUM-directed antibody. In accordance with RT-PCR, real-time PCR and Northern blot analysis, AUM was found to be expressed ubiquitously with highest expression in testis as shown in figure 25. In all investigated tissues, the AUM antibody detected a single predominant band corresponding to the expected AUM size of ~34 kDa. In

addition, faint higher molecular weight bands were detected in kidney, liver and skeletal muscle suggesting the possible existence of AUM splice variants or isoforms. By Western blotting, the relative difference in the AUM expression in testis as compared to other tissues was not as big as detected by real-time PCR (see Fig. 22). This may suggest the existence of AUM splice variants or isoforms in testis that may not be detected by the AUM antibody.

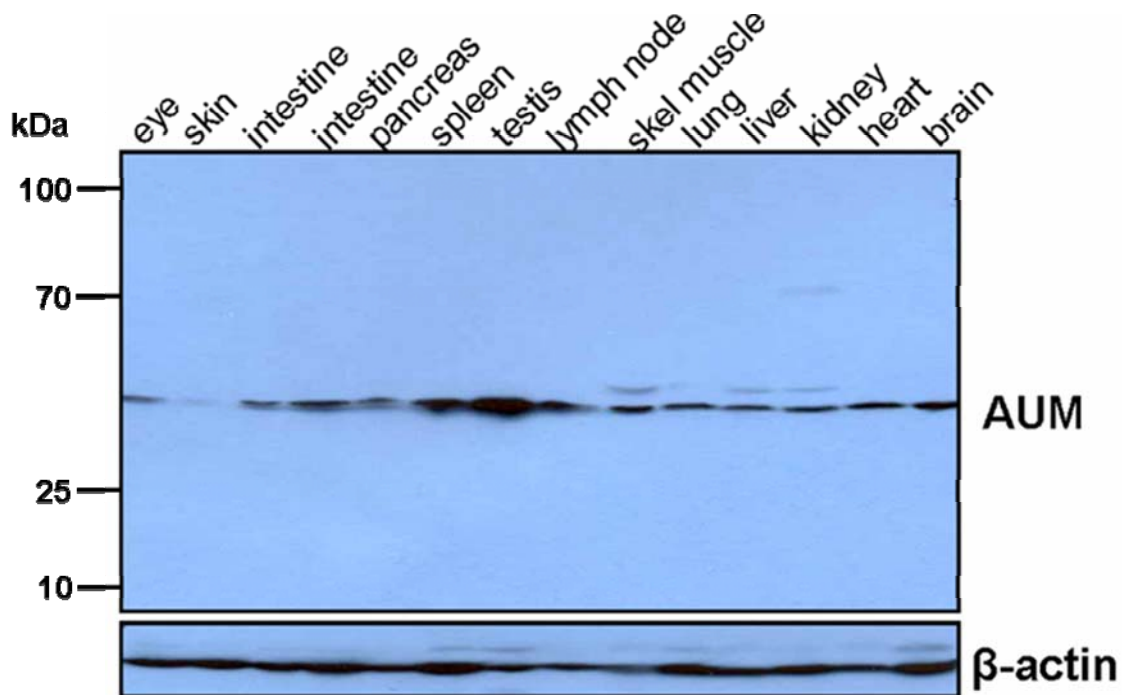


Figure 25: Analysis of AUM expression in mouse tissues

Mouse tissue lysates (60 μ g) were separated by SDS-PAGE, transferred onto nitrocellulose membrane and then analyzed by immunoblotting for AUM expression. AUM was found to be ubiquitously expressed in mouse tissues with highest expression found in testis.

Given the dominant AUM expression in testis, both at the RNA and at the protein level, we decided to investigate the AUM expression in testis in different stages of development, as well as in the male reproductive system of adult mice. Following schematic drawing illustrates the different regions of the male reproductive system and cells present in the seminiferous tubule of the testis.

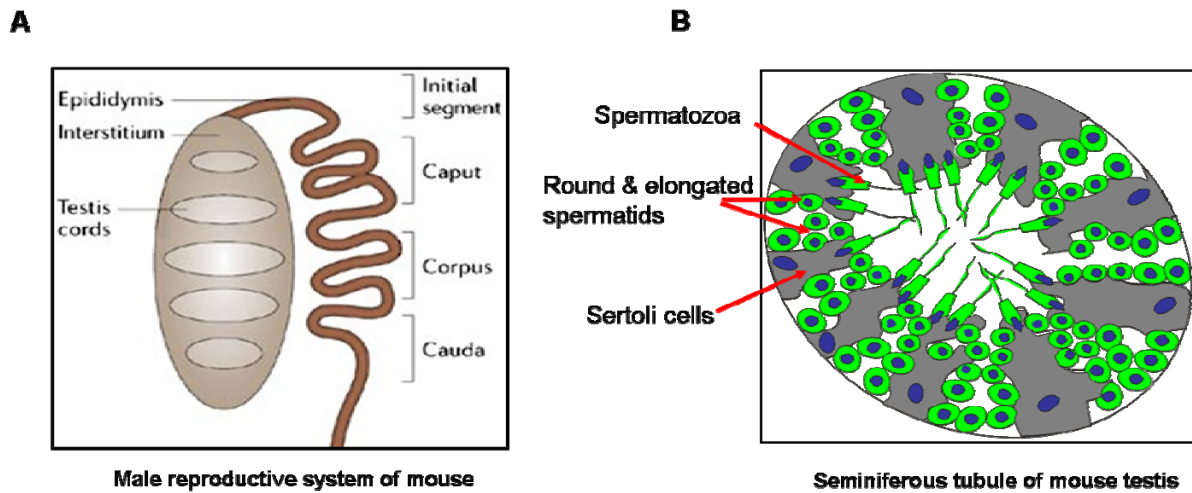


Figure 26: Schematic representation of male reproductive system of mouse

A: Major parts of male reproductive system consist of testis and sperm carrying duct called epididymis. Germ cells undergo maturation (spermatogenesis) in testis cords called seminiferous tubules. (Figure modified from Nature Reviews. Genetics 2006)

B: Seminiferous tubules of testis have germinal cells (in different stages of development) and non germinal cells called Sertoli cells interspersed between germ cells. Testosterone secreting Leydig cells are present interspersed between the seminiferous tubules (not shown in the figure)

Testis lysates were prepared from 1 day to 9 months old male mice. Whereas AUM protein expression was detectable at early embryonic stages by real-time PCR, the expression peaked at around four weeks of age as found by western blot (Fig. 27A). This time point corresponds to the age of puberty in the mouse (Murphy et al., 1994). Afterwards, the AUM protein levels reached a plateau, as shown in figure 27A. Spermatogenesis induces germ cell arrested in first meiotic division to undergo subsequent multiplication once mouse attains puberty. AUM expression corresponds to this process suggesting predominant expression in germ cells rather than non germinal cells like Sertoli or Leydig cells.

We further analyzed the AUM expression in various regions of the epididymis (the sperm carrying duct), as well as in mature mouse spermatozoa. Spermatozoa from the different regions of male reproductive system were isolated and lysates were prepared as detailed in methods (see section 4.4.4) Immature spermatozoa, formed at end of spermiogenesis undergo a maturation process called capacitation while being transported through the epididymis (Breitbart et al., 2005) The head of the epididymis is called caput whereas the tail is known as cauda epididymis. Caput sperms are less motile and cannot undergo capacitation whereas cauda epididymis contains mature spermatozoa (Bellve 1993). Interestingly, the AUM expression is higher in testis than in the epididymis or in sperm, as shown in figure 27B and 27C. Furthermore, the highest AUM abundance was detected in isolated seminiferous tubules (Fig. 27C), which contain germ cells at various stages of development (Hess et al., 1990), before the spermatozoa mature in the epididymis (Seligman et al., 2004). These results indicate that the AUM levels decrease along with process of

spermatozoa maturation. We also tested AUM antibody on the two clinical samples of normal human sperm as shown in figure 27B.

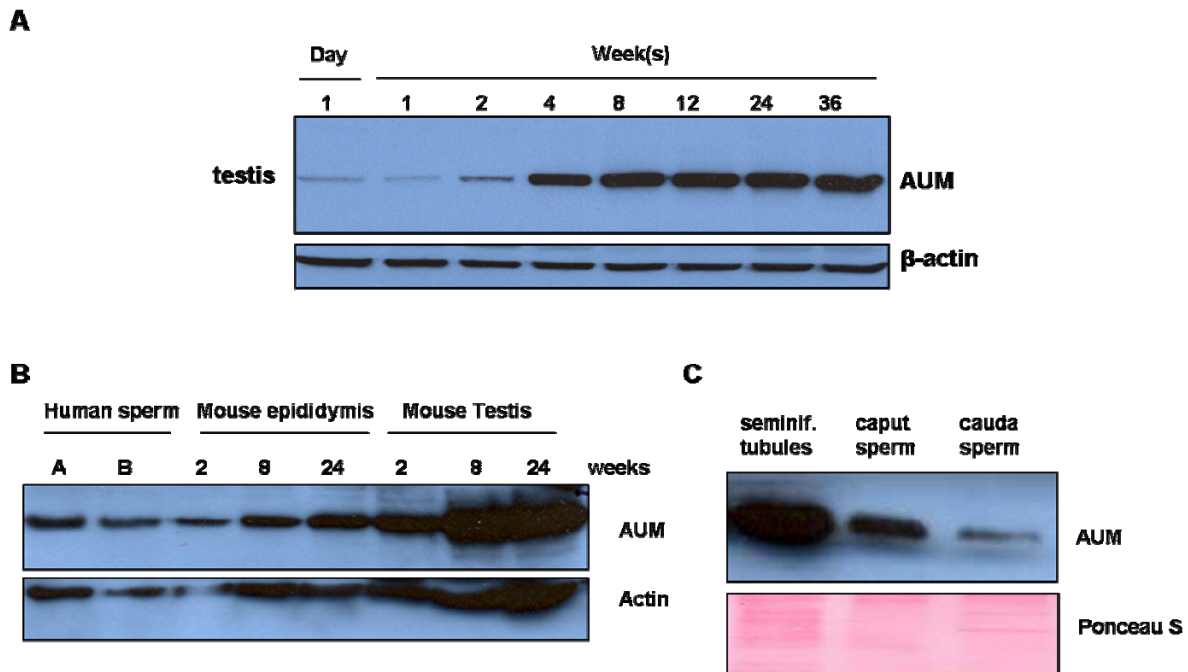


Figure 27: AUM protein expression analysis in mouse testis

A: Expression of AUM protein in mouse testis in different developmental stages.

20 μ g of testis lysate from indicated age of mouse were separated by SDS-PAGE, transferred onto nitrocellulose membrane and then analyzed by immunoblotting for AUM expression. AUM level was found to be peaking up at the age of puberty (4 weeks) in mouse.

B: AUM expression in different regions of the male reproductive system

Lysates of indicated tissues prepared in lysis buffer and were separated by SDS-PAGE, transferred onto nitrocellulose membrane and then analyzed by immunoblotting for AUM expression. Highest AUM expression was found in the seminiferous tubules of testis. The AUM antibody also recognized endogenous AUM in human sperm.

C: AUM expression during sperm maturation.

Sperm lysates were separated by SDS-PAGE, transferred onto nitrocellulose membrane and then analyzed by immunoblotting. AUM expression decreases along with process of spermatozoa maturation in the epididymis. Corresponding ponceau staining is shown as a loading control

Taken together, we have analyzed AUM expression both at the RNA and protein level in various mouse tissues. AUM is found to be expressed in ubiquitously right from early developmental stages with highest expression in seminiferous tubules of testis.

5.6 Immunohistochemical analysis of AUM in mouse testes

In order to identify the AUM-expressing cells in testis, we next performed immunohistochemical analysis on paraffin-embedded mouse testis sections. AUM was detected using the AUM-specific antibody (see Figs. 28, 29), together with either DAB detection or with fluorescently labeled secondary goat anti-rabbit antibodies as detailed in Methods (see 4.4.10). Please refer to the schematic representation of different cell types in testis in figure 26.

5.6.1 Expression pattern of AUM in mouse seminiferous tubules

In order to analyze the AUM expression pattern in mouse seminiferous tubules, paraffin-embedded sections of mouse testis were stained with the AUM-specific antibody. AUM expression was found to be restricted inside the seminiferous tubule as shown in figure 28B. In the seminiferous tubules, AUM was first detectable in round spermatids (see black star in Fig. 28C), and was maximally expressed in elongated spermatids (see red arrow in Fig. 28C) and in spermatozoa oriented towards the lumen of the tubules). In contrast, AUM was not detectably expressed in spermatogonia or in spermatocytes. These results indicate that the expression of AUM peaks only during the later stages of spermatogenesis.

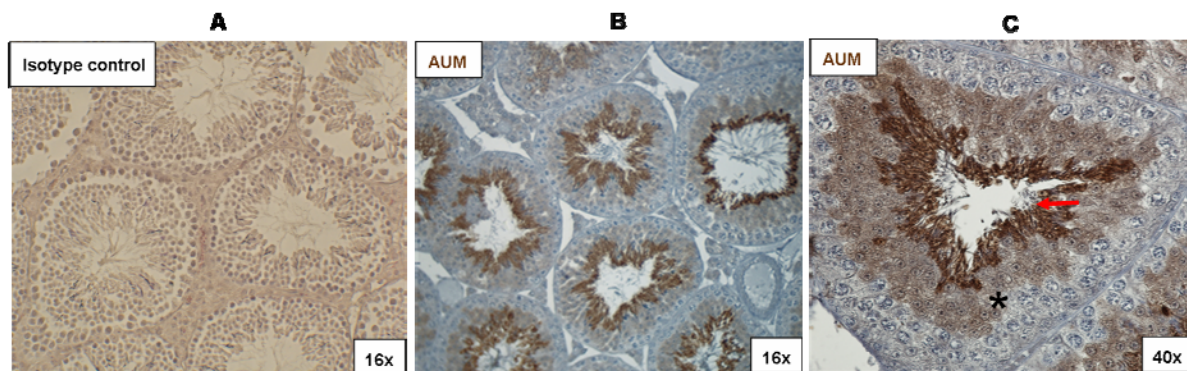


Figure 28: Immunohistochemical analysis of AUM in mouse testis

A: AUM antibody specificity. Rabbit IgG was used as isotype control.

B: AUM expression in germinal cells of seminiferous tubules. AUM-specific rabbit polyclonal antibody was used to detect the expression of AUM in mouse testis. Brown color represents AUM signal. Overview picture at 16 x magnification indicates that AUM expression is restricted to the inside of the seminiferous tubules.

C: High resolution picture shows that AUM is predominantly expressed in elongated spermatids during spermatogenesis as indicated by the red arrow. The black arrow indicates the beginning of AUM expression in round spermatids. Earlier stages of spermatogenesis such as spermatocytes present beyond black star do not show detectable AUM expression.

5.6.2 Expression pattern of AUM in male reproductive system

In order to analyze AUM expression pattern in the male reproductive system in more detail, sections of mouse testis were compared to mouse epididymis sections. In addition, mouse spermatozoa from caput and cauda epididymis were isolated, fixed on coverslips and stained with AUM-specific antibody as described in methods (see section 4.4.4). Mouse epididymis sections were also co-stained for tubulin as detailed in Methods (see 4.3.3). As shown earlier (Fig. 28), the AUM was not detected in germinal cells at the early stages of spermatogenesis. AUM expression was maximal in elongated spermatids. No AUM signal was detected in Sertoli or Leydig cells as shown in figure 29A and B. Expression of AUM in mature cauda sperms was found to be less than in immature caput sperms as shown in figure 29E and 29F. This was also confirmed by analyzing AUM expression in sections of caput and cauda epididymis as shown in figure 29C and 29D. This expression pattern supports the

biochemical data of highest AUM expression in seminiferous tubules and reduction of signal along with the sperm maturation (see Figs. 27B, C).

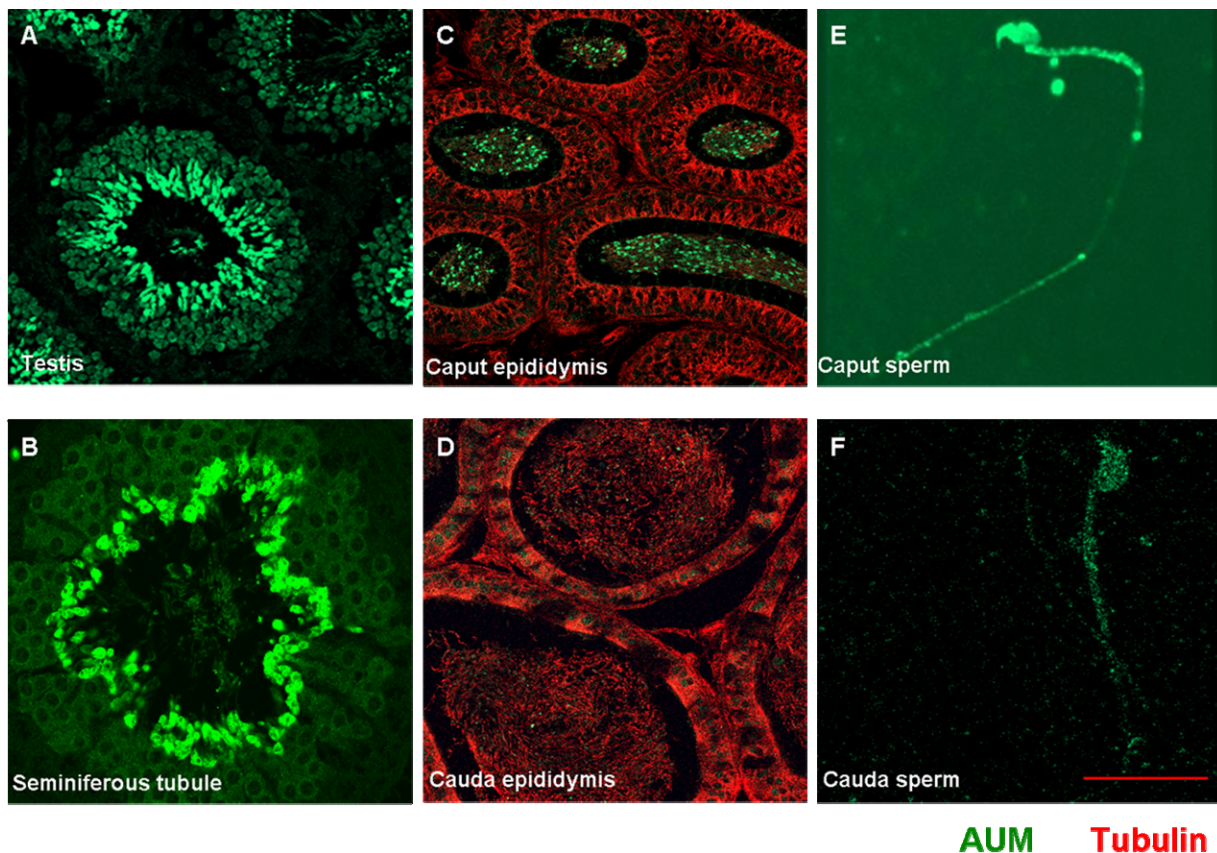


Figure 29: Expression pattern of AUM in the male reproductive system

Male reproductive tissues were stained for AUM expression using an AUM-specific rabbit polyclonal antibody. AUM signal was detected with a fluorescently-labeled secondary antibody. Antibody specificity was checked by rabbit IgG isotype control (data not shown).

A, B: Expression of AUM in testis is restricted to the germinal cells inside the seminiferous tubule.

C, D: Expression of AUM in epididymis: AUM expression goes down along with maturation from the head (caput) towards the tail (cauda).

E, F: Expression of AUM in sperms isolated from caput and cauda epididymis. Immature caput sperm have more AUM expression as compared to mature cauda sperm, suggesting a differential AUM expression during maturation process called capacitation. Scale bar represents 25 μ m.

5.6.3 Expression of AUM in developing germ cells

Germinal cells in seminiferous tubules undergo massive nuclear and cytoplasmic reorganization to form haploid, motile spermatozoa from diploid, non motile spermatogonia. This process is termed as spermatogenesis (Hess 1990). The term spermiogenesis refers to a specialized process during spermatogenesis, which is defined by the formation of mature spermatozoa from round spermatids. Spermiogenesis can be divided into 16 distinct stages in the rat (Hess et al., 1990; Zheng et al., 2007), as shown schematically in the upper panel of figure 30. During spermiogenesis, round and nonmotile spermatids (stage number 4-7 in Fig. 14) are gradually converted into motile spermatozoa (stage number 16 in Fig. 30). This differentiation process involves cell-cell interactions between germ cells and Sertoli cells

(Wang et al., 2006). Sertoli cells are the only non-germinal cells inside seminiferous tubules and play critical roles in the formation of the blood-testis barrier and for nourishing the germ cells during the process of spermatogenesis (Wang et al., 2006). In the final stages of spermiogenesis, the cytoplasm of the germ cells is reorganized, and excess cytoplasm is removed. Finally, individual spermatozoa are released into the lumen of the seminiferous tubule due to a reorganization of cell-cell adhesion junctions by a process referred to as individualization in *Drosophila* (Cagan 2003) or as spermiation in mammals (Mruk et al., 1997).

To analyze the AUM expression profile during spermiogenesis in more detail, multiple testis sections were stained for AUM and were analyzed to correlate the AUM expression with the 16 developmental stages of spermatogenesis. The lower panel of figure 30 shows representative cells. The expression of AUM peaks between stage 10 & 15 of spermiogenesis when excess cytoplasm is phagocytosed by Sertoli cells

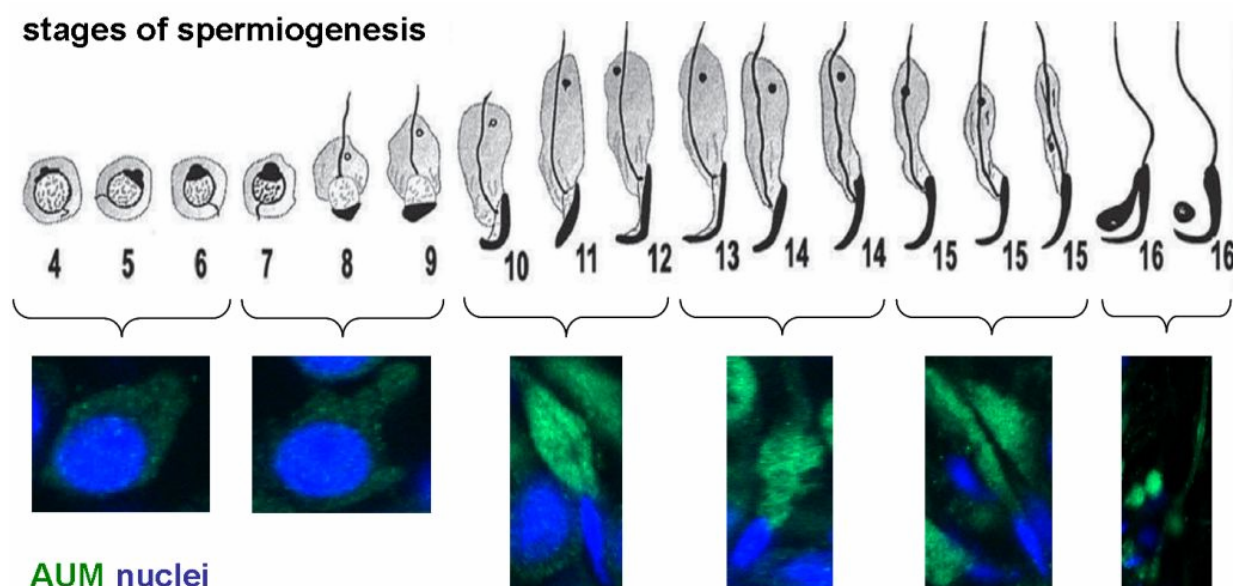


Figure 30: Expression pattern of AUM during spermiogenesis

Upper panel: Schematic representation of the process of rat spermiogenesis, divided into 16 distinct developmental stages, starting from round, non-motile spermatids (stage 4-7) up to elongated, motile spermatozoa (stage 16). Schematic representation of spermiogenesis. Numbers represent steps of spermatid development. (modified from Zheng H. et. al., 2007)

Lower panel: AUM expression pattern was analyzed from at least three separate images of seminiferous tubules stained for AUM and nucleus. Based on the nuclear shape and cell morphology, individual cells were assigned to respective stages of spermiogenesis. The AUM expression peaks between stage 10 and 15 when excess cytoplasm is shed off, giving rise to motile spermatozoa.

Taken together, our expression analysis shows that AUM is a ubiquitously expressed protein that is highly abundant in the maturing male germ cells. AUM expression peaks between stages 10 – 15 of spermiogenesis, suggesting that AUM might have a role in the reorganization of cell-cell adherence junctions between germ cells and Sertoli cells. These

expression data may be useful in the future to devise a strategy to understand the potential role of AUM in the molecular mechanism of the poorly understood processes of spermiation or capacitation.

5.7 AUM knockdown by RNA interference

To analyze the functions of AUM in male germ cells, we transiently or stably depleted the endogenous protein by RNA interference in the murine spermatogonial cell line GC-1 spg (Hofmann et al., 1992).

5.7.1 Transient AUM depletion

AUM was transiently depleted in cells by the transfection of short interfering (si)RNAs. To this end, four different mouse AUM-directed synthetic siRNA oligoribonucleotides targeting different regions of AUM were tested in comparison to a non-targeting control siRNA. Different concentrations (12.5 – 75 nM) of each siRNA oligoribonucleotide were tested in transfection experiments. The best knockdown efficiency was achieved by using siRNA oligoribonucleotides in the concentration range of 12.5 to 50 nM as shown in figure 31.

An efficient AUM knockdown was achieved with three out of the four tested siRNA oligos -041844-10 (AUM siRNA #1), J-041844-11 (AUM siRNA #3) and J-041844-12 (AUM siRNA #4). The sequences of these siRNA oligoribonucleotides along with control siRNA are shown in table 1 (section 4.3.7).

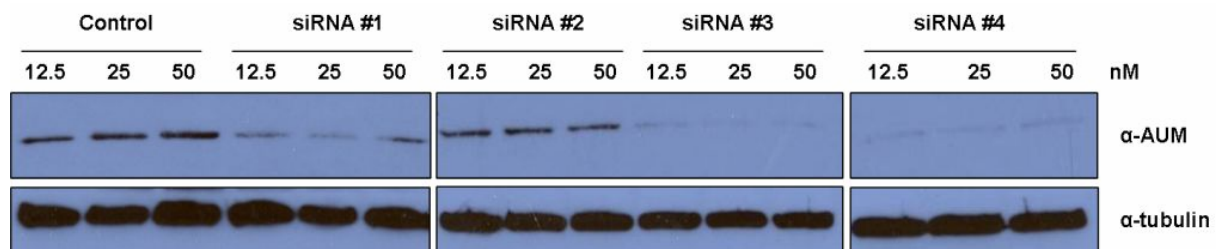


Figure 31: Transient AUM depletion by siRNA

GC-1 spermatogonial cells were transfected with 12.5 - 50 nM of control siRNA or AUM siRNAs #1-4 as described in the Methods (see 4.3.7). Cells were lysed 48 to 72 hours after transfection. Equal protein amounts (20 μ g) of the lysates were separated by SDS-PAGE, transferred onto nitrocellulose membranes and endogenous AUM levels were analyzed by immunoblotting with an AUM-specific antibody. Equal loading was controlled by immunoblotting for tubulin. SiRNA #2 and #3 showed highest knock down efficiencies.

These results demonstrate that the transient transfection of siRNA oligoribonucleotides leads to a robust AUM knock-down efficiency in cells. Nevertheless, this approach only allows the transient suppression of AUM protein expression. Furthermore, the efficiency of transfection may vary in between experiments. Together, these factors may affect the final outcome of the experiment. To solve this problem, and to achieve uniform AUM down regulation over extended time periods, we decided to use a vector-based system to express short hairpin

(sh)RNA (see 4.3.7) in cells. Such a vector-based system may also allow us to establish stable cell lines.

5.7.2 Stable AUM depletion

For a long-term and uniform depletion of AUM protein expression in GC1 cells, five different AUM-specific shRNA sequences targeting different regions of murine AUM were tested. The sequences of these shRNA constructs are shown in table 2 (see section 4.3.7). As detailed in Methods (see 4.3.6), lentiviruses harboring five different shRNAs and one established control shRNA were generated, and used for the transduction of GC1 cells. Cells stably expressing the respective shRNAs were then selected using puromycin.

Figure 32, upper panel shows that two out of five tested shRNA constructs TRCN0000081473 and TRCN0000081477 (#73 & #77), yielded an effective AUM knockdown. All further experiments were done using the stably AUM-depleted GC1 cell line obtained after the transduction of the shRNA construct #77 (referred to as M77) and with the control shRNA GC1 cell line expressing the control shRNA construct SHC002.

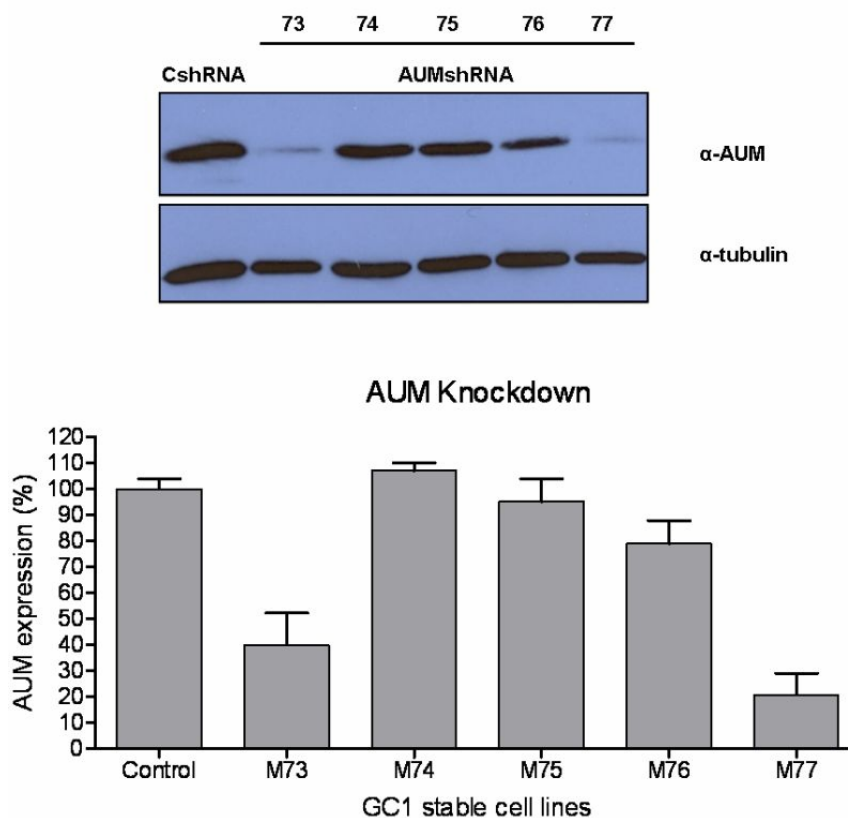


Figure 32: Stable AUM depletion by shRNA

Upper panel: GC1 cells were transduced with lentiviruses encoding for control shRNA (CshRNA) or for five different AUM-directed shRNA constructs (#73-77). Cells were lysed and equal protein amounts (20 μ g) of the lysates were separated by SDS-PAGE and were transferred onto nitrocellulose membranes. AUM levels were analyzed by immunoblotting with the AUM-specific antibody. Equal loading was assessed by immunoblotting for tubulin.

Lower panel: Densitometrical evaluation of AUM knock-down efficiency from three different Western blots.

In order to validate AUM shRNA cell lines and to test the potential function of AUM as a protein tyrosine phosphatase as shown before by overexpression studies (see 5.4.2), we induced the EGFR signaling cascade with epidermal growth factor (EGF) after overnight starvation of shRNA-expressing GC1 cells as detailed under Methods (see 4.4.14). EGF was used as a typical growth factor that is well-known to trigger cellular tyrosine phosphorylation cascades (Schlessinger 2002). GC1 cells were stimulated with 85 nM of EGF for various time points and were probed for global changes in tyrosine-phosphorylated proteins as shown in figure 33. These data suggest that AUM seems to transiently act on tyrosine-phosphorylated proteins, in particular during the initial phase after EGF stimulation. Compared to AUM overexpression studies, the depletion of endogenous AUM triggered more prominent changes in EGF-induced tyrosine phosphorylation.

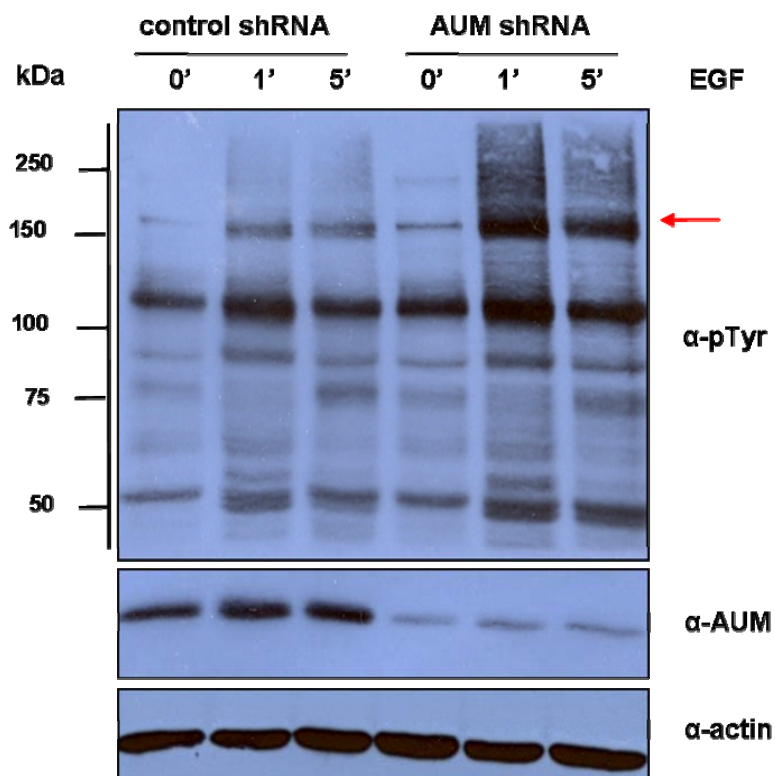


Figure 33: Effect of AUM on cellular tyrosine phosphorylation in EGF-stimulated cells

GC1 cells expressing with the indicated shRNAs were starved overnight in serum-free culture medium. Cells were stimulated with 85 nM of EGF for the indicated time points, and were subsequently lysed in lysis buffer. Equal protein amounts (20 μ g) of the lysates were separated by SDS-PAGE, transferred onto nitrocellulose membranes and tyrosine-phosphorylated levels were analyzed by immunoblotting with the phosphotyrosine-specific antibody 4G10.

Western blots shown here are representative of 3 independent experiments. The results show that AUM can act as a cellular protein tyrosine phosphatase. Arrow indicates modulation of phosphotyrosine content upon AUM depletion.

5.8 Potential role of AUM in epidermal growth factor signaling

Since we observed an increased phosphorylation of high-molecular weight proteins corresponding to the size of the epidermal growth factor receptor (EGFR) in epidermal growth factor (EGF)-stimulated, AUM-depleted cells compared to control shRNA cells (see Fig. 33), we tested the hypothesis that the EGFR itself may be an AUM substrate. The EGFR is a ~180 kDa receptor tyrosine kinase that is phosphorylated on multiple tyrosine residues upon EGF binding (Bazley and Gullick 2005). EGFR phosphorylation triggers the association of various adaptors and scaffolding molecules that propagate the growth factor signal to affect *e.g.* cytoskeletal changes, cell adhesion and motility and cell growth (Biscardi et al., 2000). The EGFR and some of its downstream signaling molecules had already appeared as a possible substrate in the phosphopeptide screen (Fig.19). Cells overexpressing AUM^{wt} or AUM^{D34N} or stably AUM-depleted cells were starved overnight and were subsequently stimulated with EGF for the indicated time points as detailed in Methods (4.4.14).

We analyzed the effect of AUM overexpression or depletion on total EGFR levels as well as on EGFR phosphorylation, using EGFR phospho-specific antibodies. Total EGFR levels were found to be increased in the absence of AUM as shown in figure 34A. Due to technical limitations, we could not reprobe the same blot for various phospho-specific EGFR antibodies. One of the tyrosine phosphorylation sites on EGFR (Tyr1045) is of particular interest due to its potential role in EGFR ubiquitination and trafficking (Levkowitz et al., 1999). Cell lysates from the same experiment were loaded on separate gels and probed with the anti-pTyr1045-EGFR antibody. One min after EGF stimulation, AUM-depleted cells showed increased pTyr1045 phosphorylation, which had disappeared at 5 min, indicating a transient effect of AUM on the EGFR signaling pathway. We used two of our efficiently AUM-depleted cell lines (#73 and #77), and found similar effects as shown in figure 34B.

To rule out cell line-restricted effects of AUM on EGFR phosphorylation, we also analyzed the EGFR pTyr1045 levels in HeLa cells transiently transfected with AUM^{wt} or AUM^{D34N} plasmids. We observed a transient effect on pTyr1045-EGFR levels upon AUM overexpression but at different time points as compared to GC1 cells (Fig. 34C). Only catalytically active AUM was to found transiently affect pTyr1045 levels at 5 min upon EGF stimulation.

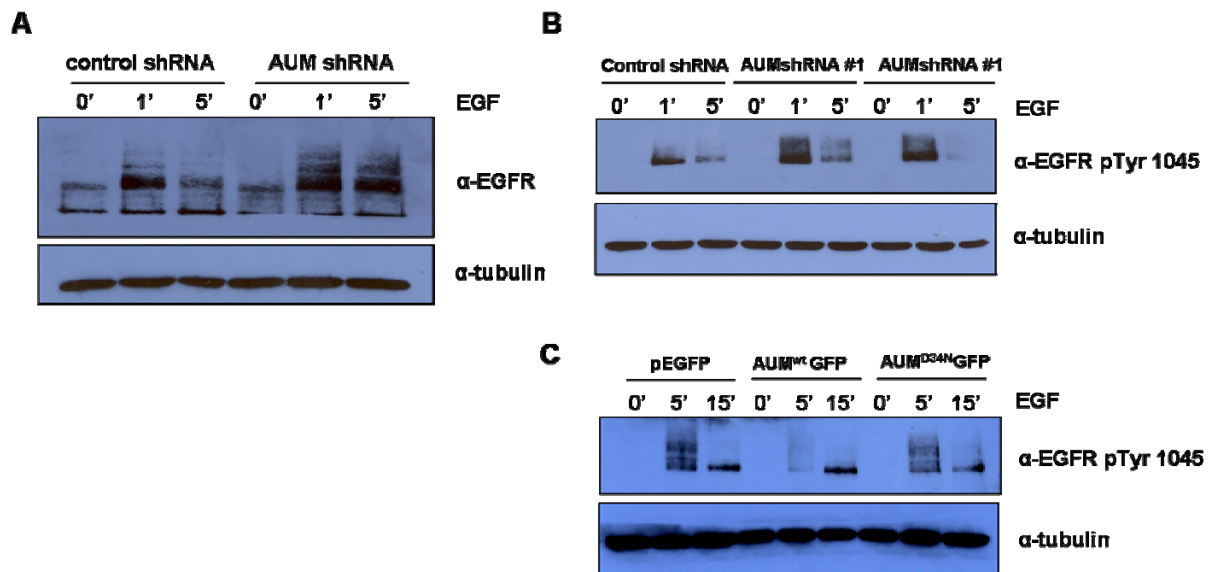


Figure 34: Effect of AUM on EGFR tyrosine phosphorylation

A, B: GC1 cells expressing with the indicated shRNA were starved overnight in serum-free culture medium. Cells were stimulated with 85 nM of EGF for the indicated time points, and were subsequently lysed in lysis buffer. Equal protein amounts (20 μ g) of the lysates were separated by SDS-PAGE, transferred onto nitrocellulose membranes and tyrosine-phosphorylated levels were analyzed by immunoblotting with the phosphotyrosine-specific antibody 4G10.

C: GC1 cells transiently transfected with the indicated plasmids were starved overnight in serum-free culture medium. Cells were stimulated with 85 nM of EGF for the indicated time points, and were subsequently lysed in lysis buffer. Equal protein amounts (20 μ g) of the lysates were separated by SDS-PAGE, transferred onto nitrocellulose membranes and tyrosine-phosphorylated levels were analyzed by immunoblotting with the phosphotyrosine-specific antibody 4G10.

Western blots shown here are representative of 3 independent experiments. The results show that AUM has role in EGFR stabilization and activation.

Taken together, these biochemical results indicate a role of AUM in EGF-mediated signaling pathways, including effects on the EGFR itself.

5.9 Effect of AUM on actin dynamics

Actin filaments are major components of at least 15 different structures such as stress fibres, endocytic pits and peri-organellar ring in multicellular organisms (Chhabra and Higgs 2007). These filaments assemble from a common pool of actin monomers depending upon the extracellular stimuli. Majority of cellular processes such as cell adhesion, migration, adhesion and proliferation involves coordinated and rapid changes in actin cytoskeleton (Mittra et al., 2005). Because of the high homology between AUM and the cofilin activating (and thus actin remodeling) phosphatase Chronophin (CIN), we next investigated the effect of AUM on actin dynamics.

We first examined the effects of AUM^{wt} or AUM^{D34N} overexpression on the actin cytoskeleton of HeLa cells. To this end, HeLa cells were spread on fibronectin (FN) coated surfaces. Serum starved cells were spread on FN coated glass coverslips and fixed at different time points. Cells were stained for microscopic observations as detailed in Methods (section 4.3.3). Figure 35 upper panel shows that AUM^{wt} overexpressing cells were small in

size, with less elaborated actin cytoskeleton and hence less adherent on fibronectin at 40 min as compared to non-transfected or AUM^{D34N} overexpressing cells as shown lower panel of figure 35.

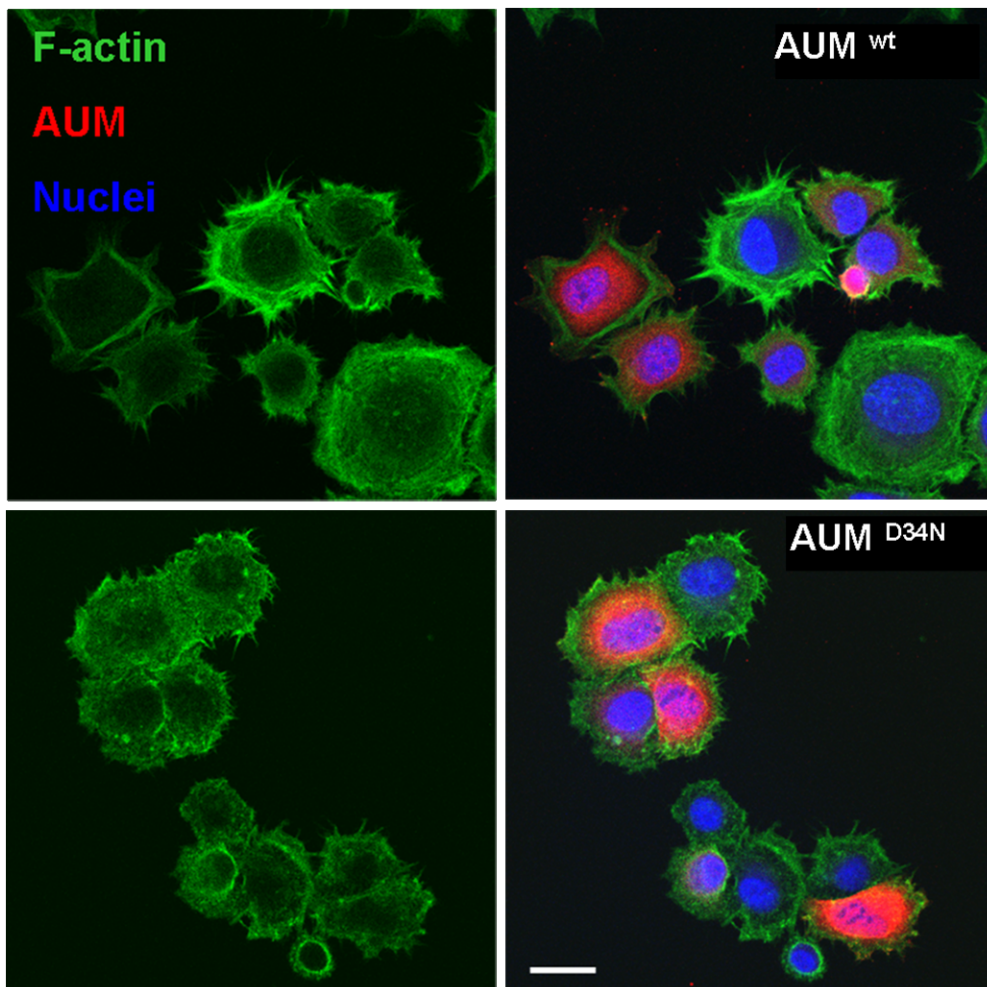


Figure 35: Effect of AUM overexpression on actin cytoskeleton in spreading HeLa cells

HeLa cells were transfected with either AUM^{wt} or AUM^{D34N} and spread on FN coated surface for 40 min. Cells were fixed in PFA and stained as indicated. AUM^{wt} transfected cells are small in size with less prominent actin cytoskeleton where as AUM^{D34N} transfected cells has no such effect as compared to non transfected cells. Scale bar represent 25 μ m.

In order to understand the potential effect of AUM overexpression (Fig. 35) on the dynamics of actin cytoskeletal reorganization, we used the G-actin sequestering drug called latrunculin A. This compound binds to G-actin monomers and thus does not allow new actin polymerization. As the actin cytoskeleton is in constant flux between filament polymerization and depolymerization (Andrianantoandro and Pollard 2006), latrunculin A treatment allows the analysis of the effect of AUM on actin dynamics. AUM overexpressing HeLa cells were treated with latrunculin A as described in Methods (see section 4.4.14).

We found that HeLa cells transfected with AUM^{wt} contain less polymerized F-actin (Fig. 36 upper panel vehicle control). Upon treatment with latrunculin A to sequester actin monomers, this effect becomes more evident as shown in the lower panel of figure 36. The differences between the F-actin structures observed upon latrunculin A treatment between

transfected and non transfected cells suggest a probable role of AUM in actin dynamics. AUM^{wt} transfected cells are characterized by a dramatic loss of polymerized actin upon latrunculin A treatment, as shown in figure 36 lower panel. Interestingly, in the absence of F-actin, AUM appears to relocalize to fibrous structures of unknown identity, as shown in latrunculin A treated cells. This effect was not observed in AUM^{D34N} transfected cells (data not shown).

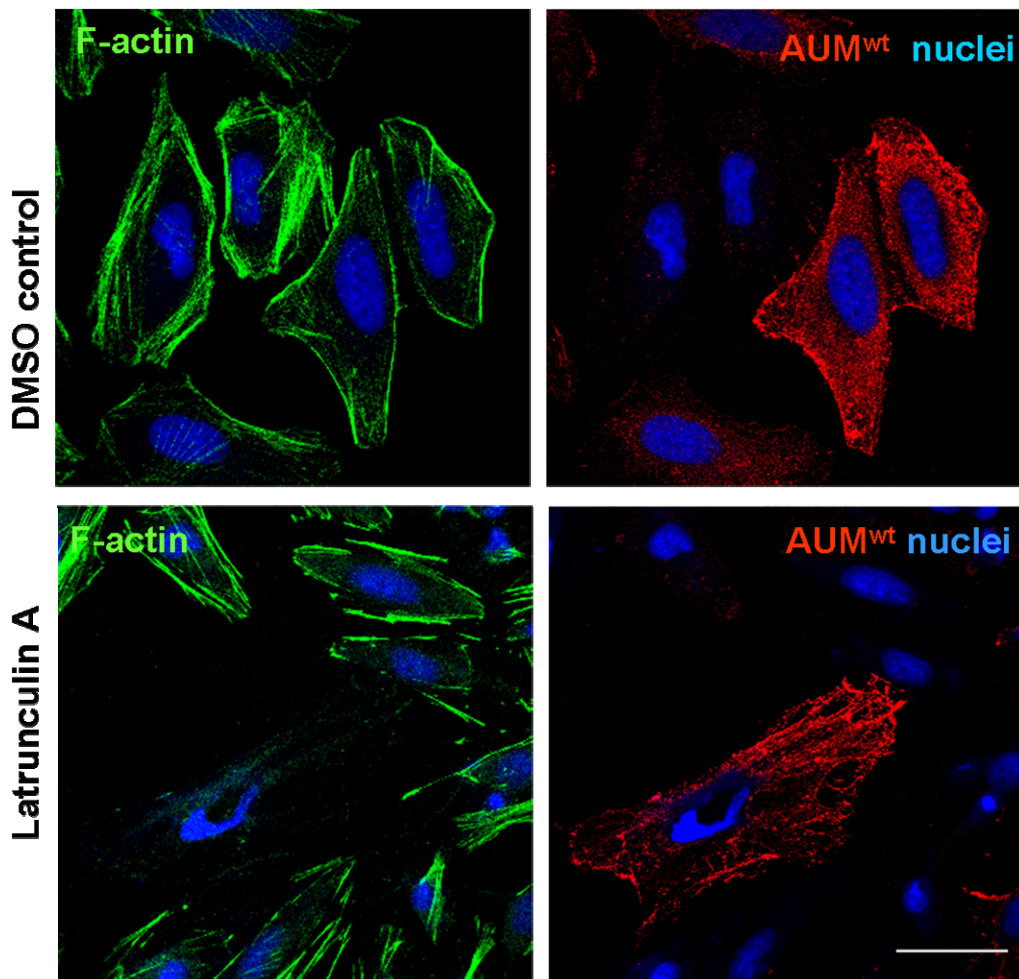


Figure 36: Effect of AUM overexpression on actin dynamics in HeLa cells

Upper panel: HeLa cells transfected with AUM^{wt} were grown in normal growth medium were treated with 2 μ l of DMSO as a vehicle control (1:1000) fixed and stained as indicated.

Lower panel: HeLa cells transfected with AUM^{wt} were grown in normal growth medium were treated with 2 μ M of latrunculin A for 20 min at 37°C. Cells were fixed and stained as indicated. Scale bar represents 50 μ m.

Latrunculin A sequesters G-actin. AUMwt transfected cells shows less F-actin structures as compared to non transfected cells indicating role of AUM in actin dynamics. In absence of F-actin, AUM localization is changed.

To investigate the effect of AUM depletion on actin dynamics in GC1 cells, the latrunculin concentration and incubation time points had to be optimized, because GC1 cells were found to be more sensitive to latrunculin A than HeLa cells. 2 to 10 min incubation at 37°C with 100 nM of latrunculin was found to be optimal for GC1 cells, because it did not cause cell detachment from the substrate or a complete destruction of the cytoskeleton.

Under basal conditions, AUM depleted cells show alteration of the actin cytoskeleton in the form of enhanced stress fibre formation and less cortical actin as compared to control shRNA expressing cells, as shown in upper panel of figure 37. The effect is more evident upon treatment with 100 nM of latrunculin A. Interestingly, AUM depleted cells show lamellopodia formation upon latrunculin A treatment, as shown in lower panel of figure 37. Taken together, these data indicate that AUM activity affects actin cytoskeletal turnover.

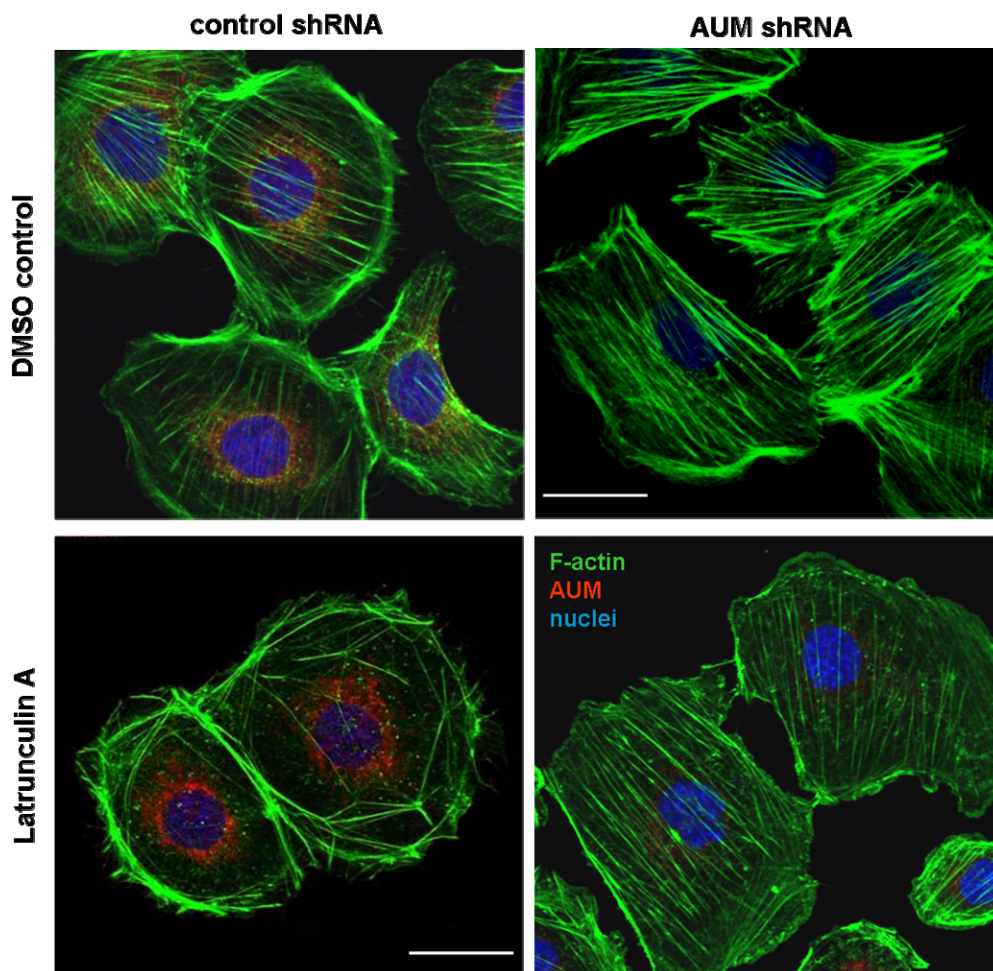


Figure 37: Effect of stable AUM depletion by shRNA on steady-state actin dynamics

Upper panel: GC1 cells stably expressing either control shRNA or AUM shRNA were grown in normal growth medium were treated with 2 μ l of DMSO as a vehicle control (1:1000), fixed and stained as indicated. Lower panel: GC1 cells transduced either with control shRNA or AUM shRNA were treated with 100 nM of latrunculin A for 10 min at 37°C. Cells were fixed and stained as indicated. Scale bar represents 25 μ m. AUM depleted cells shows more F-actin filaments as compared to control shRNA expressing cells

5.10 Role of AUM for cell adhesion

Actin cytoskeletal dynamics coordinate cell adhesion and migration by regulating the turnover of cellular adhesion complexes (Mitra et al., 2005). While working with AUM^{D34N}-expressing and AUM-depleted cells, we observed that these cells appeared more spread than their corresponding controls, and took longer to detach by trypsinization during standard subculturing. These observations suggested a potential role for AUM in cell adhesion.

5.10.1 Effect of AUM activity on cell adhesion to fibronectin

To investigate a possible effect of on AUM activity on cell adhesion, we transfected HeLa cells with AUM^{wt} and AUM^{D34N}, and tested the adhesion of these cells to fibronectin. Fibronectin is a high molecular weight extracellular matrix glycoprotein that is known to be essential for cell adhesion, migration, growth and differentiation (Sieg et al., 1998). Fibronectin binds to the surface of cells via integrin receptors (Schlaepfer et al., 1998). Integrins are clustered in adhesive structures known as focal adhesions (Zaidel-Bar 2009). Focal adhesions are composed of multiple structural and signaling molecules (Geiger et al., 2009) that provide a physical linkage to the actin cytoskeleton (Mitra et al., 2005).

Serum starved AUM^{wt} and AUM^{D34N}, transfected HeLa cells were spread on FN coated surface for 20 and 40 min and then fixed in PFA for microscopic analysis as detailed in section (4.3.3). Most of the proteins in focal adhesion complexes are tyrosine phosphorylated hence we stained cells with pTyr specific antibody. AUM^{wt} transfected cells shows less pTyr proteins and were less adherent to the extracellular matrix (ECM) as compared to AUM^{D34N} transfected cells (Fig. 38A). This observation suggests that AUM phosphatase activity regulates cell – ECM adhesion and that in the absence of catalytically active AUM, cells are strongly adherent to the substratum. As a first approach to quantify this effect, we washed cells after spreading on FN for 20 or 40 min and then measured the protein content of the cell lysates. Figure 38B shows that more AUM^{D34N} transfected cells attached to the substratum as compared to empty vector or AUM^{wt}-transfected cells, as reflected by the higher protein content.

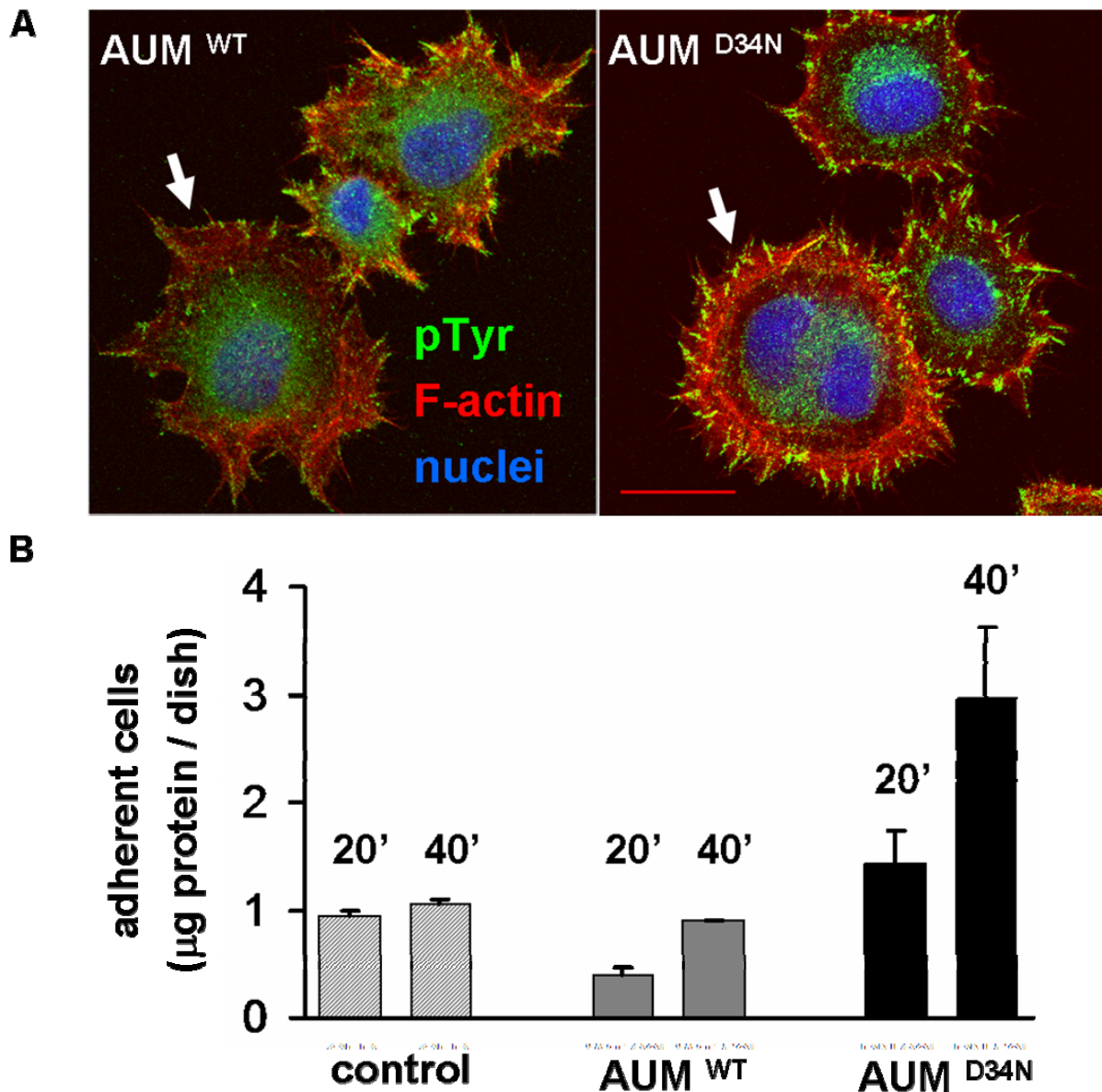


Figure 38: Effect of AUM activity on cell adhesion

A: HeLa cells either transfected with AUM^{wt} or AUM^{D34N} were spread on fibronectin coated surface upon overnight starvation. After 40 min cells were fixed in 4% PFA and stained as indicated. AUM^{wt} transfected cells have less prominent pTyr containing proteins, as compared to AUM^{D34N} transfected cells. The arrows indicate AUM^{wt} or AUM^{D34N} myc-His₆-transfected cells which were identified by staining for the myc-tag (not shown). Scale bar represents 25 µm.

B: HeLa cells either transfected with AUM^{wt} or AUM^{D34N} were starved overnight and spread on fibronectin coated surfaces for 20 or 40 min. The total protein content of the cell lysates in AUM^{D34N} transfected cells is higher at both time points as compared to AUM^{wt} or empty vector transfected cells at corresponding time point.

5.10.2 Effect of AUM depletion on cell adhesion to fibronectin

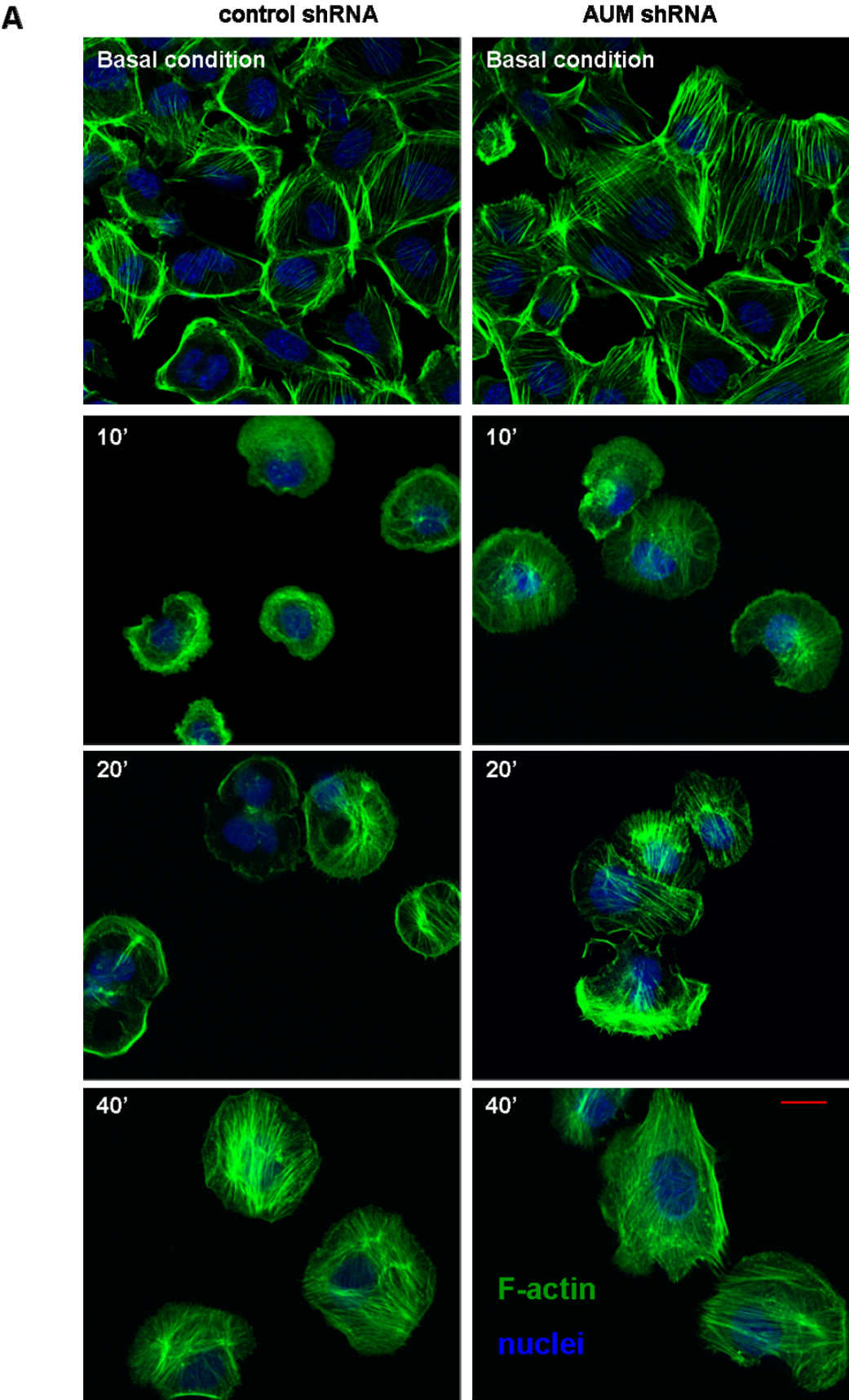
To test whether the depletion of endogenous AUM would also affect cell adhesion on fibronectin we performed microtitre plate adhesion assay. We used calcein AM (Invitrogen Karlsruhe), a nontoxic, cell permeable compound for quantitative measurement of cell adhesion. Calcein AM gets converted into negatively charged green fluorescent calcein by

esterases once entered into live cells and stained cells can be quantified fluorimetrically at 535 nm. Control shRNA or AUM shRNA expressing cells were treated with 0.1 μ M calcein for 30 min at 37°C and then equal number of cells were spread on FN coated surface for 10, 20 or 40 min. AUM depleted cells were found to be more adherent at 10 min of spreading on FN as compared to control shRNA expressing cells. This effect was less prominent at later time points suggesting that AUM has role in early events of spreading on FN (data not shown). In absence of AUM, cells appeared to be strongly adhere to the substratum and this phenomenon is being investigated in further details at the moment in our lab.

5.10.3 Effect of AUM depletion on cell area during spreading

To test the potential effect of AUM depletion on cell spreading, we next analyzed the kinetics of cell spreading by cell area measurements using a semiautomated microscopic approach. For this, cells were serum-starved, detached by limited trypsinization as described in Methods (see 4.3.1), seeded on FN-coated surfaces and were finally fixed at various time points. Cells were then stained for polymerized actin using phalloidin and nuclei were labeled using DAPI (see 4.3.3). As detailed in Methods (see 4.4.15), the cell area was detected using the stained actin, and each cell was identified by its nuclear stain. Cells were spread on 96 well plates (15 μ ibidi plates, ibidi, Munich) coated with FN. Cells were fixed after 10, 20 and 40 min of spreading on FN, and cell areas were quantified by taking four fields of view per well. For quantification, 5 replicates of each condition were used. Data shown here are from 3 independent experiments with a minimum 1000 cells counted per condition. Figure 39A shows representative pictures of each condition. AUM depleted GC1 cells at 10 min of spreading were found to be 21% larger in size as compared to control shRNA expressing cells as shown in figure 39B. The effect on cell size between control shRNA and AUM shRNA expressing cells diminishes at later time points, indicating a role of AUM in early events of spreading.

The effect of AUM on cell size could even be observed under basal conditions (that is, adherent cells growing under standard conditions). The images indicating the effect of AUM on cell size under basal conditions are taken from a separate experiment and are included in this panel for comparison.



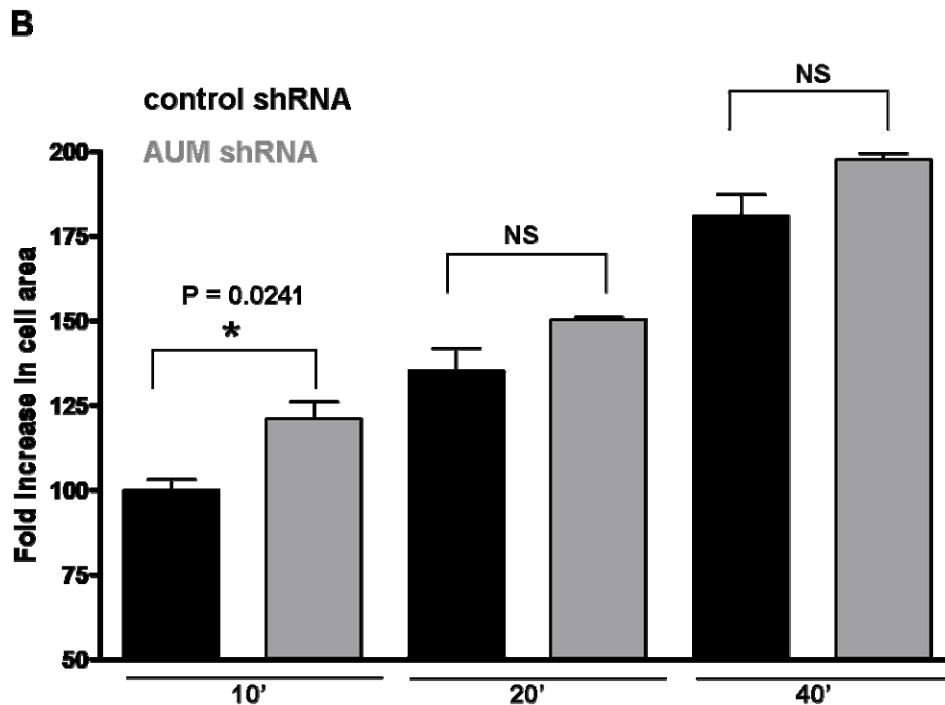


Figure 39: Effect of AUM on area of spreading cells

A: GC1 cells expressing control shRNA or AUM shRNA were spread on FN-coated microtiter plates for 10, 20 and 40 min and fixed. Cells were stained as indicated. Scale bar represents 25 μ m. Cells with AUM depletion are larger in size from early stage of spreading on, as compared to control cells.

B: Quantification of cell area of spreading cells. Minimum of 1000 cells were counted per condition. Arbitrary units of cell area were obtained and were normalized against control shRNA expressing cells at 10 min of spreading and plotted as fold increase of size with respect to it for all conditions. Cells expressing AUM shRNA are larger in size at all time points but the only the difference at 10 min is statistically significant ($P = 0.0241$), as calculated by Student's t-test. These results suggest a role of AUM in early events of cell spreading.

5.10.4 AUM localization in spreading cells

So far we have observed effect of AUM overexpression or depletion on cell spreading. The spreading of cells is largely governed by focal adhesion turnover (Geiger et al., 2009). So the next question was whether AUM is actually present in these structures. Focal adhesion (FA) structures are composed of many constitutively present proteins such as paxillin, vinculin or talin (Mitra et al., 2005). GFP-AUM^{wt} expressing HeLa cells were fixed upon spreading on fibronectin for 40 min and stained with vinculin as a marker for FA as detailed in section (4.3.3). AUM was not found to colocalize with vinculin as shown in figure 40. Interestingly there are many focal adhesion associated proteins which are recruited to adhesion sites, (Zaidel-Bar et al., 2007) and very few are constitutively present in FA. AUM localization in fact was found to be around the structures of FA at 40 min of spreading on FN in HeLa cells.

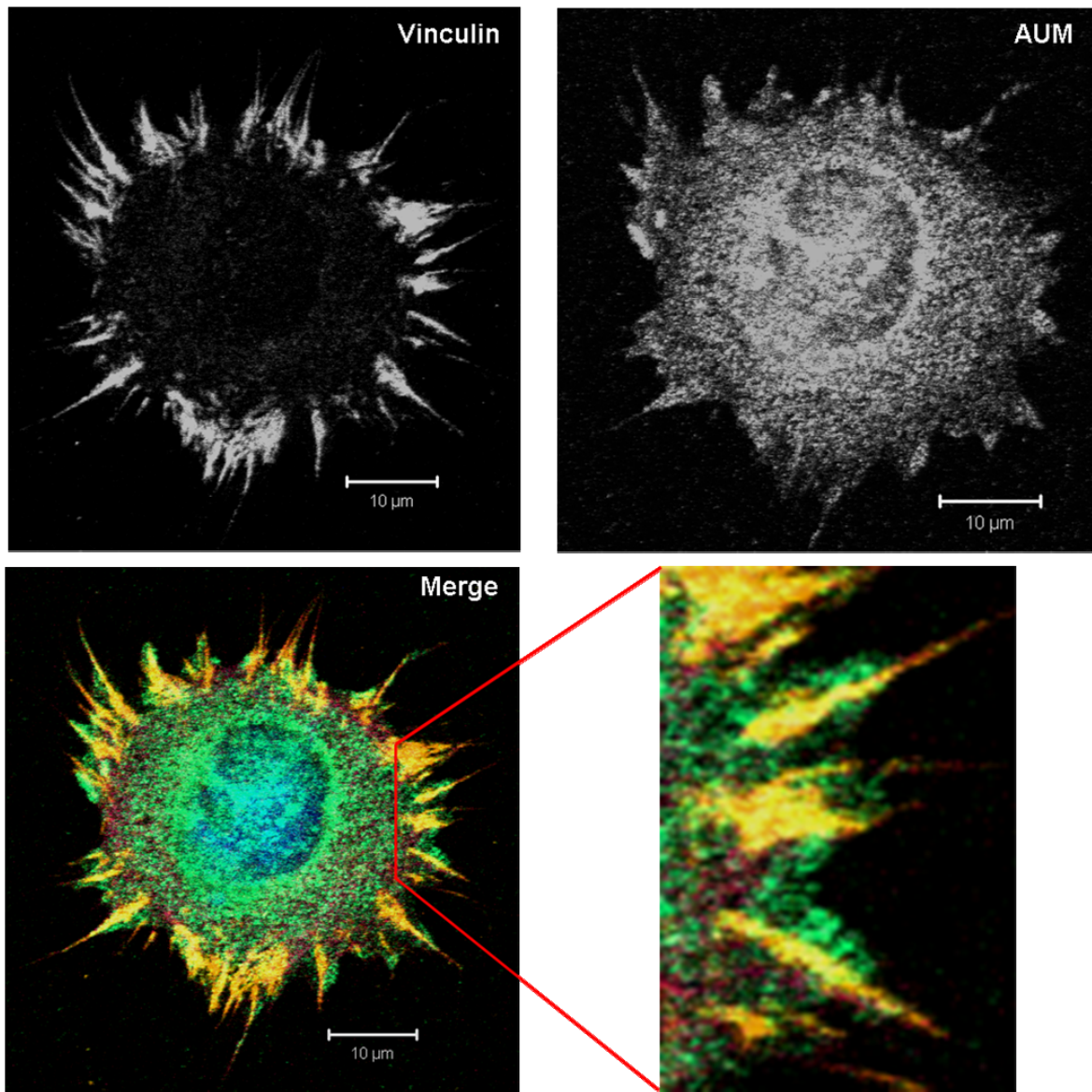


Figure 40: AUM localization in spreading cells

HeLa cells transfected with GFP-AUM^{wt} were spread on fibronectin coated glass coverslips for 40 min. The PFA-fixed cells were then stained for the focal adhesion marker vinculin. The nucleus was stained with DAPI. AUM was localized by the fluorescence of its GFP-tag. Part of the merged image is magnified in lower right panel and shown AUM localization with respect to vinculin. AUM does not colocalize with vinculin in focal adhesions at 40 min of spreading on fibronectin. Scale bar represents 10 μ m.

5.10.5 Effect of AUM depletion on phosphotyrosine content of focal adhesions in spreading cells

Even though we did not find AUM localization in focal adhesion structures, we had consistent cell morphological effects in terms of cell area, and a distinct adhesion behavior of AUM depleted cells, indicating a role of AUM in these processes. Cell area determination of spreading cells at different time points already suggested a probable role for AUM in the early events of spreading. Instead of analyzing colocalization of AUM with one of the FA markers under various spreading conditions, we decided to analyze the levels of total

phosphotyrosine content of cells under spreading conditions. Control or AUM shRNA expressing GC1 cells were serum starved and spread on fibronectin coated glass coverslips for 10 min and fixed for microscopic observations as described in Methods (see 4.3.3). AUM depleted cells showed enhanced levels of phosphotyrosine content of focal adhesion structures, as shown in figure 41 when compared to control shRNA expressing cells. Many focal adhesion proteins are known to be tyrosyl phosphorylated upon activation, which leads to a strong adhesion to the ECM (Bass et al., 2008). Thus along with the experimental evidence of role of AUM on adhesion at 10 min of spreading on fibronectin (data not shown), this functional read out suggest that AUM is specifically acting in the signaling pathway involved in early cell spreading.

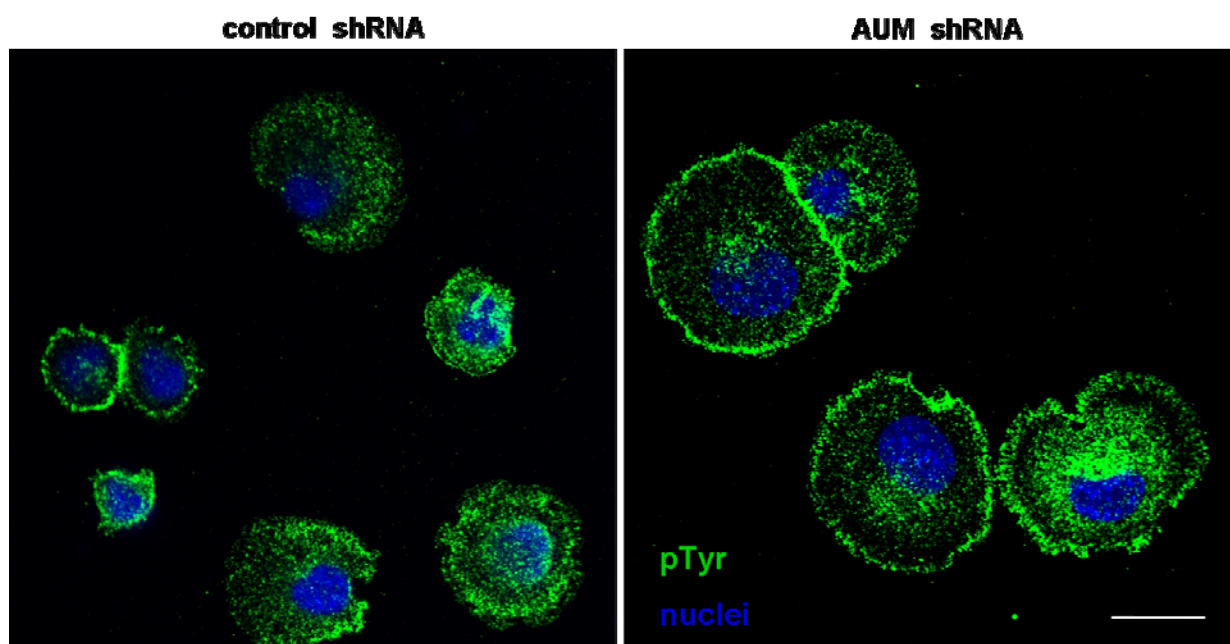


Figure 41: Effect of AUM depletion on phosphotyrosine content of focal adhesion in spreading cells

GC1 cells with either control shRNA or AUM shRNA were spread on fibronectin coated surface for 10 min. PFA fixed cells are stained as indicated. AUM depleted cells have increased phosphotyrosine content of focal adhesions leading to strong cell-ECM adhesion at 10 min of spreading on fibronectin. Scale bar represents 25 μ m.

5.10.6 Effect of AUM depletion on focal adhesion maturation in spreading cells

Focal adhesion structures are at the base of the cell surface anchoring the cell to substratum. To image these structures a variety of microscopic methods have been developed over the time (Holt et al., 2008) such as interference reflection microscopy (IRM) or total internal reflection microscopy (TIRF). We employed TIRF microscopy to visualize these structures in order to understand the effect of AUM depletion on focal adhesion maturation in spreading cells. TIRF microscopy uses an evanescent wave for the selective illumination of a fluorophore in a restricted region of the specimen immediately adjacent to

the glass-water interface. The evanescent wave is generated only when the incident light is totally reflected at the glass-water surface allowing selective visualization of surface regions. Control or AUM shRNA-expressing GC1 cells were spread on fibronectin coated glass surfaces for 40 min and fixed in PFA for microscopic analysis as detailed in Methods (see 4.3.3). Cells were then stained for polymerized actin using phalloidin, for focal adhesions using vinculin and nuclei were labeled using DAPI. As shown in figure 42 below, control shRNA expressing cells have predominantly small focal complexes at the cell periphery whereas AUM depleted cells show elongated focal adhesions oriented towards the center of the cell. Focal adhesion structures at the center are found to be at the base of F-actin stress fibres providing mechanical support to the cell during spreading and adhesion (Zaidel-Bar et al., 2007), thus allowing strong adhesion of the cells to the substratum.

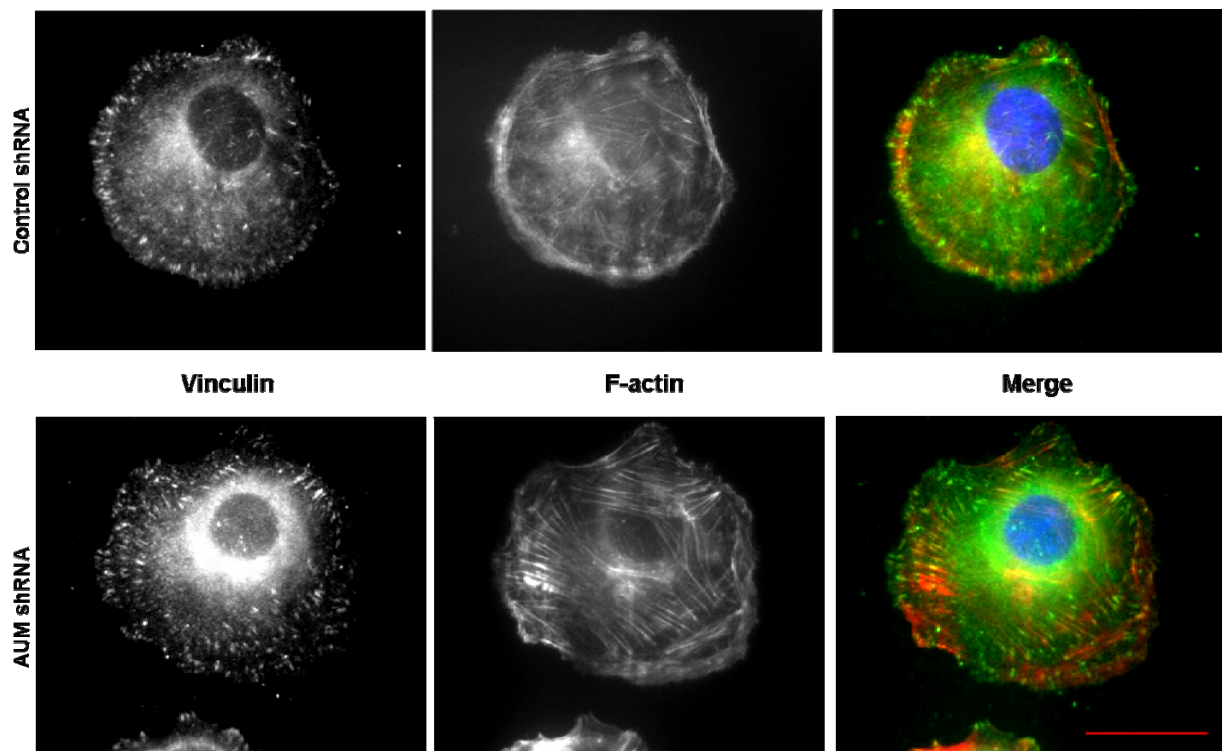


Figure 42: Effect of AUM on focal adhesion maturation in spreading cells

GC1 cells expressing control or AUM shRNA were spread on fibronectin coated surfaces for 40 min. PFA fixed cells are stained as indicated. Images are taken on a TIRF microscope for visualization of focal adhesion structures stained with vinculin. AUM depleted cells have longer focal adhesion structures towards the center of the cell suggesting a role of AUM in focal adhesion maturation during spreading. Scale bar represents 25 μm .

5.11 AUM-Src phosphocycling

In order to understand the molecular mechanisms underlying the spreading behavior of AUM depleted or overexpressed cells, we decided to investigate the status of downstream effector proteins in EGFR and integrin mediated pathways. We had an indication of Src as a probable AUM target from the genome-wide peptide screen (see section 5.3). Hence we decided to analyze the regulation of Src in further detail. Src is a non-receptor tyrosine kinase that acts as a proto-oncogene (Sheiness and Bishop 1979). There are multiple Src family members, *i.e.* c-Src, Fyn, Blk, c-Fgr, Hck, Lck, Lyn, c-Yes and Yrk that are well characterized for their role in various signaling pathways (Yeatman 2004). Src is ubiquitously expressed and plays key role in cell differentiation, motility, proliferation and survival. As Src is a central molecule in multiple signaling pathways, it is under tight regulation governed by multiple regulatory mechanism (Roskoski 2005). 95% of Src in cells is in inactive form and can transiently be targeted to the plasma membrane upon activation. A direct role of Src in focal adhesion turnover has been well documented. Src initiates the activation of various proteins such as focal adhesion kinase (FAK) involved in cell-ECM adhesion (Oberfell et al., 2002).

We first analyzed the effect of AUM on Src phosphorylation (on the phosphotyrosine sites which govern Src activity) upon FN stimulation or EGF stimulation in AUM overexpressed or depleted cells. There were no consistent results with this approach. Figure 43 shows one of the representative blots where the level of phosphorylation of Tyr416 on Src, which is important for Src activation, shows minor variations. Due to experimental limitations, we were not able to reprobe blots developed with Src-phosphospecific antibodies for total Src. Hence the blot probed for pTyr416-Src is of the same cell lysate as the blot for total Src, but was loaded on a separate gel.

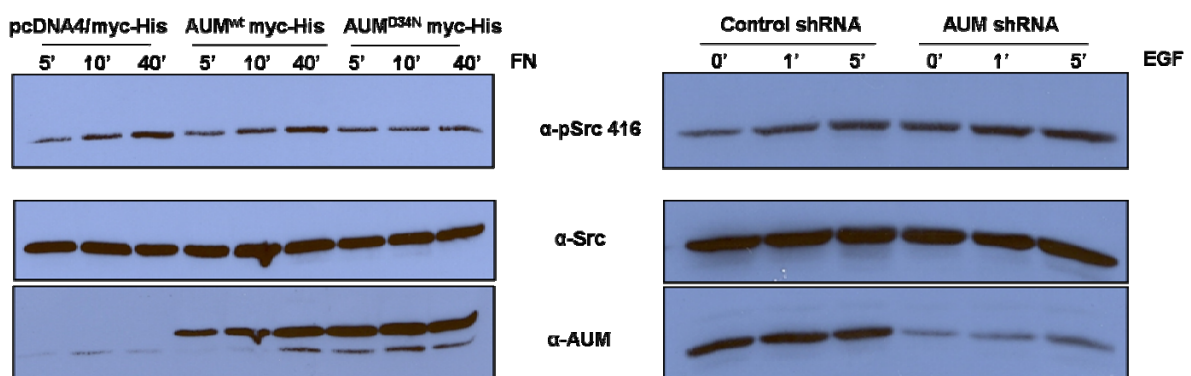


Figure 43: Effect of AUM on Src phosphorylation upon fibronectin stimulation

GC1 cells transfected with indicated plasmids or stably AUM depleted were starved overnight in serum free culture medium. Cells were spread on FN coated surfaces or stimulated with EGF for the indicated time points and lysed in lysis buffer. Equal protein amounts (20 μ g) from lysates were separated by SDS-PAGE, transferred on nitrocellulose membranes and phosphotyrosine levels were analyzed by immunoblotting with 4G10 antibody. Western blots shown here are representative of 3 independent experiments. There is no robust effect on Src phosphorylation under the given conditions.

Hence, we decided to investigate whether there is direct effect of purified AUM on activated Src as a potential substrate in *in vitro* assays. To that end, recombinantly expressed, purified GST-tagged Src was subjected to *in vitro* phosphatase assay along with recombinant AUM as detailed in Methods. AUM could partially dephosphorylate Src as shown in figure 44A. Interestingly, Src in turn was found to phosphorylate AUM. A few other phosphatases such as PTP ϵ are known to be regulated by Src-mediated phosphorylation (Berman-Golan and Elson 2007). We also analyzed the effect of AUM on two regulatory phosphorylation sites on Src (pTyr 416 and pTyr527) in a separate experiment as shown in the lower panel of figure 44A. Src-Tyr416 was not obviously dephosphorylated by AUM using this experimental approach. Also the Src-Tyr527 site was not reproducibly dephosphorylated. These results suggest that AUM may dephosphorylate Src on a different tyrosine residue, and/or that the chosen experimental approach is not sufficiently sensitive to monitor dynamic changes in the phosphorylation pattern.

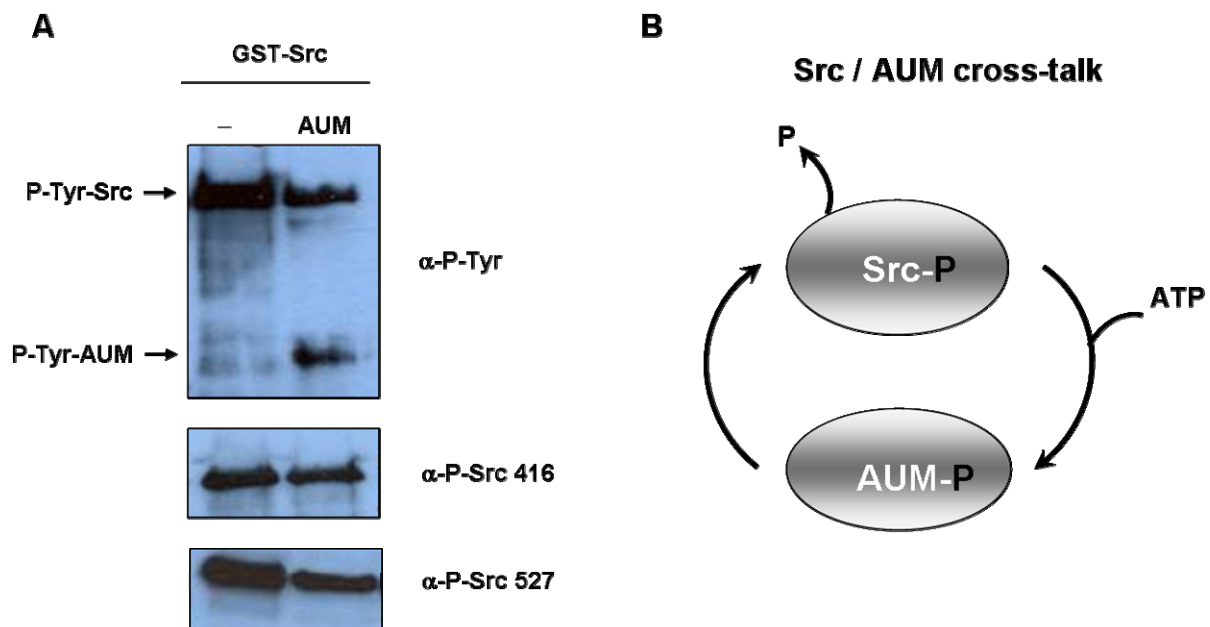


Figure 44: Cross talk between Src and AUM

A: One hundred ng of phosphorylated GST-Src was incubated with 1 μ g of purified, recombinant AUM^{wt} protein for 30 min at 30°C. The reaction was stopped by Laemmli buffer and proteins were separated by SDS-PAGE, transferred onto nitrocellulose membranes and phosphotyrosine levels were analyzed by immunoblotting with 4G10 (pTyr) antibody. AUM partially dephosphorylates Src, and Src phosphorylates AUM on tyrosine residue(s). Src dephosphorylation on pTyr 416 and pTyr 527 sites was analyzed on separate gels. No consistent dephosphorylation of Src by AUM on either site was observed.

B: Proposed model of Src-AUM interaction. In presence of ATP, active Src phosphorylates AUM on tyrosine residue and AUM in turn dephosphorylates Src at an as yet unidentified residue.

We next analyzed the potential effect of AUM on Src kinase activity. To that end we employed a biotinylated peptide which acts as Src substrate. Src kinase activity towards this substrate peptide was measured colorimetrically in the presence or absence of AUM as detailed in Methods (see section 4.4.13). Simultaneously AUM phosphatase activity was also measured in presence or absence of Src. Simultaneously, AUM phosphatase activity was also measured in presence or absence of Src. We found a strong increase in Src kinase activity towards the Src substrate peptide in the presence of AUM (Fig. 45). Unexpectedly, both AUM^{wt} and AUM^{D34N} activated Src kinase activity to a comparable extent (Fig. 45). These results indicate that AUM activates Src independent of its phosphatase activity

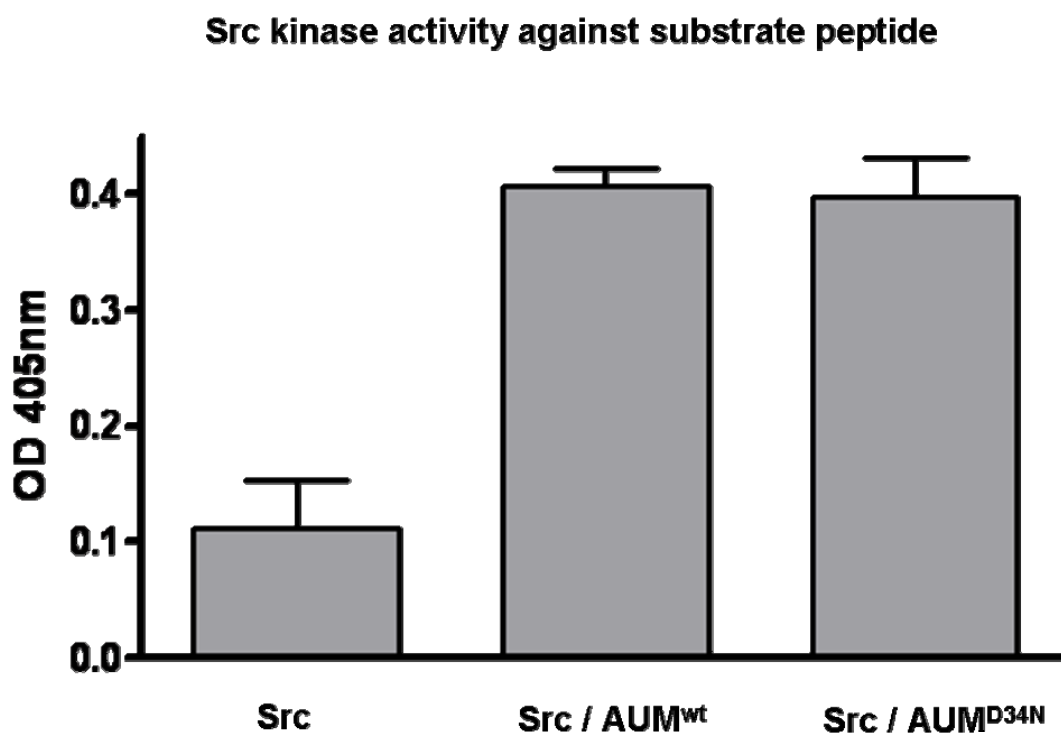


Figure 45: Effect of AUM on Src kinase activity

Fifty nanograms of purified GST-Src and 250 ng of purified AUM^{wt} or AUM^{D34N} were incubated in the presence of a biotinylated Src substrate peptide for 40 min at RT. Src kinase activity towards the peptide was measured colorimetrically at 405 nm for 30 min. Samples were tested in duplicates and the end point values of three independent experiments are plotted. Src kinase activity is increased 3-fold in the presence of catalytically active or inactive AUM

The effect of Src on AUM phosphatase activity was measured using the *p*-NPP assay as detailed in Methods (see section 4.4.11). AUM phosphatase activity towards *p*-NPP is reduced in presence of kinase-active Src, as shown in figure 46. When the Src kinase activity is inhibited by using the Src kinase inhibitor PP2, or when the Src kinase reaction is incubated with apyrase to degrade the ATP the AUM phosphatase activity towards *p*-NPP remains unaffected. Taken together, these data suggest that although AUM regulates Src

kinase activity *in vitro* in a phosphatase independent manner, Src regulates AUM phosphatase activity in kinase dependent manner.

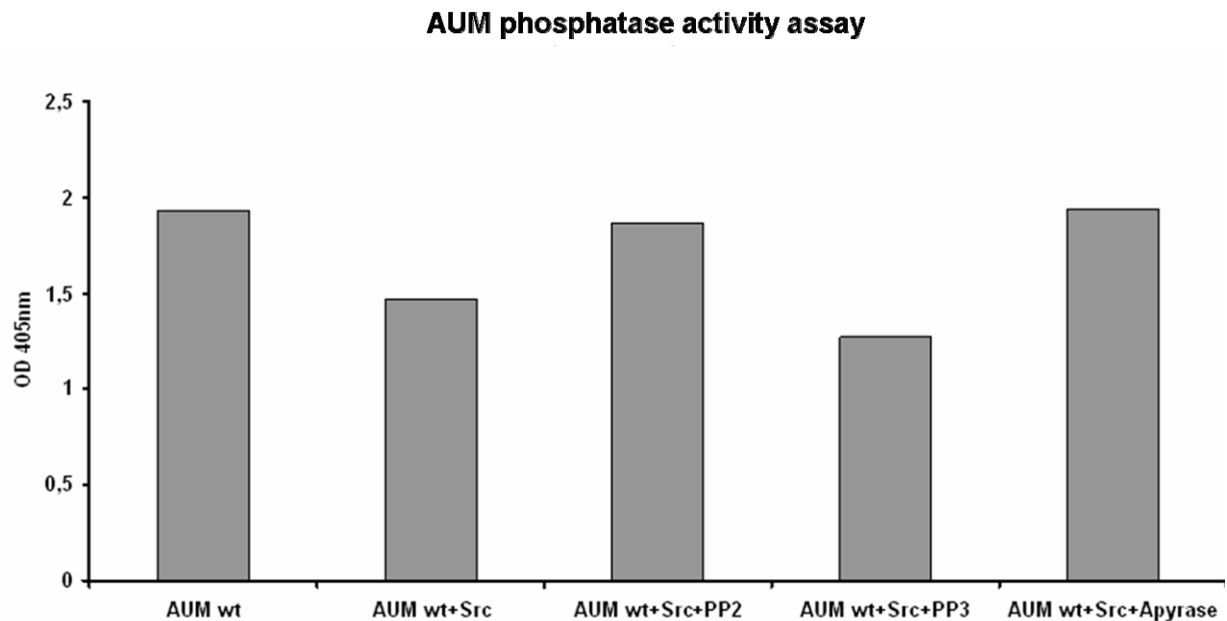


Figure 46: Effect of Src on AUM phosphatase activity

Fifty nanograms of purified GST-Src and 250 ng of purified AUM^{wt} or AUMD^{34N} were incubated for 40 min at RT. AUM phosphatase activity towards *p*-NPP was measured at 405 nm for 60 min and end point values were plotted. Samples were run in duplicates and values represent the mean of a single experiment. Active Src decreases AUM phosphatase activity. In the presence of the Src inhibitor PP2 (5 μ M) or the ATPase apyrase (0.02 U/ml), Src does not affect AUM phosphatase activity. These results suggest that Src may regulate AUM phosphatase activity in a kinase dependent manner.

Taken together, even though we are still far from concluding about the nature of the Src / AUM cross talk in cells, our *in vitro* data strongly suggest that AUM might be yet another player in the complex regulation of Src.

6 Discussion

The evolution of enzyme-mediated chemical reactions relies on mutational changes within the catalytic domain or core chemistry of the entire catalytic mechanism (Lahiri et al., 2004). The HAD superfamily of hydrolases is one such classic example which represents all known extant phyla and has undergone extensive diversification to give rise to at least five distinct subfamilies: the haloalkanoate dehalogenases (C-Cl bond hydrolysis), phosphonoacetaldehyde hydrolases (P-C bond hydrolysis), phosphate monoesterases (P-OC bond hydrolysis), ATPases (P-OP bond hydrolysis), and phosphomutases (P-OC cleavage with intramolecular phosphoryl group transfer (Allen and Dunaway-Mariano 2004). The core chemistry of this superfamily is nucleophilic catalysis mediated by an active-site aspartic acid carboxylate group. The majority of HAD hydrolases from lower organisms are assumed to be involved in nucleotidase activity, sugar and amino acid metabolism (Balakrishnan et al., 1993; Kuznetsova et al., 2006).

In addition to their phosphatase activity against sugars etc., HAD family members have also acquired protein phosphatase activity during eukaryotic evolution. Members of the HAD superfamily are therefore considered to be key players in providing raw material for the evolution of novel enzymes, leading to the diversification of enzymatic potential (Burroughs et al., 2006). These innovations were transmitted by lateral gene transfer at various time points and recruited for new functions as recently realized for many novel HAD phosphatases (aspartate-based phosphatases) in higher organisms (Collet et al., 1998; Selengut 2001; Rayapureddi et al., 2003; Singh et al., 2004; Gohla et al., 2005).

The goal of this thesis was the characterization of a previously undescribed, Chronophin (CIN)-related HAD phosphatase, which we named AUM (actin remodeling, ubiquitously expressed, magnesium-dependent HAD phosphatase). This work shows that rather than being a CIN-isoform, AUM is a novel aspartate-based phosphatase with unique enzymatic qualities.

6.1 AUM is not a CIN isoform

HAD phosphatases are typified by a highly conserved, tripartite catalytic domain, composed of the HAD motifs I-III (Ridder and Dijkstra 1999). Outside of these small conserved motifs, rarely there is an overall homology among HAD phosphatases. In spite of this fact, CIN and AUM were found to be 45% identical and 61% similar at the amino acid level (see 1.3.1). Hence we started the characterization of AUM as a putative CIN homolog in the beginning. Unexpectedly, the results of the enzymatic characterization of AUM clearly showed the distinct characteristics of AUM in comparison to CIN. By comparing the results from work on the characterization of the serine-directed phosphatase CIN (Gohla et al., 2005) and

experimental evidence from the present work on AUM, AUM emerges as a novel tyrosine phosphatase in spite of being the closest CIN homolog. These results are listed in table 4.

Table 4: Comparison of the characteristics of AUM and CIN

AUM is a CIN homolog	AUM is a novel tyrosine phosphatase
high sequence similarity (Fig. 5)	
similar gene structure (Fig. 6)	AUM and CIN map to different chromosomes in humans and mice (Fig. 6)
evolutionarily conserved (Fig. 6 & (Gohla et al., 2005))	AUM has evolved independently in higher organisms (Fig. 15)
HAD-type phosphatase (Figs.10,18 & (Gohla et al., 2005))	
AUM has (weak) activity toward the CIN substrate PLP (Fig. 17)	AUM dephosphorylates the tyrosine-like substrate <i>p</i> -NPP much more efficiently than CIN (Fig. 17)
	AUM prefers pTyr residues in peptides and proteins as substrates (Figs. 19, 20)
ubiquitously expressed (Fig. 25 & (Gohla et al., 2005))	tissue specific AUM expression is distinct from that of CIN (Fig. 25 & (Gohla et al., 2005))
role in actin cytoskeletal dynamics (Figs. 36, 37 & (Gohla et al., 2005))	AUM has a role in the early events of cell spreading that are mediated by tyrosine phosphorylation (Figs. 39, 41)
	AUM might have a role in signaling cascades initiated by transmembrane receptors (Fig. 48)
predominantly cytosolic proteins (Fig. 36 & (Gohla et al., 2005))	

We analyzed the evolutionary relationships between CIN and AUM phosphatase orthologs by constructing phylogenetic trees (Fig. 15) and found that both evolved together in lower organisms where they might exert similar functions. However, in vertebrates CIN and AUM orthologs have evolved independently and may thus have acquired novel functions.

We then analyzed the pattern of CIN/AUM evolution in the context of other known human HAD phosphatases in two model organisms as shown in Fig.16. The availability of raw material in the form of novel catalytic characteristics is a prerequisite for the diversification of enzymatic potential during the course of evolution as discussed earlier (Burroughs et al., 2006). At least eight distinct signaling pathways are known to have evolved exclusively in multicellular organisms. These are nuclear hormone receptor pathways, WNT, TGF- β , JAK/STAT, Notch/Delta, hedgehog, toll-like receptors and phosphotyrosine (pTyr) mediated signaling pathways (Pires-daSilva and Sommer 2003).

P-Tyr signaling has played a prominent role in the expansion of metazoans by creating a versatile three component system in the form of a “writer” (a tyrosine kinases), a “reader” [Src homology 2 (SH2) domain containing proteins], and an “eraser” (tyrosine phosphatases) (Pincus et al., 2008). Each component of this three component system has evolved at different stages of evolution. However, effective pTyr signaling was possible only when all three components were present together. Hence even though in yeast, proteins with SH2 domains and PTP domains were present, there was no pTyr signaling due to the absence of protein tyrosine kinase (PTK)-domain containing proteins. It is only in metazoans that all three components are present, which gave rise to efficient pTyr signaling (Pincus et al., 2008). Figure 16 and our data showing AUM as an efficient *p*-NPP phosphatase (Fig. 17) clearly suggest that the independent evolution of AUM was a prerequisite for AUM to act as novel pTyr phosphatase in metazoans. These results are corroborated by the data showing that AUM acts as a protein tyrosine phosphatase (see 6.5).

6.2 AUM expression analysis

In order to analyze the expression pattern of this novel protein, we generated an AUM specific rabbit polyclonal peptide antibody. The sensitivity and specificity of this antibody allowed us to analyze the AUM expression pattern in various mouse tissues and cells in culture by multiple approaches. AUM peptide antibody is able to detect as little as 10 ng of recombinant protein without cross reacting with its closest homolog CIN (Fig. 24). AUM was found to be a ubiquitously expressed protein of 34 kDa (Figs. 22, 23, 25, 27). Both at the RNA and protein level AUM expression was highest in male germinal cell (Figs. 27, 28, 29). AUM expression was maximal around 4 weeks of age in mouse testis (Fig. 27), corresponding to the age of puberty (Livera et al., 2006). This information indicated a probable physiological role for AUM in spermatogenesis. Immunohistochemical approaches

confirmed this assumption (Figs. 27, 28, 29). The AUM expression profile in male germ cells coincides with the poorly understood process of individualization or spermiation (Cagan 2003).

Nevertheless, this descriptive expression analysis can not be translated into a functional understanding of the role of AUM in testis without a primary knowledge of AUM biology. Given the ubiquitous expression of AUM, which suggests a broader and fundamental role for AUM outside testis, the subsequent functional analysis of AUM was conducted by biochemical and cell biological approaches using a mouse spermatogonial cell line, GC1-spg. Given the fact that spermiation is essentially an actin-dependent process involving massive cytoskeletal reorganization and cell-matrix and cell-cell adhesion modulations between germ cells and Sertoli cells (Xiao and Yang 2007), the role of AUM in cell adhesion to the extracellular matrix was analyzed in greater detail.

6.3 Role of AUM in actin dynamics

Actin filaments are polarized structures with fast growing barbed ends and slow growing pointed ends. The dynamics of actin filaments is under tight regulation which is necessary for cell migration, proliferation and polarity formation (Revenu et al., 2004). As CIN was shown to be cofilin phosphatase (Gohla et al., 2005) and AUM found to be at least partially affecting the cellular phosphocofilin pool (Duraphe Prashant, Diploma thesis 2006) we decided to analyze the effect of AUM on actin dynamics.

In vitro polymerization or depolymerization assays of pyrene-labeled actin in the presence of recombinant, purified AUM did not show any direct effects of AUM on actin dynamics (data not shown). However, a preliminary analysis of AUM overexpressing cells by scanning electron microscopy suggested an effect of AUM on cell morphology (data not shown). AUM overexpressing or AUM depleted cells were consistently found to display altered F-actin structures (Fig. 35). Hence we concluded that AUM affected actin remodeling indirectly. This hypothesis was tested by employing the G-actin sequestering drug, latrunculin A. Cells treated with latrunculin A allowed us to analyze the effect of AUM on actin turnover by sequestering newly formed G-actin molecules. We found a stabilization of actin stress fibres in cells overexpressing AUM^{D34N} (data not shown) as well as in AUM depleted cells (Fig. 37). In contrast, AUM^{wt} overexpressing cells showed fewer F-actin structures than control cells (Fig. 36). These data strongly support the hypothesis that AUM is involved in the regulation of actin filament turnover in cells.

Even though the exact role of AUM in these processes remains to be identified, we found that the subcellular AUM localization changes in the absence of F-actin structures (Fig. 36). When we treated AUM depleted cells with latrunculin A, an interesting differential effect on cortical actin turnover and the formation of lamellipodia was observed. AUM depleted

cells were found to have less cortical actin but more stress fibres as compared to control shRNA expressing cells (Fig. 37).

Another actin dependent process which was found to be modulated by AUM is cell adhesion. Actin cytoskeletal dynamics coordinate cell adhesion and migration by regulating the turnover of cellular adhesion complexes (Mitra et al., 2005) We found that AUM^{wt} overexpressing cells were less adherent to the substratum and smaller in size when spread on fibronectin (Fig. 35). In contrast, AUM^{D34N} expressing cells were found to be advanced in spreading under similar conditions. Focal adhesion structures formed at the end of actin stress fibres regulate cell adhesion and its turnover is an important measure of spreading behavior of the cell (Geiger et al. 2009). AUM depleted cells showed matured focal adhesions and advanced spreading as compared to control cells (Fig. 42). The majorities of the cell adhesion experiments were carried out in an AUM depleted cell line and are discussed in next section.

6.4 Consequences of AUM depletion

To investigate the physiological roles of AUM in cells, we realized that overexpression analysis has experimental limitations in terms of inconsistencies in transfection efficiency and the possibility of mislocalization of tagged AUM to unusual cellular compartments. We therefore depleted endogenous AUM by RNA interference methods and investigated the cellular consequences of AUM depletion.

We have established effective AUM knockdown both by siRNA as well as shRNA (Figs. 31, 32) methods by targeting different mRNA sequences (Fig.12). To avoid inconsistencies arising from varying transfection efficiencies in individual experiments, we primarily relied on the shRNA clone M77 that showed highest AUM knockdown efficiency (Fig. 32). All knockdown studies were done primarily in the mouse spermatogenic cell line GC1-spg. This AUM depleted, stable cell line proved to be a key tool for the functional characterization of AUM. We could reproducibly observe distinct morphological characteristics such as altered spreading behavior, effects on actin turnover and morphological differences in terms of cell size with AUM depleted cells. Similarly, the biochemical analysis of signaling pathways produced a more consistent picture after knocking down of AUM as compared to AUM overexpression studies.

We analyzed the spreading pattern of AUM depleted cells both by live cell imaging and by immunofluorescence studies. Fibronectin (FN) is one of the broadly expressed ECM molecules which induce integrin mediated cell adhesion (Sieg et al., 1998). Cells were spread on FN and analyzed at different time points for focal adhesion (FA) marker proteins and the actin cytoskeleton. Vinculin, the first molecular component identified to be constitutively present in FA (Geiger 1979), was chosen as a primary marker for focal

adhesions for cellular studies along with other FA markers such as focal adhesion kinase (FAK), Paxillin, Src and antibodies targeted against total tyrosine phosphorylated proteins.

A wealth of information has been generated about the molecular components of focal adhesion plaques. There are more than 150 proteins involved in the formation, stability and dynamics of focal adhesions (Zaidel-Bar et al., 2007). Details can be found at <http://www.adhesome.org/>. These proteins are classified as focal adhesion components or as focal adhesion associated proteins. AUM was found to be localized around the FA structures (Fig. 40), suggesting AUM as a focal adhesion associated protein. Interestingly, AUM is not colocalizing with any of the FA proteins that we tested (data not shown for markers other than vinculin and pTyr). As FA structures act as anchors of the cells, FAs are present across the base of the cell under standard two-dimensional culture conditions and thus can be best visualized with specialized imaging techniques such as TIRF or IRM microscopy (Holt et al., 2008).

We used TIRF microscopy for FA imaging in this study. Focal adhesions are classified depending upon their size, location and molecular components (Worth and Parsons 2008). These distinct classes are referred to as focal complexes, focal adhesions and fibrillar adhesions. Focal complexes are small transient structures seen immediately behind the leading edge of a spreading cell. These structures support actin based events such as filopodial growth and lamellipodial protrusions (Geiger and Bershadsky 2001). Focal adhesions (FAs) are located across the base of an adherent cell and larger than focal complexes. FAs contain multiple signaling and actin-binding proteins responsible for mechanical stability (Geiger et al., 2009). Fibrillar adhesions have been described in three dimensional matrix systems and are thought to be derived from subset of FAs (Cukierman et al., 2001).

We observed that when AUM depleted cells are spread on FN surface for different time points, they are always characterized by extensive F-actin and mature FA structures as compared to control shRNA cells. One of the representative cells is shown in figure 42. AUM depleted cells contain larger FA structures oriented towards the centre of the cell, whereas control shRNA expressing cells contain more small focal complexes at the cell periphery. These data indicate a probable role of AUM in FA maturation. The potential involvement of AUM in FA turnover is currently under investigation. Here, the kinetics of the recruitment of various focal adhesion marker proteins (GFP-actinin, GFP-alpha 5 integrin, GFP-paxillin, GFP-vinculin) to focal adhesion structures is compared in AUM-depleted versus control cells.

The cellular spreading behavior was analyzed at three distinct time points (10, 20 and 40 min), which cover the early as well as the late spreading behaviour of cells (Figs. 39, 41). We

combined biochemical analysis, immunofluorescent staining and live cell imaging of AUM depleted cells to understand the potential role of AUM in this process. Interestingly, AUM depletion has characteristic effects in the early stages of cell spreading and migration. This effect was found to be specific for fibronectin, indicating a preferential activation $\alpha 5\beta 1$ integrin (Bass et al., 2008) mediated signaling pathways. We consistently observed that after 10 min of spreading on FN, more cells were attached to the substrate in the absence of AUM. The effect seemed to be less prominent at later time points (data not shown and Fig. 39). Most of the proteins in adhesion complex are tyrosyl phosphorylated (Geiger et al., 2009). Thus, the total phosphotyrosine content of FAs can be used as a functional readout for the spreading behavior of a cell. We found that AUM depleted cells are characterized by a higher pTyr content at 10 min after spreading on FN (Fig. 41). Upon phosphorylation, most of the proteins involved in FA signalling generate binding sites for downstream effectors and can thus be targeted to the plasma membrane (Parsons 2003). The elevated pTyr content in AUM depleted cells indicates an effect of AUM on the phosphorylation status of one or more proteins involved in focal adhesion signalling, thus leading to advanced adhesion as compared to control shRNA expressing cells.

AUM depleted cells are characterized by a significantly larger cell area at 10 min after seeding on FN, as quantified by a Metamorph-based microscopic analysis (detailed in Methods, see section 4.4.15). Consistent with the effect of AUM on the pTyr content in fixed cells at 10 min spreading on FN (Fig. 41), we observed a similar and statistically significant effect of AUM on the cell area at early stages of spreading as shown in figure 42. AUM depleted cells were larger in size up to 40 min of analysis, likely due to advanced spreading (Fig. 42B).

Taken together, our data clearly demonstrate that AUM has a role in spreading and adhesion, likely due to a function in FA maturation and actin cytoskeletal dynamics. The phenotype of AUM depleted cells (increased stress fiber formation, increased focal adhesion formation) are suggestive of an increased activation of the small GTPase Rho (Raftopoulos and Hall 2004). Our current experimental efforts are directed at testing the role of AUM in Rho-GTPase signaling.

6.5 Ways and means of finding AUM substrates

Primary efforts of linking a novel enzyme to its biology are typically focused on substrate determination. It is widely accepted that disrupting the equilibrium of cellular tyrosine phosphorylation can cause a plethora of diseases and that both protein tyrosine kinases (PTKs) and protein tyrosine phosphatases (PTPs) have an equal stake in the process (Hunter 2002). Our understanding of PTKs is far advanced as compared to PTPs, not only

due to historical reasons but also due to existing experimental challenges in the PTP field (Tiganis and Bennett 2007). Even after substantial progress in the field of PTP research, physiological substrate identification still remains a major task. Particularly the identification of substrates for non-transmembrane PTPs is even today primarily governed by a trial and error approach.

Although initially viewed as non-specific 'housekeeping' enzymes, it is now well established that PTPs are selective in their choice of substrates (Garton et al., 1996; Tonks 2003). The ability of PTPs to differentiate between individual substrates can be attributed to the specificity within the PTP catalytic domain. Traditionally, active-site sequence HC(X5)R has defined the PTP family, and a cysteine was known to act as nucleophile in their catalytic mechanism. An additional level of substrate specificity was achieved through non-catalytic N- and C-terminal residues which govern the spatial and temporal localization of PTPs (Tonks 2006). Recently, a novel class of PTPs, traditionally known as HAD-type or aspartate-based phosphatases, has been reported (Aravind and Koonin 1998). These aspartate-based phosphatases are typified by an unconventional catalytic mechanism and are known to dephosphorylate both pSer/pThr (Gohla et al., 2005) or pTyr residues (Rayapureddi et al., 2003).

The approaches for defining the function of PTPs have heavily relied on a combination of biochemical and genetic techniques. The current consensus for assigning a *bona fide* PTP substrate is shown in figure 47 (Tiganis and Bennett 2007). It certainly will help to standardize the experimental set up as compared to current 'best guess' approach.

We followed a similar approach in trying to identify AUM substrates. In the following section, the pros and cons of the tools that were generated in this thesis work and the assays that were performed will be discussed.

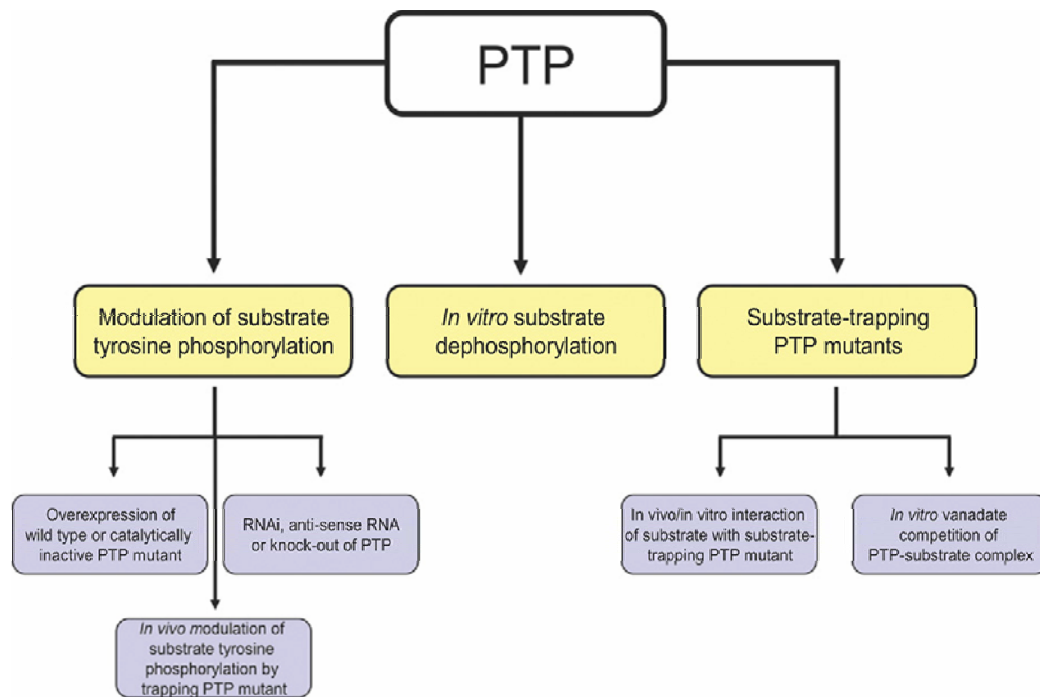


Figure 47: Approach for the characterization of PTP substrates

Proposed criteria for the assignment of a tyrosine-phosphorylated protein as a PTP substrate. A combination of overexpression and knockdown studies of PTP can be employed in order to experimentally confirm *bona fide* PTP substrate (from Tiganis and Bennett 2007).

Generation of a catalytically dead mutant of AUM

A phosphatase dead mutant of AUM was generated by site directed mutagenesis, whereby the nucleophilic aspartate was mutated conservatively to asparagine (see section 4.2.9). The catalytic impairment was unequivocally shown by lack of activity towards *p*-NPP (Fig. 18). Plasmid containing AUM^{D34N} was used in overexpression studies along with AUM^{wt} constructs with suitable tags. We analyzed the effect of AUM overexpression on actin dynamics, cell spreading, and in biochemical studies. AUM^{D34N} expressing cells show characteristically altered cell morphology in comparison to AUM^{wt} expressing cells. The overexpression of catalytically dead AUM leads to more stabilized F-actin as well as to mature focal adhesions (Figs. 35, 38). AUM^{D34N} expressing cells are advanced in spreading on FN coated surface. We also tested AUM^{D34N} as a putative substrate trapping mutant in biochemical studies focusing on likely target molecules such as Src or EGFR which are known to play central role in cell adhesion and migration (Biscardi et al., 2000; Huvneers and Danen 2009) and also because we had indication of these molecules as probable AUM substrates in phosphopeptide screen (see Fig. 19). So far we could not successfully show stable PTP-substrate complex formation using AUM^{D34N} either indicating its limitations to act as efficient substrate trapping mutant. It is possible that additional mutations need to be introduced in order to stabilize the association of AUM with its substrates.

PTP-substrate complexes could be isolated in the case of PTP-PEST or SHP2 (Garton et al., 1996; Agazie and Hayman 2003). There are certain limitations to this approach owing to the

possibility of mislocalization of AUM^{D34N} in cells, granting it access to substrates that might not otherwise be encountered under physiological conditions. Along with spatial issues of PTP-substrate complex formation in cells, there is another level of complexity in terms of temporal regulation of PTP activity in cells. Substrate trapping mutants might interfere with the propagation of downstream signaling, resulting in changes in net tyrosyl phosphorylation patterns of other PTP substrates and thus preventing their detection by this method. Hence this approach needs to be used with caution and complemented by knockdown studies which we established using RNA interference.

High throughput peptide screen

With the advent of genomic and proteomic scale screening technologies, we have yet another possibility of searching PTP substrates. Such screens are costly and demand dedicated instrumentations. Secondly, information generated at peptide level might not be translated directly into the biological context. In spite of these limitations, such screens may be a useful starting point for the characterization of novel proteins.

We employed 720 pTyr, pSer or pThr-phosphorylated 13-mer human peptides and analyzed the dephosphorylation pattern in presence of recombinant, purified AUM. The relevance of the phosphopeptides contained in these screens has either experimentally confirmed at the protein level for about half of the peptides. The remaining phosphopeptides contained in the screen were experimentally identified by mass spectrophotometric analysis. Among all of the human phosphopeptides analyzed, we found that AUM prefers certain pTyr peptides indicating its enzymatic preferences and specificity. There are only 2% of pTyr peptides above a cut off limit of 66% as enlisted in figure 19, belonging to receptor tyrosine signaling proteins, adhesion proteins, and proteins involved in cytoskeletal dynamics. There are as many as ~150 pTyr peptides dephosphorylated by AUM as enlisted in supplementary data (10.1). This screening approach helped us to direct our efforts towards certain pathways and narrowing down the search for molecules involved therein. Predominantly we focused on EGFR signaling pathway and integrin mediated adhesion pathways for future substrate hunt.

Interestingly, the putative “consensus sequence peptide” designed from this screen (see 10.1) could not be dephosphorylated by AUM (data not shown), raising questions about extrapolating the information and emphasizing the requirement for a physiological protein conformation for PTP catalysis.

Modulation of substrate tyrosine phosphorylation

Demonstrating effect of PTP on endogenous tyrosine phosphorylation can be considered as unequivocal assignment of a PTP substrate used as starting point in many novel phosphatases such as Eyes absent (Rayapureddi et al., 2003). It is possible to analyze effect of overexpression or depletion of PTP by either demonstrating changes in global phosphotyrosine levels (Selengut 2001) or by discretely analyzing individual phosphosites on proteins (Lee and Chang 2008). We identified AUM as a *bona fide* phosphotyrosine protein phosphatase by overlay assay (Fig. 20) and by *in vitro* phosphatase assays (Figs. 21, 33) both by overexpression and depletion of AUM.

We next decided to analyze the effect of AUM overexpression or loss-of-function approaches for individual phosphorylated sites on specific proteins for reasons discussed above. Epidermal growth factor receptor (EGFR) and Src, well known signaling molecules having central role in vital cellular processes are tyrosyl phosphorylated at multiple residues (Roskoski 2005; Wolf-Yadlin et al., 2006). We induced specific signaling pathways by ligands such as EGF or ECM molecules such as FN, and analyzed the effect on tyrosine phosphorylation upon overexpression or depletion of AUM. Unfortunately, we were not successful in obtaining consistent results with any of the phosphosites under various experimental conditions. We tried to immunoprecipitate either endogenous EGFR or Src at various time points after stimulation, but could not see the effect on tyrosine phosphorylation biochemically even when the obvious effect on cell adhesion by AUM overexpression or depletion was visible in cell biological analyses (Figs. 35-39). This can partly be attributed to unknown regulation of AUM in cells and to the transient effect of this phosphatase during cell spreading or EGF induced cell proliferation. It was evident in *in vitro* phosphatase assays that the effect of AUM overexpression or depletion can only be observed during the initial phases within 5 min (Figs. 21, 33) or within 10 min in FN spreading assays (Fig. 39). In spite of these limitations, we could consistently observe a stabilization of signaling molecules in absence of AUM such as EGFR (Fig. 34), and $\alpha 5\beta 1$ integrins and Src (data not shown) under spreading conditions or upon growth factor stimulation. Tyr1045 is one of the phosphosites on EGFR which upon phosphorylation generates a major docking site for c-Cbl, an adaptor protein and ubiquitin ligase that leads to receptor ubiquitination and degradation or trafficking (Biscardi et al., 1999). We found consistent modulation of phosphorylation status of Tyr1045 upon AUM depletion (Fig. 34) as compared to control shRNA expressing cells. We could not confirm the hyperphosphorylation status of Tyr1045 with endogenous immunoprecipitated EGFR, and secondly there was concomitant increase in total EGFR level in the absence of AUM (Fig. 34) suggesting hyperphosphorylation of Tyr1045 as a consequence of increased EGFR levels and not due to depletion of AUM. We

have not systematically analyzed yet the reason of stabilization of EGFR in AUM depleted cells as early as 1 min after EGF stimulation.

We now know that majority of signaling molecules are multisite phosphorylated (Cohen 2000), which often has contrasting effects on the final outcome of protein activation. This may be one reason why it is difficult to correlate changes in the phosphorylation status of individual sites to certain functions by employing the currently available biochemical approaches.

In vitro substrate dephosphorylation

Probably the most straightforward approach of confirming the PTP substrate is an *in vitro* phosphatase assay where recombinant PTP and substrate are incubated together under defined conditions to monitor dephosphorylation of the potential substrate using anti-phosphotyrosine antibodies or the release of phosphate colorimetrically or by release of radiolabelled phosphate.

On the basis of the results of the phosphopeptide screen, we chose recombinant Src, FAK and phospholipids scramblase 1 for *in vitro* assays. Upon *in vitro* phosphorylation either alone with ATP or along with suitable upstream kinases, the phosphorylated protein was subjected to *in vitro* phosphatase reaction in the presence of recombinant, purified AUM as detailed in Methods (see section 4.4.13). There was no conclusive pattern with any of the proteins (data not shown), suggesting that either the data obtained on the peptide level may not be true at the protein level, or that there might be additional factors such as binding partners or phosphorylation status of PTP itself that govern the phosphatase efficiency (Chan et al., 2008)

In case of *in vitro* phosphatase assay with Src, there are some interesting observations even though there was no unambiguous AUM mediated dephosphorylation on either of the two regulatory sites (Fig. 44A). Our data indicate the existence of AUM / Src cross talk in cells due to our observation of Src mediated AUM phosphorylation. Experiments aimed at investigating a potential physical interaction of AUM and Src are currently ongoing.

We measured the effect of AUM on Src kinase activity towards a phosphorylated Src substrate peptide (for assay details, see section 4.4.13), and reproducibly found that AUM enhances Src kinase activity, albeit in a phosphatase-independent manner (Fig. 45). This finding may partially explain why we did not obtain consistent results when testing the effect of AUM on Src dephosphorylation in biochemical assays, as the AUM phosphatase activity might not be required for the regulation of Src kinase activity according to *in vitro* experiments.

We also analyzed the effect of Src on AUM phosphatase activity towards p -NPP because Src was found to phosphorylate AUM on a thus far unidentified tyrosine residue (Fig. 5). We found that Src inhibits AUM phosphatase activity. This effect is dependent on Src kinase activity as shown in figure 46.

These results so far indicate a potential role of AUM as a structural component in Src regulation. Hence we put forward the hypothesis that AUM is involved in the regulation of Src activity by binding with one of its tyrosine residues to the Src SH2 domain as schematically shown in figure 48. It is known in the literature that there are a few phosphatases such as PTP ϵ that act as “competitive” Src activators by competing the intramolecular interaction between the pTyr527 residue and the Src SH2 domain, thus releasing the Src autoinhibitory loop (Berman-Golan and Elson 2007). This mechanism makes the Src autophosphorylation site Tyr416 accessible for phosphorylation and leads to a Src kinase activation.

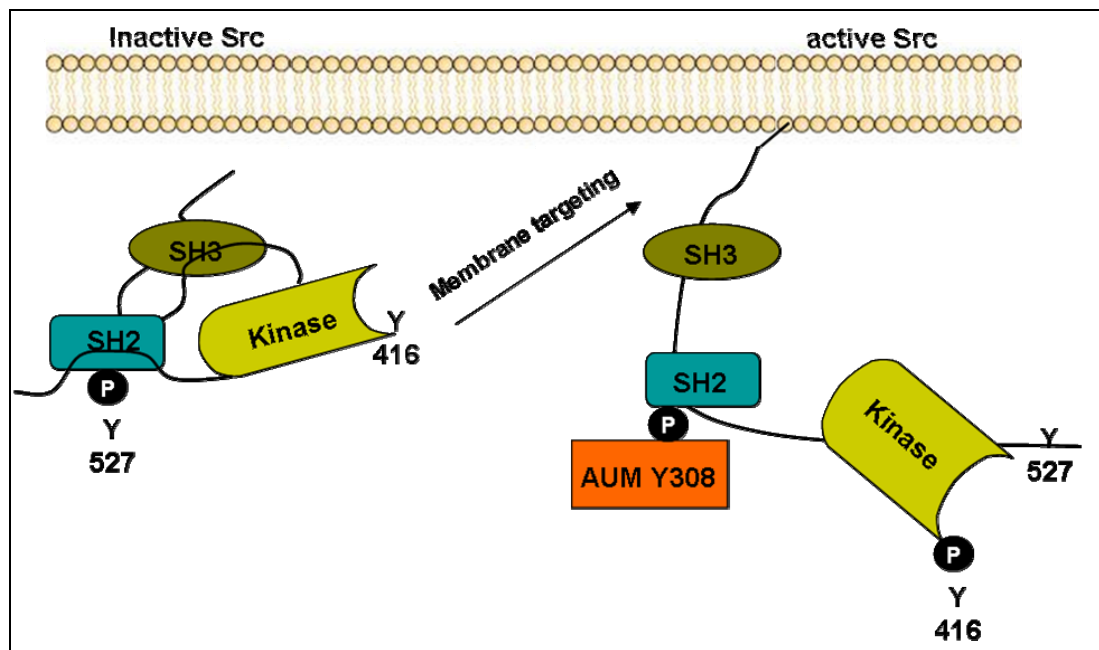


Figure 48: Suggested mechanism for AUM acting as a novel Src kinase activator
AUM may bind to the Src SH2 domain and thus release Src from its autoinhibited conformation. AUM may thus act as a Src kinase activator in a phosphatase independent manner.

AUM is predicted to be tyrosine phosphorylated on 8 residues (figure 4) as analyzed by one of the available post translational modification prediction tools (<http://www.cbs.dtu.dk/services/NetPhos/>). Out of these 8 residues 3 have been experimentally confirmed by mass spectrophotometric analysis (<http://www.phosida.com/>). These sites are Tyr108, 178 and 308. Two tyrosine residues at the C-terminal region are found to be particularly interesting. Tyr248 is found to be conserved only in vertebrates whereas Tyr308 is found to be evolutionarily conserved from bacteria to humans. At present,

we are in the process of generating and testing the corresponding AUM mutants. The effect of these mutants on Src activity will allow us to experimentally test our proposed hypothesis.

So far, our biochemical and cell biological data suggest that AUM has a role in the early spreading events of cells on FN coated surfaces. Src is known to be involved in the process of early stages of spreading by regulating the phosphorylation status of p190RhoGAP which in turn activates Rho activity of the cell (Huveneers and Danen 2009). If indeed our *in vitro* results indicating that AUM acts as a Src activator hold true under cellular and under *in vivo* conditions, then we should be able to observe an effect on Src kinase activity upon overexpression or depletion of AUM in cells. The use of pharmacological inhibitors of Src such as PP2 in cellular assays may be helpful to investigate the nature of the AUM / Src cross talk under physiological conditions.

To summarize, our identification and characterization of AUM place this molecule as an interesting novel player in vital cellular processes such as cell adhesion and migration. A conditionally AUM-deficient mouse model has recently been generated by our laboratory. It can be expected that this model will hold the key to unlock the mystery of this novel aspartate based phosphotyrosine phosphatase.

7 Summary

Protein phosphatases can be classified into at least three major families based on amino acid sequences at their active sites. A newly emerging phosphatase family contains the active site sequence DXDX(T/V), and belongs to the haloacid dehalogenase (HAD) superfamily of hydrolases, a ubiquitous and evolutionarily conserved enzyme family. Although the existence of 58 human HAD enzymes has been predicted by database analysis, our understanding of their biological functions remains rudimentary.

By database mining and phylogenetic analysis of human HAD phosphatases, we have found a previously unidentified enzyme with homology to Chronophin, a cytoskeletal regulatory HAD phosphatase. We have cloned and characterized this novel enzyme and named it AUM, for actin remodeling, ubiquitously expressed, magnesium-dependent HAD phosphatase. By Northern blot, real-time PCR and Western blot analysis, we show that AUM is broadly expressed in all major human and mouse tissues with highest levels found in testis. Using immunohistochemistry, we can show that AUM is specifically expressed in maturing germ cells and that its expression peaks during spermiogenesis.

To characterize the substrate preference of AUM, we have conducted an *in vitro* phosphatase substrate screen with 720 phosphopeptides derived from human phosphorylation sites. AUM exclusively dephosphorylates phosphotyrosine (pTyr)-containing peptides. Furthermore, only 17 pTyr peptides (~2% of all pTyr peptides investigated) acted as AUM substrates, indicating a high degree of substrate specificity. Putative AUM substrates include proteins involved in cytoskeletal dynamics and tyrosine kinase signaling. In accordance with the phosphopeptide screen, phosphatase overlay assays employing whole-cell extracts of pervanadate-treated HeLa cells show that AUM dephosphorylates only a limited number of tyrosyl-phosphorylated proteins.

The role of AUM for cellular signaling was investigated in response to epidermal growth factor (EGF) stimulation in a spermatogonial cell line (GC-1 spg). The overexpression of AUM reduces, whereas the RNAi-mediated depletion of endogenous AUM increases EGF-induced tyrosine phosphorylation, including changes in the phosphorylation of the EGF receptor itself. Interestingly, *in vitro* kinase/phosphatase assays with purified Src and AUM indicate that AUM can activate Src, which in turn phosphorylates and inactivates AUM. Although it is at present unclear how Src and AUM regulate each other, our initial findings suggests that AUM enhances Src kinase activity independently of its phosphatase activity, whereas Src diminishes AUM phosphatase activity in a kinase dependent manner.

On a cellular level, AUM-depleted cells are characterized by altered actin cytoskeletal dynamics and adhesion, as indicated by stabilized actin filaments, enlarged focal adhesions,

a marked increase in cell area of spreading cells, as well as accelerated cell spreading on fibronectin.

Taken together, we have identified and characterized AUM as a novel member of the emerging family of aspartate-dependent protein tyrosine phosphatases. Our findings implicate AUM as an important regulator of Src-dependent cytoskeletal dynamics during cell adhesion and migration.

8 Zusammenfassung

Protein Phosphatasen werden aufgrund der Aminosäuresequenzen ihrer aktiven Zentren in drei große Familien unterteilt. In einer neu entdeckten Familie von Phosphatasen ist das aktive Zentrum durch die Sequenz DXDX(T/V) charakterisiert. Diese Aspartat-abhängigen Phosphatasen gehören zu der Superfamilie der Hydrolasen vom Haloazid Dehalogenase (HAD)-Typ, einer evolutionär konservierten und ubiquitär verbreiteten Enzymfamilie. Bislang konnten 58 menschliche HAD Enzyme durch Datenbankanalysen identifiziert werden. Ihre Funktionen sind jedoch nach wie vor nur rudimentär verstanden.

Im Rahmen dieser Arbeit wurde zunächst das Komplement aller menschlichen HAD Phosphatasen durch Datenbank-Recherchen erfasst. Zusammen mit phylogenetischen Analysen gelang es, eine zum damaligen Zeitpunkt unbekannte, putative Phosphatase zu identifizieren, die eine vergleichsweise hohe Sequenz-Homologie zu der Zytoskelett-regulierenden HAD Phosphatase Chronophin aufweist. Dieses neuartige Enzym wurde kloniert und mit biochemischen und zellbiologischen Methoden charakterisiert. Auf der Basis dieser Befunde bezeichnen wir dieses neuartige Protein als AUM (*actin remodeling, ubiquitously expressed, magnesium-dependent HAD phosphatase*). Mittels Northern blot, *real-time* PCR und Western blot Analysen konnte gezeigt werden, dass AUM in allen untersuchten menschlichen und murinen Geweben exprimiert wird. Die höchste Expression konnte in Hodengewebe nachgewiesen werden. Durch immunohistochemische Untersuchungen konnte gezeigt werden, dass AUM spezifisch in reifenden Keimzellen mit einem Expressionsmaximum zum Zeitpunkt der Spermiogenese exprimiert wird.

Um die Substratpräferenz von AUM zu charakterisieren, wurde zunächst ein peptidbasierter *in vitro* Phosphatase-Substrat-Screen durchgeführt. Hierbei wurden 720 aus menschlichen Phosphoproteinen abgeleitete Phosphopeptide untersucht. Interessanterweise dephosphorylierte AUM ausschließlich Phosphotyrosin (pTyr)-enthaltende Peptide. Nur 17 pTyr-Peptide (~2% aller untersuchten Peptide) fungierten als AUM-Substrate. Diese Daten legen eine hohe Substratspezifität von AUM nahe. Zu den putativen AUM Substraten gehören Proteine, die in die Dynamik der Zytoskelett-Reorganisation sowie in Tyrosin Kinase-vermittelte Signalwege eingebunden sind. In Übereinstimmung mit den Ergebnissen dieses Phosphopeptid-Screens konnte mittels Phosphatase *overlay* assays sowie in Zellextrakten aus Pervanadat-behandelten HeLa Zellen demonstriert werden, dass AUM eine begrenzte Anzahl Tyrosin-phosphorylierter Proteinen dephosphorylieren kann.

In zellulären Untersuchungen wurde die mögliche Rolle von AUM im Rahmen der durch den epidermalen Wachstumsfaktor (EGF) ausgelösten Tyrosin-Phosphorylierung in einer Spermatozyten Zelllinie (GC-1 spg-Zellen) analysiert. So konnte nachgewiesen werden, dass die Überexpression von AUM zu einer moderaten Abnahme Tyrosin-phosphorylierter Proteine nach EGF-Stimulation führte. Im Gegensatz dazu löste jedoch die durch RNA-Interferenz vermittelte Depletion von endogenem AUM einen robusten Anstieg Tyrosin-phosphorylierter Proteine aus, zu denen auch der EGF-Rezeptor selbst zählt.

Zusätzlich zu dem EGF-Rezeptor wurde die Src-Kinase im Zuge des Phosphopeptid-Screens als mögliches AUM Substrat identifiziert. Daher wurden *in vitro* Kinase/Phosphatase-Assays mit gereinigtem Src und AUM durchgeführt. Mit diesem Ansatz konnte erstmals gezeigt werden, dass AUM in der Lage ist, die Src-Kinase zu aktivieren, während Src AUM phosphoryliert und die AUM Phosphatase-Aktivität blockiert. Diese Ergebnisse deuten auf eine gekoppelte, wechselseitige Regulation von AUM und Src hin. Obwohl die Details dieser Regulation derzeit noch unklar sind, zeigen unsere initialen Ergebnisse, dass AUM die Src-Aktivität unabhängig von seiner Phosphatase-Aktivität steigert, während Src die AUM Phosphatase-Aktivität Kinase-abhängig vermindert.

Auf zellulärer Ebene sind AUM-depletierte Zellen durch Veränderungen der Aktin-Zytoskelett-Dynamik und der Zelladhäsion charakterisiert. So weisen AUM-defiziente Zellen stabilisierte Aktin-Streißfasern und vergrößerte fokale Adhäsionen auf. Weiterhin sind AUM-depletierte Zellen durch ein beschleunigtes *spreading* auf Fibronektin gekennzeichnet.

Wir haben mit AUM ein bisher nicht beschriebenes Mitglied der Familie Aspartat-abhängiger Phosphatasen entdeckt. In dieser Arbeit ist es gelungen, AUM phylogenetisch, biochemisch und zellbiologisch zu charakterisieren. Unsere Ergebnisse legen nahe, dass AUM einen wichtigen, neuartigen Regulator der Src-vermittelten Zytoskelett-Dynamik im Rahmen der Zelladhäsion und Migration darstellt.

9 References

- Agazie, Y. M. and M. J. Hayman (2003). "Development of an efficient "substrate-trapping" mutant of Src homology phosphotyrosine phosphatase 2 and identification of the epidermal growth factor receptor, Gab1, and three other proteins as target substrates." *J Biol Chem* **278**(16): 13952-8.
- Allen, K. N. and D. Dunaway-Mariano (2004). "Phosphoryl group transfer: evolution of a catalytic scaffold." *Trends in Biochemical Sciences* **29**(9): 495-503.
- Almo, S. C., J. B. Bonanno, J. M. Sauder, S. Emtage, T. P. Dileo, et al. (2007). "Structural genomics of protein phosphatases." *J Struct Funct Genomics* **8**(2-3): 121-40.
- Alonso, A., J. Sasin, N. Bottini, I. Friedberg, A. Osterman, et al. (2004). "Protein tyrosine phosphatases in the human genome." *Cell* **117**(6): 699-711.
- Altschul, S. F., W. Gish, W. Miller, E. W. Myers and D. J. Lipman (1990). "Basic local alignment search tool." *J Mol Biol* **215**(3): 403-10.
- Andersen, J. N., R. L. Del Vecchio, N. Kannan, J. Gergel, A. F. Neuwald, et al. (2005). "Computational analysis of protein tyrosine phosphatases: practical guide to bioinformatics and data resources." *Methods* **35**(1): 90-114.
- Andrianantoandro, E. and T. D. Pollard (2006). "Mechanism of actin filament turnover by severing and nucleation at different concentrations of ADF/cofilin." *Mol Cell* **24**(1): 13-23.
- Aravind, L. and E. V. Koonin (1998). "The HD domain defines a new superfamily of metal-dependent phosphohydrolases." *Trends Biochem Sci* **23**(12): 469-72.
- Archambault, J., G. Pan, G. K. Dahmus, M. Cartier, N. Marshall, et al. (1998). "FCP1, the RAP74-interacting subunit of a human protein phosphatase that dephosphorylates the carboxyl-terminal domain of RNA polymerase II." *J Biol Chem* **273**(42): 27593-601.
- Balakrishnan, R., M. Frohlich, P. T. Rahaim, K. Backman and R. R. Yocum (1993). "Appendix. Cloning and sequence of the gene encoding enzyme E-1 from the methionine salvage pathway of *Klebsiella oxytoca*." *J Biol Chem* **268**(33): 24792-5.
- Bamburg, J. R. and G. S. Bloom (2009). "Cytoskeletal pathologies of Alzheimer disease." *Cell Motil Cytoskeleton* **66**(8): 635-49.
- Bamburg, J. R. and O. P. Wiggan (2002). "ADF/cofilin and actin dynamics in disease." *Trends Cell Biol* **12**(12): 598-605.
- Bass, M. D., M. R. Morgan, K. A. Roach, J. Settleman, A. B. Goryachev, et al. (2008). "p190RhoGAP is the convergence point of adhesion signals from alpha 5 beta 1 integrin and syndecan-4." *J Cell Biol* **181**(6): 1013-26.
- Bazley, L. A. and W. J. Gullick (2005). "The epidermal growth factor receptor family." *Endocr Relat Cancer* **12 Suppl 1**: S17-27.

- Bellve, A. R. (1993). Recovery, Capacitation, Acrosome reaction, Fractionation of sperm. *Methods in Enzymology*. **225**: 113 - 136.
- Berman-Golan, D. and A. Elson (2007). "Neu-mediated phosphorylation of protein tyrosine phosphatase epsilon is critical for activation of Src in mammary tumor cells." *Oncogene* **26**(49): 7028-37.
- Biscardi, J. S., R. C. Ishizawar, C. M. Silva and S. J. Parsons (2000). "Tyrosine kinase signalling in breast cancer: epidermal growth factor receptor and c-Src interactions in breast cancer." *Breast Cancer Res* **2**(3): 203-10.
- Biscardi, J. S., M. C. Maa, D. A. Tice, M. E. Cox, T. H. Leu, et al. (1999). "c-Src-mediated phosphorylation of the epidermal growth factor receptor on Tyr845 and Tyr1101 is associated with modulation of receptor function." *J Biol Chem* **274**(12): 8335-43.
- Blevins, T., R. Rajeswaran, P. V. Shivaprasad, D. Beknazariants, A. Si-Ammour, et al. (2006). "Four plant Dicers mediate viral small RNA biogenesis and DNA virus induced silencing." *Nucleic Acids Res* **34**(21): 6233-46.
- Bradshaw, R., & Dennis, E., Ed. (2003). *Handbook of Cell Signaling*, Elsevier Science (USA). **1**: 373 - 377.
- Bradshaw, R., & Dennis, E., Ed. (2003). *Handbook of Cell Signaling*, Elsevier Science (USA). **1**: 593-600.
- Breitbart, H., G. Cohen and S. Rubinstein (2005). "Role of actin cytoskeleton in mammalian sperm capacitation and the acrosome reaction." *Reproduction* **129**(3): 263-8.
- Burroughs, A. M., K. N. Allen, D. Dunaway-Mariano and L. Aravind (2006). "Evolutionary genomics of the HAD superfamily: understanding the structural adaptations and catalytic diversity in a superfamily of phosphoesterases and allied enzymes." *J Mol Biol* **361**(5): 1003-34.
- Cagan, R. L. (2003). "Spermatogenesis: borrowing the apoptotic machinery." *Curr Biol* **13**(15): R600-2.
- Chan, G., D. Kalaitzidis and B. G. Neel (2008). "The tyrosine phosphatase Shp2 (PTPN11) in cancer." *Cancer Metastasis Rev* **27**(2): 179-92.
- Chhabra, E. S. and H. N. Higgs (2007). "The many faces of actin: matching assembly factors with cellular structures." *Nat Cell Biol* **9**(10): 1110-21.
- Chomczynski, P. and N. Sacchi (1987). "Single-step method of RNA isolation by acid guanidinium thiocyanate-phenol-chloroform extraction." *Anal Biochem* **162**(1): 156-9.
- Cohen, P. (1992). "Signal integration at the level of protein kinases, protein phosphatases and their substrates." *Trends in Biochemical Sciences* **17**(10): 408-413.
- Cohen, P. (2000). "The regulation of protein function by multisite phosphorylation - a 25 year update." *Trends in Biochemical Sciences* **25**(12): 596-601.
- Collet, J. F., V. Stroobant, M. Pirard, G. Delpierre and E. Van Schaffingen (1998). "A new class of phosphotransferases phosphorylated on an aspartate residue in an amino-terminal DXDX(T/V) motif." *J Biol Chem* **273**(23): 14107-12.
- Cukierman, E., R. Pankov, D. R. Stevens and K. M. Yamada (2001). "Taking cell-matrix adhesions to the third dimension." *Science* **294**(5547): 1708-12.

- Das, A. K., N. R. Helps, P. T. Cohen and D. Barford (1996). "Crystal structure of the protein serine/threonine phosphatase 2C at 2.0 Å resolution." *EMBO J* **15**(24): 6798-809.
- Eckhart, W., M. A. Hutchinson and T. Hunter (1979). "An activity phosphorylating tyrosine in polyoma T antigen immunoprecipitates." *Cell* **18**(4): 925-33.
- Elbashir, S. M., J. Harborth, W. Lendeckel, A. Yalcin, K. Weber, et al. (2001). "Duplexes of 21-nucleotide RNAs mediate RNA interference in cultured mammalian cells." *Nature* **411**(6836): 494-8.
- Gao, G. J. and M. L. Fonda (1994). "Kinetic analysis and chemical modification of vitamin B6 phosphatase from human erythrocytes." *J Biol Chem* **269**(10): 7163-8.
- Garton, A. J., A. J. Flint and N. K. Tonks (1996). "Identification of p130(cas) as a substrate for the cytosolic protein tyrosine phosphatase PTP-PEST." *Mol Cell Biol* **16**(11): 6408-18.
- Geiger, B. (1979). "A 130K protein from chicken gizzard: its localization at the termini of microfilament bundles in cultured chicken cells." *Cell* **18**(1): 193-205.
- Geiger, B. and A. Bershadsky (2001). "Assembly and mechanosensory function of focal contacts." *Curr Opin Cell Biol* **13**(5): 584-92.
- Geiger, B., J. P. Spatz and A. D. Bershadsky (2009). "Environmental sensing through focal adhesions." *Nat Rev Mol Cell Biol* **10**(1): 21-33.
- Gohla, A., J. Birkenfeld and G. M. Bokoch (2005). "Chronophin, a novel HAD-type serine protein phosphatase, regulates cofilin-dependent actin dynamics." *Nat Cell Biol* **7**(1): 21-9.
- Gordon, J., Ed. (1991). *Methods in Enzymology*. **201**: 477-482.
- Guo, Y., N. Cheong, Z. Zhang, R. De Rose, Y. Deng, et al. (2004). "Tim50, a component of the mitochondrial translocator, regulates mitochondrial integrity and cell death." *J Biol Chem* **279**(23): 24813-25.
- Hanahan, D. (1983). "Studies on transformation of *Escherichia coli* with plasmids." *J Mol Biol* **166**(4): 557-80.
- Hanks, S. K. and T. Hunter (1995). "Protein kinases 6. The eukaryotic protein kinase superfamily: kinase (catalytic) domain structure and classification." *FASEB J* **9**(8): 576-96.
- Hendrickx, A., M. Beullens, H. Ceulemans, T. Den Abt, A. Van Eynde, et al. (2009). "Docking motif-guided mapping of the interactome of protein phosphatase-1." *Chem Biol* **16**(4): 365-71.
- Hess, R. A. (1990). "Quantitative and qualitative characteristics of the stages and transitions in the cycle of the rat seminiferous epithelium: light microscopic observations of perfusion-fixed and plastic-embedded testes." *Biol Reprod* **43**(3): 525-42.
- Hess, R. A., D. J. Schaeffer, V. P. Eroschenko and J. E. Keen (1990). "Frequency of the stages in the cycle of the seminiferous epithelium in the rat." *Biol Reprod* **43**(3): 517-24.

- Hofmann, M. C., S. Narisawa, R. A. Hess and J. L. Millan (1992). "Immortalization of germ cells and somatic testicular cells using the SV40 large T antigen." *Exp Cell Res* **201**(2): 417-35.
- Holt, M. R., Y. Calle, D. H. Sutton, D. R. Critchley, G. E. Jones, et al. (2008). "Quantifying cell-matrix adhesion dynamics in living cells using interference reflection microscopy." *J Microsc* **232**(1): 73-81.
- Hornberg, J. J., F. J. Bruggeman, B. Binder, C. R. Geest, A. J. de Vaate, et al. (2005). "Principles behind the multifarious control of signal transduction. ERK phosphorylation and kinase/phosphatase control." *Febs J* **272**(1): 244-58.
- Hotulainen, P., E. Paunola, M. K. Vartiainen and P. Lappalainen (2005). "Actin-depolymerizing factor and cofilin-1 play overlapping roles in promoting rapid F-actin depolymerization in mammalian nonmuscle cells." *Mol Biol Cell* **16**(2): 649-64.
- Hunter, T. (1998). "The Croonian Lecture 1997. The phosphorylation of proteins on tyrosine: its role in cell growth and disease." *Philos Trans R Soc Lond B Biol Sci* **353**(1368): 583-605.
- Hunter, T. (2000). "Signaling--2000 and Beyond." *Cell* **100**(1): 113-127.
- Hunter, T. (2002). "Tyrosine phosphorylation in cell signaling and disease." *Keio J Med* **51**(2): 61-71.
- Hunter, T., Ed. (2004). *Protein phosphorylation: What does the future hold in life sciences for the 21st century?* NJ, Wiley Hoboken pp 191-223.
- Hunter, T. (2007). "The Age of Crosstalk: Phosphorylation, Ubiquitination, and Beyond." *Molecular Cell* **28**(5): 730-738.
- Huveneers, S. and E. H. Danen (2009). "Adhesion signaling - crosstalk between integrins, Src and Rho." *J Cell Sci* **122**(Pt 8): 1059-69.
- Jang, Y. M., D. W. Kim, T. C. Kang, M. H. Won, N. I. Baek, et al. (2003). "Human pyridoxal phosphatase. Molecular cloning, functional expression, and tissue distribution." *J Biol Chem* **278**(50): 50040-6.
- Kannan, N. and S. S. Taylor (2008). "Rethinking pseudokinases." *Cell* **133**(2): 204-5.
- Kim, Y., M. S. Gentry, T. E. Harris, S. E. Wiley, J. C. Lawrence, Jr., et al. (2007). "A conserved phosphatase cascade that regulates nuclear membrane biogenesis." *Proc Natl Acad Sci U S A* **104**(16): 6596-601.
- Kolokoltsov, A. A., S. C. Weaver and R. A. Davey (2005). "Efficient functional pseudotyping of oncoretroviral and lentiviral vectors by Venezuelan equine encephalitis virus envelope proteins." *J Virol* **79**(2): 756-63.
- Koonin, E. V. and R. L. Tatusov (1994). "Computer analysis of bacterial haloacid dehalogenases defines a large superfamily of hydrolases with diverse specificity. Application of an iterative approach to database search." *J Mol Biol* **244**(1): 125-32.
- Kuznetsova, E., M. Proudfoot, C. F. Gonzalez, G. Brown, M. V. Omelchenko, et al. (2006). "Genome-wide analysis of substrate specificities of the *Escherichia coli* haloacid dehalogenase-like phosphatase family." *J Biol Chem* **281**(47): 36149-61.

- Laemmli, U. K. (1970). "Cleavage of structural proteins during the assembly of the head of bacteriophage T4." *Nature* **227**(5259): 680-5.
- Lahiri, S. D., G. Zhang, J. Dai, D. Dunaway-Mariano and K. N. Allen (2004). "Analysis of the substrate specificity loop of the HAD superfamily cap domain." *Biochemistry* **43**(10): 2812-20.
- Lahiri, S. D., G. Zhang, D. Dunaway-Mariano and K. N. Allen (2002). "Caught in the act: the structure of phosphorylated beta-phosphoglucomutase from *Lactococcus lactis*." *Biochemistry* **41**(26): 8351-9.
- Larkin, M. A., G. Blackshields, N. P. Brown, R. Chenna, P. A. McGettigan, et al. (2007). "Clustal W and Clustal X version 2.0." *Bioinformatics* **23**(21): 2947-8.
- Lee, H. H. and Z. F. Chang (2008). "Regulation of RhoA-dependent ROCKII activation by Shp2." *J Cell Biol* **181**(6): 999-1012.
- Levkowitz, G., H. Waterman, S. A. Ettenberg, M. Katz, A. Y. Tsygankov, et al. (1999). "Ubiquitin ligase activity and tyrosine phosphorylation underlie suppression of growth factor signaling by c-Cbl/Sli-1." *Mol Cell* **4**(6): 1029-40.
- Livera, G., G. Delbes, C. Pairault, V. Rouiller-Fabre and R. Habert (2006). "Organotypic culture, a powerful model for studying rat and mouse fetal testis development." *Cell Tissue Res* **324**(3): 507-21.
- Manning, G., G. D. Plowman, T. Hunter and S. Sudarsanam (2002). "Evolution of protein kinase signaling from yeast to man." *Trends Biochem Sci* **27**(10): 514-20.
- Mitra, S. K., D. A. Hanson and D. D. Schlaepfer (2005). "Focal adhesion kinase: in command and control of cell motility." *Nat Rev Mol Cell Biol* **6**(1): 56-68.
- Moffat, J., D. A. Grueneberg, X. Yang, S. Y. Kim, A. M. Kloepper, et al. (2006). "A lentiviral RNAi library for human and mouse genes applied to an arrayed viral high-content screen." *Cell* **124**(6): 1283-98.
- Moorhead, G. B., V. De Wever, G. Templeton and D. Kerk (2009). "Evolution of protein phosphatases in plants and animals." *Biochem J* **417**(2): 401-9.
- Morrison, D. K., M. S. Murakami and V. Cleghon (2000). "Protein kinases and phosphatases in the *Drosophila* genome." *J Cell Biol* **150**(2): F57-62.
- Mruk, D., L. J. Zhu, B. Silvestrini, W. M. Lee and C. Y. Cheng (1997). "Interactions of proteases and protease inhibitors in Sertoli-germ cell cocultures preceding the formation of specialized Sertoli-germ cell junctions in vitro." *J Androl* **18**(6): 612-22.
- Murphy, L., I. A. Jeffcoate and P. J. O'Shaughnessy (1994). "Abnormal Leydig cell development at puberty in the androgen-resistant Tfm mouse." *Endocrinology* **135**(4): 1372-7.
- Obergfell, A., K. Eto, A. Mocsai, C. Buensuceso, S. L. Moores, et al. (2002). "Coordinate interactions of Csk, Src, and Syk kinases with [alpha]IIb[beta]3 initiate integrin signaling to the cytoskeleton." *J Cell Biol* **157**(2): 265-75.
- Okabe, Y., T. Sano and S. Nagata (2009). "Regulation of the innate immune response by threonine-phosphatase of Eyes absent." *Nature* **460**(7254): 520-4.

- Olsen, J. V., B. Blagoev, F. Gnad, B. Macek, C. Kumar, et al. (2006). "Global, in vivo, and site-specific phosphorylation dynamics in signaling networks." *Cell* **127**(3): 635-48.
- Pardo, M. and P. Nurse (2005). "The nuclear rim protein Amo1 is required for proper microtubule cytoskeleton organisation in fission yeast." *J Cell Sci* **118**(Pt 8): 1705-14.
- Parsons, J. T. (2003). "Focal adhesion kinase: the first ten years." *J Cell Sci* **116**(Pt 8): 1409-16.
- Peisach, E., J. D. Selengut, D. Dunaway-Mariano and K. N. Allen (2004). "X-ray crystal structure of the hypothetical phosphotyrosine phosphatase MDP-1 of the haloacid dehalogenase superfamily." *Biochemistry* **43**(40): 12770-9.
- Pincus, D., I. Letunic, P. Bork and W. A. Lim (2008). "Evolution of the phospho-tyrosine signaling machinery in premetazoan lineages." *Proc Natl Acad Sci U S A* **105**(28): 9680-4.
- Pires-daSilva, A. and R. J. Sommer (2003). "The evolution of signalling pathways in animal development." *Nat Rev Genet* **4**(1): 39-49.
- Raftopoulou, M. and A. Hall (2004). "Cell migration: Rho GTPases lead the way." *Dev Biol* **265**(1): 23-32.
- Rayapureddi, J. P., C. Kattamuri, B. D. Steinmetz, B. J. Frankfort, E. J. Ostrin, et al. (2003). "Eyes absent represents a class of protein tyrosine phosphatases." *Nature* **426**(6964): 295-8.
- Revenu, C., R. Athman, S. Robine and D. Louvard (2004). "The co-workers of actin filaments: from cell structures to signals." *Nat Rev Mol Cell Biol* **5**(8): 635-46.
- Ridder, I. S. and B. W. Dijkstra (1999). "Identification of the Mg²⁺-binding site in the P-type ATPase and phosphatase members of the HAD (haloacid dehalogenase) superfamily by structural similarity to the response regulator protein CheY." *Biochem J* **339** (Pt 2): 223-6.
- Roskoski, R., Jr. (2005). "Src kinase regulation by phosphorylation and dephosphorylation." *Biochem Biophys Res Commun* **331**(1): 1-14.
- Schlaepfer, D. D., K. C. Jones and T. Hunter (1998). "Multiple Grb2-mediated integrin-stimulated signaling pathways to ERK2/mitogen-activated protein kinase: summation of both c-Src- and focal adhesion kinase-initiated tyrosine phosphorylation events." *Mol Cell Biol* **18**(5): 2571-85.
- Schlessinger, J. (2002). "Ligand-induced, receptor-mediated dimerization and activation of EGF receptor." *Cell* **110**(6): 669-72.
- Selengut, J. D. (2001). "MDP-1 is a new and distinct member of the haloacid dehalogenase family of aspartate-dependent phosphohydrolases." *Biochemistry* **40**(42): 12704-11.
- Seligman, J., Y. Zipser and N. S. Kosower (2004). "Tyrosine phosphorylation, thiol status, and protein tyrosine phosphatase in rat epididymal spermatozoa." *Biol Reprod* **71**(3): 1009-15.
- Sheiness, D. and J. M. Bishop (1979). "DNA and RNA from uninfected vertebrate cells contain nucleotide sequences related to the putative transforming gene of avian myelocytomatosis virus." *J Virol* **31**(2): 514-21.

- Sieg, D. J., D. Ilic, K. C. Jones, C. H. Damsky, T. Hunter, et al. (1998). "Pyk2 and Src-family protein-tyrosine kinases compensate for the loss of FAK in fibronectin-stimulated signaling events but Pyk2 does not fully function to enhance FAK- cell migration." *EMBO J* **17**(20): 5933-47.
- Singh, S. K., K. Yang, S. Karthikeyan, T. Huynh, X. Zhang, et al. (2004). "The thrH gene product of *Pseudomonas aeruginosa* is a dual activity enzyme with a novel phosphoserine:homoserine phosphotransferase activity." *J Biol Chem* **279**(13): 13166-73.
- Smith, P. K., R. I. Krohn, G. T. Hermanson, A. K. Mallia, F. H. Gartner, et al. (1985). "Measurement of protein using bicinchoninic acid." *Anal Biochem* **150**(1): 76-85.
- Soufi, B., F. Gnad, P. R. Jensen, D. Petranovic, M. Mann, et al. (2008). "The Ser/Thr/Tyr phosphoproteome of *Lactococcus lactis* IL1403 reveals multiply phosphorylated proteins." *Proteomics* **8**(17): 3486-93.
- Stewart, S. A., D. M. Dykxhoorn, D. Palliser, H. Mizuno, E. Y. Yu, et al. (2003). "Lentivirus-delivered stable gene silencing by RNAi in primary cells." *Rna* **9**(4): 493-501.
- Taylor, D. L. and Y. L. Wang (1980). "Fluorescently labelled molecules as probes of the structure and function of living cells." *Nature* **284**(5755): 405-10.
- Tiganis, T. and A. M. Bennett (2007). "Protein tyrosine phosphatase function: the substrate perspective." *Biochem J* **402**(1): 1-15.
- Tonks, N. K. (2003). "PTP1B: From the sidelines to the front lines!" *FEBS Letters* **546**(1): 140-148.
- Tonks, N. K. (2006). "Protein tyrosine phosphatases: from genes, to function, to disease." *Nat Rev Mol Cell Biol* **7**(11): 833-46.
- Towbin, H., T. Staehelin and J. Gordon (1979). "Electrophoretic transfer of proteins from polyacrylamide gels to nitrocellulose sheets: procedure and some applications." *Proc Natl Acad Sci U S A* **76**(9): 4350-4.
- Tuschl, T. and A. Borkhardt (2002). "Small interfering RNAs: a revolutionary tool for the analysis of gene function and gene therapy." *Mol Interv* **2**(3): 158-67.
- Wang, H., W. Xiong, Y. Chen, Q. Ma, J. Ma, et al. (2006). "Evaluation on the phagocytosis of apoptotic spermatogenic cells by Sertoli cells in vitro through detecting lipid droplet formation by Oil Red O staining." *Reproduction* **132**(3): 485-92.
- Wishart, M. J. and J. E. Dixon (1998). "Gathering STYX: phosphatase-like form predicts functions for unique protein-interaction domains." *Trends Biochem Sci* **23**(8): 301-6.
- Wolf-Yadlin, A., N. Kumar, Y. Zhang, S. Hautaniemi, M. Zaman, et al. (2006). "Effects of HER2 overexpression on cell signaling networks governing proliferation and migration." *Mol Syst Biol* **2**: 54.
- Worth, D. C. and M. Parsons (2008). "Adhesion dynamics: Mechanisms and measurements." *The International Journal of Biochemistry & Cell Biology* **40**(11): 2397-2409.
- Xiao, X. and W. X. Yang (2007). "Actin-based dynamics during spermatogenesis and its significance." *J Zhejiang Univ Sci B* **8**(7): 498-506.

- Yamashita, M., K. Yamagata, K. Tsumura, T. Nakanishi and T. Baba (2007). "Acrosome reaction of mouse epididymal sperm on oocyte zona pellucida." *J Reprod Dev* **53**(2): 255-62.
- Yeatman, T. J. (2004). "A renaissance for SRC." *Nat Rev Cancer* **4**(6): 470-80.
- Zaidel-Bar, R. (2009). "Evolution of complexity in the integrin adhesome." *J Cell Biol* **186**(3): 317-21.
- Zaidel-Bar, R., S. Itzkovitz, A. Ma'ayan, R. Iyengar and B. Geiger (2007). "Functional atlas of the integrin adhesome." *Nat Cell Biol* **9**(8): 858-67.
- Zhang, G., A. S. Mazurkie, D. Dunaway-Mariano and K. N. Allen (2002). "Kinetic evidence for a substrate-induced fit in phosphonoacetaldehyde hydrolase catalysis." *Biochemistry* **41**(45): 13370-7.
- Zhang, W. and L. Shi (2004). "Evolution of the PPM-family protein phosphatases in *Streptomyces*: duplication of catalytic domain and lateral recruitment of additional sensory domains." *Microbiology* **150**(Pt 12): 4189-97.
- Zheng, H., C. Ji, S. Gu, B. Shi, J. Wang, et al. (2005). "Cloning and characterization of a novel RNA polymerase II C-terminal domain phosphatase." *Biochem Biophys Res Commun* **331**(4): 1401-7.
- Zheng, H., C. J. Stratton, K. Morozumi, J. Jin, R. Yanagimachi, et al. (2007). "Lack of Spem1 causes aberrant cytoplasm removal, sperm deformation, and male infertility." *Proc Natl Acad Sci U S A* **104**(16): 6852-7.

10 Supplementary data

10.1 JPT phosphopeptide screen analysis

AUM was analyzed with Ser/Thr or Tyr phosphopeptides as a first approach to identify physiological substrates. As per convention, hits above a 66% cut off of the highest OD obtained in this assay were considered meaningful and were analyzed as possible AUM substrates as discussed in section 5.3. There are around 150 hits below this cut off. These hits may still be useful to understand the role of AUM in signaling pathways.

Below is the complete list of phosphopeptides dephosphorylated by AUM in descending order of OD. For each phosphopeptide, the 13-mer sequence, SwissProt ID and the known main biological function of the respective proteins are listed. The phosphorylated tyrosine, serine or threonine residue is always the central amino acid. Physiologically relevant phosphorylation sites for the first 17 peptides (those above the 66% cut off) and for all EGFR family proteins were identified by BLAST analysis (Altschul et al., 1990) of the human protein data base. A theoretical AUM substrate “consensus peptide” sequence was derived from the first 17 hits and from all EGFR hits enlisted. Interesting hits were grouped under well characterized protein families.

Table S1: Phosphotyrosine peptides dephosphorylated by AUM

Phosphopeptide	SwissProt ID	Details	pTyrosine
LSEDCLYLNIIYTP	P23141	Liver carboxylase 1 precursor	Y118
MEGQHNYLCAGRN	P06401	Progesterone receptor	Y601
DGFYYLYANICFR	O14788	TNF ligand superfamily member 11	Y217
RDINSLYDVSRMY	P16885	PLC-gamma-2	Y753
ASSQDCYDIPRAF	Q13480	GRB2-associated binding protein 1	Y406
LLEQQKYTVTVDY	O14920	Inhibitor of nuclear factor kappa B kinase beta subunit	Y199
RYQPGKYPMPNQS	Q9NRQ2	Phospholipid scramblase 4	Y88
AAFQFSYTAVFGA	Q9Y256	CAAX prenyl protease 2	Y236
NEDYAGYIIPPAP	Q9UNH7	Sorting nexin 6	Y89
LCQSGIYINVLDI	O00476	Sodium-dependent phosphate transport protein 4	Y337
EAALNEYLRVKTV	O75891	10-formyltetrahydrofolate dehydrogenase	Y892
VPNQPVYNQPVYN	O15162	Phospholipid scramblase 1	Y69
SEEIRFYQLGEEA	P22001	Potassium voltage-gated channel subfamily A member 3	Y187
YCPDPLYEVMLKC	P08581	Hepatocyte growth factor receptor precursor (c-met)	Y1313
DAEKPFYVNVFEH	P11274	Breakpoint cluster region protein	Y177
DSPPALYAEP L DS	Q99704	Docking protein 1 (p62dok)	Y296
AFDNLYYWDQDPP	P04626	C-erbB-2 precursor	Y1221
ENPIDLYIYVIDM	P55823	Cadherin-4 precursor	Y264
LSEDCLYLVNWIIP	P06276	Cholinesterase	Y122
LYAGDYRVRVQGRA	Q08345	Epithelial discoidin domain receptor 1 precursor	Y797
ESEELYSSCRQL	P16885	PLC-gamma-2	Y1197
PSDKFIYATVKQS	Q05586	Glutamate (NMDA) receptor subunit zeta 1 precursor	

PLDSTFYRSLLED	P04626	C-erbB-2 precursor	Y1005
LEEILAYQPDILC	Q9UK39	Nocturnin (CCR4 protein homolog)	
DAEMTGYYVTRWY	O15264	Mitogen -activated protein kinase 13	
IGVRESYVNLCSN	Q93034	Cullin homolog 5	
WIRYHRYHGRSAA	P11309	Proto-oncogene serine/threonine-protein kinase pim-1	
LKMKEKYLNVSAC	O75343	Guanylate cyclase soluble, beta-2 chain	
FLRCINYYVFFPSL	P17181	Interferon-alpha/beta receptor alpha chain precursor	
AYQNTIYLNLDWH	P15144	Aminopeptidase N	
PPERIIYANPCKQ	P11926	Ornithine decarboxylase	
LLLANAYIYVQQL	P32004	Neural cell adhesion molecule L1 precursor	
GPNNNNYANVELI	O00763	Coactosin-like protein	
ALDNPEYHNASNG	Q15303	erbB-4 precursor	Y1188
MLNSKGYTKSIDI	P28482	Mitogen-activated protein kinase 1 (ERK-2)	
SIKMQQYTEHFMA	P29317	Ephrin type-A receptor 2 precursor	
LMEKDSYPRFLKS	Q08116	Regulator of G-protein signaling 1	
QLSDPDYINQYVI	Q9Y5W8	Sorting nexin 13	
NLYAGDYRVQGR	Q08345	Epithelial discoidin domain receptor 1 precursor	
RSSLKAYGNGYSS	P07550	Beta-2 adrenergic receptor	
EVHKSGLSSERL	P15311	Ezrin (Cytovillin)	
TAENAEYLRVAPQ	P00533	ErbB-1 precursor	Y1197
TSSSEYGSVSPD	Q99683	Mitogen -activated protein kinase kinase kinase	
EDNVKSYMMDQRR	Q13075	Neuronal apoptosis inhibitory protein	
SIESDIYAEIPDE	Q14289	Focal adhesion kinase 2	
LNTTATYAEPYRP	Q99569	Plakophilin 4	
KKSLTIYAQVQKP	Q13291	Signaling lymphocyte activation molecule precursor	
LSPAFRYQDPWK	P29473	Nitric-oxide synthase, endothelial	
TLPPCIYMAPMNQ	P55286	Cadherin-8 precursor	
RLSGELYGRATAW	Q99999	Galactosylceramide sulfotransferase	
NCTHDLYMIMREC	P22607	Fibroblast growth factor receptor 3 precursor	
RQPFVKYATLISN	P48357	Leptin receptor precursor	
EAPTTAYKKTPI	P14317	Hematopoietic lineage cell specific protein	
IHLEKKYVRRDSG	P07333	Macrophage colony stimulating factor I receptor	
GVCAERYSQEVFE	O15304	Apoptosis regulatory protein Siva	
LNQSSGYRYGTDP	P06241	Proto-oncogene tyrosine-protein kinase FYN	
FRHDSGYEVHHQK	P05067	Amyloid beta A4 protein precursor	
SPGMKIYIDPFTY	P54762	Ephrin type-B receptor 1 precursor	
ARTGILYVNASLD	Q9NYQ8	Multiple epidermal growth factor-like domains 1	
GAFGTVYKGIWIP	P04626	C-erbB-2 precursor	Y735
MTCAELYEKLPQG	P35590	Tyrosine-protein kinase receptor Tie-1 precursor	
SDTSSYCIPTAG	Q13480	GRB2-associated binding protein 1	
MDLLRQYLRVETQ	Q13085	Acetyl-CoA carboxylase 1	
LGTVMRYEEIELR	Q9BZQ4	Nicotinamide mononucleotide adenylyltransferase 2	
AFDNPDYWHSRLF	P21860	c-erbB-3	Y1328
LASEEIYINQLEA	Q12979	Active breakpoint cluster region-related protein	
STSLVGYLRVQGV	Q9UKG9	Peroxisomal carnitine O-octanoyltransferase	
YSTKYFYKQNGRI	Q15303	erbB-4 precursor	Y1268
PPDHQYYNDFPGK	P29353	SHC transforming protein 1	
SQEELHYATLNFP	Q96LC7	Sialic acid binding Ig-like lectin 10 precursor	
CIVENEYGSINHT	P11362	Basic fibroblast growth factor receptor 1 precursor	
HRQGHYMEMNFT	P63010	Adapter-related protein complex 2 beta 1 subunit	
EVTFHLYLIPSDC	Q9C000	NACHT-, LRR-, and PYD- containing protein 2	
QLRDCIYLNAGIM	P56937	Estradiol 17-beta-dehydrogenase 7	
WIEDTLYANVDF	P78363	Retinal-specific ATP-binding cassette transporter	
AEPYNLYSSLKEL	Q92569	PI3-kinase p85-gamma subunit	
EDCGGGYTPDCSS	P11274	Breakpoint cluster region protein	
SYEGNSYTFIDPT	P07333	Macrophage colony stimulating factor I receptor	

MEDSTYYKASKGK	Q05397	Focal adhesion kinase 1 (pp125FAK)	
NLYSGDYRIQGR	Q16832	Discoidin domain receptor 2 precursor	
TGENPIYKSAVTT	P05556	Integrin beta-1 precursor (FN receptor beta subunit)	
YDVSRMYVDPSEI	P16885	PLC-gamma-2	
GRNPGFYVEANPM	P19174	PLC-gamma-1	
LMSEGLYKALEAA	Q15750	Mitogen-activated protein kinase kinase kinase 7 interacting protein 1	
EENWSFYPNVART	P78509	Reelin precursor	
MPSEEGYQDYEP	P37840	Alpha-synuclein (Non-A4 component of amyloid precursor)	
SENFDDYMKEVGV	P15090	Adipocyte lipid-binding protein	
SIRMKRYILHFHS	P21709	Ephrin type-A receptor 1 precursor	
RSSLKAYGNGYSS	P07550	Insulin receptor substrate-1	
TPGMKIYIDPFTY	P29323	Ephrin type-B receptor 2 precursor	
YQYMETYMGPALF	Q14974	Imortin beta-1 subunit	
LTPSFEYQPDPNW	P29475	Nitric-oxide synthase	
ASVMQEYTSQGGV	P25787	Proteasome subunit alpha type 2	
FERASEYQLNDSA	P11488	Guanine nucleotide-binding protein G(t) alpha-1 subunit	
GIIATIIIPGDI	P82251	Glycoprotein-associated amino acid transporter b0,+AT1	
KLSGEAYGFVARI	P04275	Von Willebrand factor precursor	
IFPQPNYVDMLIS	Q9Y5G6	Protocadherin gamma A7 precursor	
PNEDCLYLNIVYP	Q9Z94	Neuroigin 3 precursor	
CFSPNRYWLCAAT	P25388	Guanine nucleotide-binding protein beta subunit-like protein 12.3	
LTSNQEYLDLSMP	P11362	Basic fibroblast growth factor receptor 1 precursor (FGFR-1)	
GEEDTEYMTSSR	P22681	CBL E3 ubiquitin protein ligase	
DPDNEAYEMPSEE	P37840	Alpha-synuclein (Non-A4 component of amyloid precursor)	
LEVGAPLYLRVDGK	Q08174	Protocadherin 1 precursor	
TFPPISYLNIAISW	P53602	Diphosphomevalonate decarboxylase	
GECSIDYVEMAVN	O75891	10-formyltetrahydrofolate dehydrogenase	
TNSITVYASVTLP	Q13291	Signaling lymphocyte activation molecule precursor	
AFDNPDYWNHSLP	Q15303	erbB-4 precursor	Y1242
PPFKSAYSSFVNL	Q9Y2I7	FYVE finger-containing phosphoinositide kinase	
CYLLIRYCSGKSK	P29033	Gap junction beta-2 protein (Connexin 26)	
GTAEPDYGALYEG	P19174	PLC-gamma-1	
LQMAQIYINALSE	Q92858	Atonal protein homolog 1	
SIFFIIIIIVAF	Q01668	Voltage-dependent L-type calcium channel alpha-1D subunit	
IIQAEFYLNPDQS	P01903	HLA class II histocompatibility antigen	
EETREAYANIAEL	P33076	MHC class II transactivator	
LVIPDLYLNAGGV	P49448	Glutamate dehydrogenase 2	
DCAHFHYENVDFG	O14559	Sorting nexin 26	
TAENPEYLGLDVP	P04626	C-erbB-2 precursor	Y1248
VAENPEYLSEFSL	Q15303	erbB-4 precursor	Y1268
MVLKHPYPRKVEE	Q9UN19	Dual adapter for phosphotyrosine and 3 phosphoinositide	
PAVPSIYATLAIH	Q8NHL6	Leucocyte immunoglobulin-like receptor subfamily B member 1	
AAAAETYANISWE	Q92823	Neuronal cell adhesion molecule precursor	
KHATGNYIIIMDA	O60762	Dolichol-phosphate mannosyltransferase	
TRICKIYDSPCLP	Q06609	DNA repair protein RAD51 homolog 1	
TFGAKPYDGIPAR	P04626	C-erbB-2 precursor	Y923
DMGDEVYDDVDTS	O15117	FYN-binding protein	
FITEEDYQALRTS	Q00610	Clathrin heavy chain 1	
SENFDDYMKALGV	P02689	Myelin P2 protein	
TSTEPQYQPGENL	P12931	Proto-oncogene tyrosine-protein kinase Src (p60-Src)	
DIHVGDIYIIPKNT	O15528	25-hydroxyvitamin D-1 alpha hydroxylase, mitochondrial precursor	
GIICTFYTAVGGM	Q92911	Sodium/iodide cotransporter	
GLARDIYKDPDYV	P35968	Vascular endothelial growth factor receptor 2 precursor (VEGFR-2)	

NLEQEEYEDPDIP	P02730	Band 3 anion transport protein (CD233 antigen)	
CSPPPDYNSVVLV	P17948	Vascular endothelial growth factor receptor 1 precursor (VEGFR-1)	
SPGMKIYIDPFTY	P54762	Ephrin type-B receptor 1 precursor	
DDFDGTYETQGGK	P21709	Ephrin type-A receptor 1 precursor	
SIFFIYIIIIAF	Q13936	Voltage-dependent L-type calcium channel alpha-1C subunit	
QGEDQYYLRVTTV	P10909	Clusterin precursor	
DKDLRHVYLNRFQ	Q86UL8	Atrophin-1 interacting protein 1	
IAANCIYLNIPNK	O94760	Dimethylarginine dimethylaminohydrolase 1	
MVIPDLYLNAGGV	P00367	Glutamate dehydrogenase 1	
PASEQGYEEMRAF	P21860	C-erbB-3 precursor	Y1289
SRGEEVYVKKTMG	P35590	Tyrosine-protein kinase receptor Tie-1 precursor	
PTAGALYSGSEGD	P11831	Serum response factor	
SQQTNDYMQPEED	P12814	Non-muscle alpha-actinin 1 (F-actin cross linking protein)	
RPEDTFYFDPEFT	P51812	Ribosomal protein S6 kinase alpha 3	
RRYGDRYINLRGP	P12821	Angiotensin-converting enzyme	
		Tyrosine-protein kinase ITK/TSK (T-cell specific kinase)	
TVVIALYDYQTND	Q08881		
YQKLYTYIQSRFY	O43781	Dual-specificity tyrosine-phosphorylation regulated kinase 3	
ATDDDFYDDPCFD	P15172	Myoblast determination protein 1	
MDEELHYASLNHFH	P20138	Myeloid cell surface antigen CD33 precursor	
PKAEDEYVNEPLY	Q15303	erbB-4 precursor	Y1202
LYEKFTYAGIDCS	Q02763	Angiopoietin 1 receptor precursor	
SLDNPDYQQDFPF	P00533	ErbB-1 precursor	Y1172
SFLDSGYRILGAV	P18206	Vinculin	Y822
TLQHPDYLQEYST	Q15303	erbB-4 precursor	Y1258
KIGEGTYGTVFKA	Q00535	Cell division protein kinase 5	
SSSIDEYFSEQPL	P17181	Interferon-alpha/beta receptor alpha chain precursor	
IMNDSNYIVKGNA	P07333	Macrophage colony stimulating factor I receptor precursor	
PAFDNLYYWDQDP	P04626	C-erbB-2 precursor	Y1221
EELGYEYMDVGS	P21860	c-erbB-3 precursor	Y1222
GAFGTVYKGLWIP	P00533	ErbB-1 precursor	Y727
PSRDPHYQDPHST	P00533	ErbB-1 precursor	Y1056
GAFGTVYKGIWVP	Q15303	erbB-4 precursor	Y733
DKPKQEYLNPEVE	Q15303	erbB-4 precursor	Y1162
AAEQPLYLNPLDP	Q8N566	Arp8 homolog (Consensus AUM substrate peptide)	Y173
A/PADNPEYLGEDLP	P04626	Consensus EGFR peptide	Y1248

Total hits	Class of proteins
16	EGF receptor family
12	EGFR downstream proteins
4	MAPK/ interacting proteins
13	cell adhesion molecules
7	Other growth factor receptors
3	Voltage gated channels

11 Curriculum Vitae

Persönliche Daten:

Nachname	Duraphe
Vorname	Prashant
Geschlecht	männlich
Geburtstag	25/09/1973
Geburtsort	Pune, Indien
Staatsangehörigkeit	indisch
Familienstand	ledig
Arbeitsplatz	Rudolf Virchow Zentrum für experimentelle Biomedizin Universität Würzburg, Versbacherstr. 9 97078 Würzburg, Deutschland Tel.: 0931 201 48763 Prashant.Duraphe@virchow.uni-wuerzburg.de
Wohnsitz	Neutorstrasse 4 97070 Würzburg, Deutschland Tel.: 0176 800 36173

Hochschulbildung und Berufstätigkeit:

seit 08/2008	Doktorand am Rudolf Virchow Zentrum für experimentelle Biomedizin, Universität Würzburg
07/2006 - 07/2008	Doktorand am Institut für Biochemie und Molekularbiologie II, Heinrich- Heine Universität Düsseldorf

- 07/2006 Master of Science, Hauptfach Molekularbiologie,
University of Skövde, Schweden
- 02/2006 - 06/2006 Diplomand am Institut für Biochemie und Molekularbiologie II, Heinrich
Heine Universität Düsseldorf
- 01/2005 - 12/2005 Aufbaustudium am Institut für Molekularbiologie, Universität von
Skövde, Schweden
- 07/1999 - 06/1999 Wissenschaftlicher Assistent in der Abteilung für Molekulare
Diagnostik, Grant Medical Foundation in Pune, Indien
- 06/1996 - 06/1999 Privatlehrer für Studenten des Grundstudiums
- 06/1994 - 04/1996 Hauptstudium im Hauptfach Zoologie an der Universität Pune, Indien
- 06/1991 - 04/1996 Grundstudium der Naturwissenschaften an der Universität Pune, Indien

Schulbildung:

- 06/1989 - 04/1991 Oberstufenkolleg in Pune, Indien
- 06/1979 - 04/1989 Grund- und Mittelschule in Pune , Indien

Liste von Vorträgen:

Duraphe P., Odersky A., Jonkheijm P., Zanger K., Nürnberg B. and Gohla A.

Titel: Identification and characterization of AUM, a novel mammalian haloacid
dehalogenase phosphatase involved in spermiogenesis

Europhosphatase Meeting 2007, Aveiro, Portugal (EMBO Conference Series, 24-28/05/
2007)

Duraphe P., Odersky A., Jonkheijm P., Zanger K., Waldmann H., Nürnberg B. and Gohla A.

Titel: Identification and characterization of AUM, a novel mammalian haloacid dehalogenase phosphatase involved in spermiogenesis

Jahrestagung der deutschen Gesellschaft für Pharmakologie und Toxikologie 2008, Mainz, Deutschland (11-13/03/2008)

Duraphe P. and Gohla A.

Titel: Identification and characterization of AUM, a novel mammalian aspartate-based phosphatase

Rudolf Virchow Zentrum Retreat 2009, Klöster Höchst, Deutschland (04-06/10/2009)

Erklärung

Hiermit erkläre ich an Eides statt dass ich die vorliegende Dissertation mit dem Title 'Identifizierung und Charakterisierung von AUM, einer neuen humanen Tyrosin-Phoshatase' selbständig angefertigt und keine anderes als die von mir angegebenen Quellen und Hilfsmittel verwendet habe.

Weiterhin erkläre ich dass diese dissertation weder in gleicher noch in ähnlicher form bereits ein einem anderen Prüfungsverfahren vorgelegen ist.

Würzburg, November 2009

Prashant S. Duraphe

12 Acknowledgments

I would like to thank Prof. Dr. Antje Gohla for her inspiring guidance and providing me the opportunity to conduct this PhD thesis in her research group. Not everyone get opportunity to work on a novel protein and privilege of naming it. I had both, in spite of having nothing extraordinary track record. It is her commitment and perseverance could make it possible to complete the project. I am grateful to her for guiding me throughout the work.

I would like to thank Prof. Dr. Dr. M. Scharl for his interest in this work and his willingness to represent this work at Natural science faculty of prestigious Würzburg University.

I am thankful to Drs. Elisabeth Jeanclos, Oleg Fedorchenko, Axel Hoffmann and Ms. Andrea Odersky for stimulating discussions and showing keen interest in the project. I also would like to thank Prof. Dr. Dr. B. Nürnberg for providing me financial assistance during initial phase of my doctoral studies.

I had an opportunity to work at universities of Düsseldorf and Würzburg. I am thankful to all the colleagues at both the laboratories for their kind support. I am particularly happy to pass on my project to compatriot, Ambrish Saxena and would like to thank him for his help during final stages of the project.

It is of my great pleasure to see the project that I initiated along with all the colleagues is at very interesting stage. We will have AUM mouse soon and a young, enthusiastic graduate student, Annegrit Seifried had recently started working on structure of AUM.

It would be unfair if I do not mention the affection I received everywhere in this great *land der ideen*. I would like to express my gratitude towards Germany and her people for establishing successful system and scientific atmosphere to help moving human knowledge ahead.

At the end, I am indebted to everyone back home. I am what I am, is only because of my nation, and support of my family & friends.

I dedicate this work to seers of eastern philosophy who gave us 'AUM'

| ॐ तत् सत् |

|AUM...TAT...SAT|

(Bhagavad Gita 17.23)

